MAGNETIC FIELDS AND SUPERGRANULE VELOCITY FIELDS ON THE QUIET SUN

Thesis by

Haimin Wang

In Partial Fulfillment of the Requirements

for the Degree of

Doctor of Philosophy

California Institute of Technology

Pasadena, California

1988

(Submitted April 25, 1988)

ACKNOWLEDGEMENTS

I am indebted to Professor Harold Zirin, my thesis advisor, for his constant guidance and encouragement on my work, for countless number of helpful discussions and suggestions, and for many kinds of support. I can not express enough gratitude to him.

I am grateful to the other members of my oral examination committee, Professors Peter Goldreich, Ken G. Libbrecht and Sterl Phinney for many useful criticisms and suggestions, those are very helpful in my thesis work.

I express my deepest appreciation to Sara F. Martin for many helpful discussions, comments and suggestions, for her cooperation in several observation projects, and for reading draft and correcting English.

My special thanks to Jim Kaufman for reading the draft of part of my thesis, and many discussions on physics and computer programming; to Dean-Yi Chou for his cooperation on chapter 4, and other helpful discussions; to Pawan Kumar and Kwok-Wai Cheung for being my officemates in my first two years at Caltech, I enjoy the wonderful time I had; to my fellow graduate students, particularly John A. Biretta, Richard Edelson,Jim McCarthy, Dave Hough, Alain Porter, Fernando Selman, Mingshen Han and Lin Zhou, for many discussions and friendship.

I would like to thank the professors at Caltech who taught me physics and astronomy.

I am also indebted to the research staff in the solar group of Caltech, Gordon Hurford, Frances Y. Tang, Dale Gary, Bruce D. Popp, Martin F. Wodard and Margaret A. Liggett for reading draft, and for helpful discussions; to the Big Bear staff, Alan P. Patterson, William Marquette, Randy J. Fear, and other members for kind and useful support on observation; to staff at National Solar Observatories for the support on several observation runs; to Jeff Nenow for processing films; and to Helen Z. Knudsen, the librarian, for her kind assistance.

I must thank my wife, Chunping, for her love, understanding and support.

Finally, I would like to thank every one at Caltech for providing such an inspiring and exciting atmosphere to work in.

ABSTRACT

I have carried out detailed study on the quiet sun magnetic fields and supergranule velocity fields. This thesis consists of 6 themes. 1. I studied the statistical properties of quiet sun magnetic fields, including size distribution, evolution, flux budget of magnetic flux elements, and the magnetic diffusion constant. From the observations, I derived that the magnetic diffusion constant is $\leq$150 km^2/sec in the quiet region. I found that cancelling features and Ephemeral Regions are major sources of magnetic flux disappearance and replenishment. 2. I studied the supergranule velocity fields. Supergranule vertical velocities have a r.m.s. speed of 0.03 km/s. By observing the evolution of individual supergranule cells, I found that the average lifetime of supergranules is $\geq$50 hours. 3. I measured the contrast of faculae near the solar limb. The measurements show no obvious contrast increase or decrease near the solar limb. The observation fits neither the "hot wall" nor "hot cloud" fluxtube model. 4. I measured the separation velocities of new bipoles. The observed values are several times smaller than the values estimated by the theory of magnetic buoyancy. 5. I applied the local correlation tracking technique to BBSO Videomagnetogram data and detected an approximate radial intranetwork flow pattern. 6. I studied the relationship between magnetic fields and convection velocity fields. I found that ephemeral regions have a light tendency to emerge at or near the boundaries of supergranules; supergranules have the same scale, correlation lifetime and mean horizontal speed in the enhanced network region as in the mixed polarity quiet sun; the velocity of moving magnetic features that surround sunspots is consistent with the direct Doppler measurement.

TABLE OF CONTENTS

Chapter 1

Introduction

1. Supergranule and Solar Convection Modes

It is well known that the sun has a convection zone which transfers energy from the solar radiative zone to the photosphere. There are four scales of convection which have been observed or proposed in the sun: granulation, mesogranulation, supergranulation and giant cell.

Although the existence of granules has been known for nearly two centuries, the first modern high resolution photographs were obtained by Schwarzchild (1959) with the stratoscope balloon-born telescope. His pictures confirmed that the bright granules are separated by narrow dark lanes, like Benard cells. The subject of granulation has been thoroughly reviewed in "The Solar Granulation" by Bray *et al.* (1984). The typical granule has the following properties: radial velocity 1-2 km/s; scale 1000 km; lifetime 10 minutes; temperature fluctuation $\geq 100°$. Data from the SOUP experiment on Spacelab 2 have provided several new and exciting results concerning granules. For example, the results of Title *et al.* (1987) show that the granule lifetime is much longer near active regions than in the quiet sun.

The supergranulation was the second kind of convection to be discovered. Its velocity pattern was discovered by Hart (1954, 1956). Supergranulation was first named and studied extensively by Leighton *et al.* (1962). Some properties of supergranules are: scale 3×10^4 km; lifetime 20-24 hours; the motion within each cell has a horizontal outflow from a source inside the cell, the peak velocity of horizontal flow is about 0.5 km/s. Although the horizontal component of supergranule velocity

has been well studied, its vertical component is still a matter of dispute. Different authors had very different supergranule vertical speed from in the order of 0.01 km/s (Musman and Rust, 1970; Giovanelli, 1980) to about 0.4 km/s (Deubner, 1971; Skumanich *et al.*, 1975).

November *et al.* (1981, 1982) introduced the term mesogranulation for the observed velocity fluctuation on a scale intermediate between those of granulation and supergranulation. It was found that the mesogranulation has a r.m.s. vertical velocity amplitude of 60 m/s superposed on the larger scale supergranular flows. Mesogranulation also has pattern of cellular flow with a spatial scale of 5 to 10 Mm. The lifetime appears to be at least 2 hours. No related magnetic feature has been found.

Numerical simulations of giant cells have been performed quiet extensively (Young, 1974; Gilman, 1978a,b). Giant cells may have the scale of hundreds of Mm, extending throughout the entire convection zone. Their lifetime is in the order of a few months. So far, their is no solid observing evidence to confirm the existence of giant cells. Some indirect evidences show that the giant cell might be related to the activity complexes (Bumba, 1975). Based on that fact, Wilson (1987) proposed the idea that the solar magnetic cycle may relate to the giant convection cell.

In table 1, I summarize the physical properties of 4 different convection modes, including their relationship with solar magnetic phenomena.

Table 1 Solar Convection Modes

Convection Mode	Size	Lifetime	Velocity	Related Magnetic Phenomena
Giant cell	100 Mm	a few months	0.1 km/s	active complex
Supergranule	30 Mm	1-2 days	0.5 km/s	magnetic network
Mesogranule	5 Mm	2 hours	0.1 km/s	none
Granule	1000 Km	10-20 min.	1.0 km/s	filigree

2. Quiet Sun Magnetic Fields

The hierarchy of solar magnetic fields has been reviewed by Zwaan (1987). In a quiet region, magnetic fields can be generally divided into two categories: network fields and intranetwork fields, covering the entire solar surface. The fields are all in the form of discrete magnetic elements.

Network fields have been found in the boundaries and, in particular in the vertices of supergranular velocity cells (Simon and Leighton, 1964). Field elements are constantly changing in shape, but usually they retain a recognizable coherence throughout an observing day (Martin, 1983; Livi *et al.*, 1985, Zirin, 1985a). The magnetic flux of network elements ranges from 2×10^{18} mx to 3×10^{19} mx. They show a little motion, some of them move along the supergranule boundaries with a speed of 0.1 km/s. Over periods of hours, some network elements change markedly either by splitting, by merging with a field fragment of the same polarity or by cancelling with a field element of opposite polarity.

The intranetwork fields were first discovered by Livingston and Harvey (1975, also Harvey 1977) with the 512-channel magnetograph at Kitt Peak. The polarities of intranetwork fields are mixed on a scale of a few arcseconds, they are independent of the dominant polarity of the surrounding network fields. The lifetime of intranetwork fields ranges from 1 to several hours. The sensitivity improvement of the VMG system at BBSO makes it possible to study the intranetwork fields in detail. The magnetic flux in the intranetwork elements are from the detection limit i.e. a few times 10^{16} Mx to 10^{17} Mx (Wang *et al.* 1985a). The intranetwork fields move with a typical velocity of 0.3 km/s, approximately toward the boundaries of the supergranule cell (Martin, 1987).

The ephemeral region (ER) is another important and interesting magnetic phenomenon. An ER is an emergence of a small bipolar magnetic flux. Harvey and Martin (1973) did the first comprehensive study of ERs. They also studied the correlation between the birthrate of ERs and the phase of the solar cycle (Martin and Harvey, 1979). ERs have a typical flux of 3×10^{18} Mx to 1×10^{20}. The birthrate of ERs strongly depends on the sensitivity of observation. Tang (personal communication) estimated that it is between 0.1 to 0.6/hour/10^{10}km^2.

Recently, the Caltech group determined that the magnetic cancelling features are the major sources responsible for the disappearance of magnetic flux on the quiet sun (Martin 1983; Wang *et al.* 1985b; Livi *et al.* 1985, Martin *et al.* 1985; Zirin 1985a, 1987). They defined cancellation as the mutual disappearance of magnetic

flux in closely spaced features of opposite polarity. For a typical pair of bipolar features, cancellation requires several hours, implying a flux loss rate of 10^{18} Mx/hour. During the cancelling events, the approaching speed of two elements is around 0.5 km/s. Cancellation may take place among network fields, intranetwork fields and ERs. Cancellation between two network magnetic elements contributes most of the flux disappearance. Number of cancellation varies from 1 to 8 per supergranule per day. The physical mechanism of cancellation could be submergence (Parker 1984; Zirin 1985b) or magnetic reconnection. No conclusive model has been established for it.

The intrinsic strength of quiet sun magnetic fields is a problem which has not been settled. The apparent magnetic strength of a network element is on the order of 100 to 200 gauss. Due to the resolution limit and atmospheric seeing of ground based observations, the intrinsic magnetic strength of network fields might be much higher than the apparent strength. Stenflo (1976 and the references cited therein) developed a line ratio technique, i.e. they observed the magnetic field simultaneously by two spectrum lines of same atom with different g factor. Their results show that the network fields are on the order of 2 to 3 kilo gauss. However, the intranetwork fields were generally believed to be intrinsically weak (Zirin, 1987; Spruit *et al.* 1987).

Finally, I would like to introduce the work in the transportation of magnetic fields. Leighton (1964, 1969) developed a model of the solar cycle, in which the

supergranules transport magnetic flux from sunspots to quiet regions by means of a random walk process. An important parameter in his model is the diffusion constant. For a diffusion constant of 10^4 km^2/s, the observations fit the theory pretty well. Mosher (1977) derived the following expression for the cross-correlation coefficient of network magnetic fields in terms of diffusion constant:

$$CC(t) = 1 - (\sqrt{\pi Dt}/1.7r_0)\mathrm{erf}(1.7r_0/\sqrt{4Dt})$$

where CC(t) is the cross-correlation coefficient of magnetic fields as a function of time, D is the effective diffusion constant, erf is the error function and r_0 is the average size of network magnetic elements. He fitted the Hα and CaK cross-correlation data to the above formula, obtaining diffusion constant of 200 to 300 km^2/s, much less than that required by Leighton's solar cycle model. He proposed that a meridional flow of order of 3 m/s may contribute to the long term magnetic diffusion. Marsh's mechanism (Marsh 1978) gives another source of magnetic diffusion. The cancellation of ER with network magnetic elements of opposite polarity may give an effective diffusion constant of 800 km^2/s.

3. Magnetoconvection

This subject deals with the interaction between magnetic fields and the convection velocity fields. The early work was based on the fact that the bright patches of chromospheric calcium emission which make up the network are located at the boundaries of supergranules (Leighton *et al.* 1962, Simon and Leighton 1964). Early

workers also found that regions of strong photospheric magnetic fields tend to occur directly below the bright calcium emission. An explanation of this correlation has been given by Simon and Leighton (1964; Simon 1963). The supergranule motions accumulate magnetic fields in the cell boundaries where the flow is strongly converging, these enhanced fields are then responsible for the calcium emission above the cell boundaries.

As Spruit (1984) discussed, the interaction of flux tubes with convection has two aspects: (1) the formation of flux tubes by the interaction of a weak diffused field with convection; (2) the interaction of already established flux tubes with the convective flow. Numerous authors have studied this subject theoretically. Clark (1968), for example, calculated the motion of chromospheric fields under the influence of supergranule velocity fields. Channeled magnetic fields were found from his calculation, which might correspond to the network fields. Galloway and Weiss (1981) presented results from numerical experiments on magnetoconvection. They discussed the concentration of magnetic flux into isolated ropes in the turbulent convective zones of the sun and other late type stars. The diffused magnetic fields were swept to the boundaries of convection cells after a few turn-over times. Meyer *et al.* (1979) constructed a 2-D model to study the interaction of isolated magnetic flux tubes with convection in the Sun. In 1985, they described the 3-D behavior of buoyant magnetic flux tubes in the granules and supergranules (Schmidt *et al.* 1985). They concluded that small fluxtubes are swept to the boundaries while larger

more buoyant tubes with flux larger than 10^{19} Mx are dragged to the axis of the cell. New flux emerges at the center of the cell.

I distinguish two types of observational tests of the theory of interacting magnetic fields with convective motion. (1) Static test, i.e. observation of the relative location of magnetic features within the convection cell. (2) Dynamic test, i.e. observation of the relationship between the motion of various photospheric and chromospheric features and the convection velocity fields. Howard *et al.* (1979), for example, studied the birthplace of active regions and X-ray bright points which were believed corresponding to ephemeral regions. They concluded that the X-ray bright points tend to emerge randomly throughout the CaK network pattern, active regions were found to emerge at the boundaries of network cells. They suggested that the magnetic flux of active regions comes from deeper in convection zone than the flux that gives rise to bright points. Excellent white light granulation images have been obtained by the Solar Optical Universal Polarimeter (SOUP) instrument on Spacelab 2 (Title *et al.*, 1986; November *et al.* 1986; Simon *et al.* 1988). The SOUP team developed and applied the local correlation technique to granulation data. They detected several types of transverse flows including systematic outflow from the sunspot penumbra and the cellular flow patterns on supergranule and mesogranule scales. They also began a comparative study of white light movies from SOUP and simultaneous Hα, Cak and magnetogram images from Big Bear Solar Observatory (Topka *et al.* 1987). The studies revealed the evolution of weak

intranetwork fields. They showed how horizontal flows coincide spatially with the network pattern. Recently, the VMG system at BBSO is modified to produce very sensitive magnetograms appropriate for studies of the intranetwork flow pattern (Martin 1987, Zirin 1987).

Moving magnetic features (MMF) may add more interest to the interaction of magnetic fields with convection. MMFs are magnetic features which flow radially away from the well developed sunspots (Sheeley and Bhatnagar, 1971; Sheeley, 1972; Harvey and Harvey, 1973; Vrabec, 1974). The speed of the outflow is about 1 km/s. Because of its strong magnetic fields, the spot inhibits normal convection, so one might expect the upflow would be diverted radially outward from the sunspot (Meyer *et al.*, 1974).

4. Introduction to the Thesis

Based on the review above, some problems with the quiet sun magnetic fields and supergranule velocity fields need further study. How do supergranules evolve? What is the detailed magnetic flux budget on the quiet sun? What are the quantitative properties of the intranetwork flow pattern and how well does it match the supergranule velocity field? How do magnetic fields affect the convection? How do some magnetic features (e.g. ERs and cancellation features) relate to the supergranule velocity fields? The study of these problems constitutes my thesis.

In Chapter 2, I discuss the general properties of magnetic fields on the quiet sun.

Auto- and cross-correlation techniques have been used to describe the temporal and spatial information of quiet sun magnetic fields. The diffusion constant was derived from the magnetogram correlation curve; it is about 150 km^2 km/s. After studying the flux budget in detail, I propose that the cancelling features and ERs might be major sources of flux disappearance and replenishment.

In Chapter 3, I present the results on the general properties of supergranule, including the horizontal and vertical velocity structure, evolution, and the lifetime of supergranules and magnetic network. In particular, I found the lifetime of supergranules is $\geq$ 50 hours.

In Chapter 4, I measured the contrast of solar faculae near the solar limb. I found that contrast increases monotonically towards the limb for shorter wavelengths (3400Å to 4600Å); for longer wavelengths (5200Å to 7100Å), contrast has a tendency to peak around $\cos\theta$=0.15, and then decrease towards the extreme limb. The observation does not agree with either "hot wall" or "hot cloud" model.

In Chapter 5, I investigated the separation velocity of emerging magnetic flux. I measured the separation velocity of 24 new bipoles, and compared them with the theoretical values estimated by the theory of magnetic buoyancy. The predicted velocities are higher than those observed. There is no correlation between the separation velocity and magnetic flux of the new bipoles.

In Chapter 6, I show the results for the intranetwork flow pattern(IFP). I applied the local correlation track technique to the magnetogram and found an

approximately radial flow pattern from the supergranule center. The IFP is roughly consistent with supergranule velocity fields.

In Chapter 7, I discuss the effect of magnetic fields on the supergranule. I analyzed the amplitude of supergranule velocity fields, supergranule size and lifetime in regions with different magnetic activity. Properties of moving magnetic features are studied. I also discuss the relationship between ERs and cancellation features and supergranules. The ERs tend to occur at or near the boundary of supergranule boundaries; cancellation of magnetic flux usually occurs in such a manner that two magnetic elements of opposite polarity approach along the boundary of supergranules and disappear mutually.

References

Bray, R.J. , Longhlead, R.E. and Durrant, C.J. 1984, *The Solar Granulation* , 2nd ed., Cambridge University Press, Cambridge.

Bumba V. 1975, in V. Bumba and J. Kleczek (eds.) *Basic Mechanism of Solar Activity*, IAU Symp. **71**, 47.

Clark, A. Jr. 1968, *Solar Physics* **4**, 386.

Deubner, F. 1971, *Solar Physics* **17**, 6.

Galloway, D.J. and Weiss, N.O. 1981, *Ap. J.* **243**, 945.

Gilman, P.A. 1978a, *Geophys. Astrophy. Fluid Dyn.* **11**, 157.

Gilman, P.A. 1978b, *Geophys. Astrophy. Fluid Dyn.* **11**, 181.

Giovanelli, R.G. 1980, *Solar Physics* **67**, 211.

Hart, A.B. 1954, *Monthly Notice of Roy. Astro. Soc.* **114**, 2.

Hart, A.B. 1956, *Monthly Notice of Roy. Astro. Soc.* **116**, 38.

Harvey, J. 1977, *Highlight of Astronomy* **4(2)**, 223.

Harvey, J. and Harvey K. 1973, *Solar Physics* **28**, 61.

Harvey, K. and Martin, S.F. 1973, *Solar Physics* **32**, 389.

Howard *et al.* 1979, *Solar Physics* **63**, 105.

Leighton, R. B. 1964, *Ap. J.* **140**, 1547.

Leighton, R. B. 1969, *Ap. J.* **156**, 1.

Leighton R.B., Noyes, R.W. and Simon, G.W. 1962 , *Ap. J.* **135**, 474.

Livi, S.H.B., Wang, J. and Martin, S.F. 1985, *Australian Journal of Physics* **38**[6], 855.

Livingston, W.C. and Harvey, J. 1975, *Bull. AAS* **7**, 346.

Marsh, K.A. 1978, *Solar Physics* **59**, 105.

Martin, S.F. 1983, BBSO preprint No. 0159.

Martin, S.F. 1987, To Appear in Solar Physics.

Martin, S.F. and Harvey, K. 1979, *Solar Physics* **64**, 93.

Martin, S.F., Livi, S.H.B. and Wang, J. 1985, *Australian Journal of Physics* **38**[6], 929.

Meyer, F., Schimdt, H.U., Weiss N.O. and Wilson, P.R. 1974, *Monthly Notice Roy. Astro. Soc.* **169**, 35.

Meyer, F., Schimdt, H.U., Simon, G.W. and Weiss N.O. 1979, *Astro. and Astrophys.* **76**, 35.

Mosher, J. 1977, Ph. D. Thesis, California Institute of Technology.

Musman, S. and Rust, D.M. 1970, *Solar Physics* **13**, 261.

November, L.J., Toomre, J. and Gebbie, K.B. 1981, *Ap. J.* **245**, L123.

November, L.J., Toomre, J., Gebbie, K.B. and Simon, G.W. 1982, *Ap. J.* **258**, 846.

November, L.J., Simon, G.W., Tarbell, T.D., Title, A.M. and Ferguson, S.H. 1986, Proceeding of Workshop on Theoretic Problems in High Resolution Solar Physics II, in Boulder, CO, p121 .

Parker, E. 1984, *Ap. J.* **280**, 423.

Schimdt, H.U., Simon, G.W. and Weiss N.O. 1985, *Astro. and Astrophys.* **148**, 191.

Schwarzchild, M. 1959, *Ap. J.* **130**, 345.

Sheeley, N.R. Jr. 1972, *Solar Physics* **25**, 98.

Sheeley, N.R. Jr. and Bhatnagar, A. 1971, *Solar Physics* **19**, 338.

Skumanich, A., Smythe, C. and Frazier, E.N. 1975, *Ap. J.* **200**, 747.

Simon, G.W. 1963, Ph.D. Thesis, California Institute of Technology.

Simon, G.W. and Leighton, R.B. 1964, *Ap. J.* **140**, 1120.

Simon, G.W., Title, A.M., Topka, K.P., Shine, R.A., Ferguson, S.H., Zirin, H. and the SOUP Team 1988, To Appear in Ap. J..

Stenflo, J.O. 1976, in Bumba V. and Kleczek J. (eds.) *Basic Mechanism of Solar Activity*, IAU Symp. **71**, 69.

Spruit, H.C. 1984, in Keil, S.L. (ed.) *Small Scale Dynamical Processes in Quiet Stellar Atmosphere*, NSO/SP, p249.

Spruit, H.C., Title, A.M. and Van Ballegooijen, A.A. 1987, *Solar Physics* **110**, 115.

Title, A.M., Tarbell, T.M. and the SOUP Team 1986, Proceeding of Workshop on Theoretic Problems in High Resolution Solar Physics II, in Boulder, CO, p55

Title, A.M., Tarbell, T.D., and Topka, K.P. 1987, *Ap. J.* **317**, 892.

Topka, K.P., Ferguson T., Title, A.M., Tarbell, T.D., Zirin, H, Simon, G.W. and November, L. 1987, *AAS. Bull.* **19**, 927.

Vrabec, D. 1974, in R.G. Athay (ed), *Chromospheric Fine Structure*, D. Reidel Pulb. Co., Dordrecht, Holland, p201.

Wang, J., Zirin, H. and Shi, Z. 1985a, *Solar Physics* **98**, 241.

Wang, J., Shi, Z., Martin, S.F. and Livi, S.H.B. 1985b, Submitted to Solar Physics.

Wilson, P. 1987, *Solar Physics* **110**, 59.

Young, R.E. 1974, *J. Fluid Mech.* **63**, 695.

Zirin, H. 1985a, *Australian Journal of Physics* **38**[**6**], 961.

Zirin, H. 1985b, *Ap. J.* **291**, 858.

Zirin, H. 1987, *Solar Physics* **110**, 101.

Zwaan, C. 1987, *Ann. Rev. Astro. Astrophys* **25**, 83.

Chapter 2

Structure of Magnetic Fields on the Quiet Sun

Accepted by **Solar Physics**

ABSTRACT

To obtain quantitative temporal and spatial information on the network magnetic fields, we applied auto- and cross-correlation techniques to the Big Bear video-magnetogram (VMG) data. The average size of the network magnetic elements derived from the auto-correlation curve is about 5,700 km. The distance between the primary and secondary peak in the auto-correlation curve is about 17,000 km, which is half of the size of the supergranule as determined from the velocity map. The correlation time is about 10 to 20 hours. The diffusion constant derived from the cross-correlation curve is 150 km^2/sec. We also found that in the quiet regions the total magnetic flux in a window $3' \times 4'$ changes very little in nearly 10 hours. That means the emergence and the disappearance of magnetic flux are in balance. The cancelling features and the emergence of ephemeral regions are the major sources for the loss and replenishment of magnetic flux on the quiet sun.

1. Introduction

Auto-correlation and cross-correlation techniques are powerful tools to obtain statistical information about some structures on the sun. Leighton's (1957) measurements of the lifetime of granulation was one of the first applications used in the study of solar features. To study the structure and the time scale of the supergranulation, Leighton and his colleagues applied the correlation technique to Dopplergrams taken at Mount Wilson (Leighton et al., 1962; Simon and Leighton, 1964). From the auto-correlation curve, they found that the size of the supergranulation, the next larger convective structure above the granulation, is about 32,000 km. From the cross-correlation curve, they found a lifetime of 20 hours for this cell structure. Several other authors, e.g. Simon (1963), Roger (1974), Worden and Simon (1976), found various values of the supergranule lifetime from 20 to 40 hours by calculating the cross-correlation of images related to the supergranule and chromospheric network. By assuming the magnetic flux is diffused by the supergranular motion, Mosher (1976) derived a diffusion constant of 200-400 km^2/sec from the K-line and H_α cross-correlation data. Duvall (1980) applied the cross-correlation method to Dopplergrams to derive the solar differential rotation rate.

The improvement of the Big Bear VMG system (Mosher, 1976; Zirin, 1985) makes it possible to study the weak magnetic fields in the quiet sun better than before. Several members of Caltech group have studied the VMG data in great detail (Martin, 1983; Wang et al., 1985; Livi et al., 1985; Martin et al., 1985;

Zirin, 1985, 1987; Chou and Wang, 1987). They described the evolution, physical properties and the classification of the weak magnetic fields. In the quiet sun, magnetic flux can be classified into two categories: network fields and intranetwork (IN) fields. The former is stronger and its proper motion speed is smaller; the latter is weaker and moves faster. They also studied the appearance and disappearance of magnetic fields such as ephemeral regions (ER), cancelling features and merging and fragmentation of flux.

At BBSO, it is now possible to record every magnetograph image on magnetic tape in digital form, greatly facilitating quantitative analysis.

In this work we apply the auto-correlation and cross-correlation technique to BBSO magnetograms to find the average magnetic structures. The magnetic diffusion constant is derived. Finally, we will present the results of study on the budget of magnetic flux on quiet sun.

2. Instrumentation, Data Collection and Reduction

The VMG system at Big Bear Solar Observatory was described in detail by Zirin (1985). Data used for this paper were collected in the summers of 1985 and 1986. One set of VMG data which was obtained on June 22, 1985 is shown in Figure 1. The observation was made at the solar disk center.

The magnetic fields are calibrated by the technique described by Shi et al.

(1986). The radial velocity of sidereal rotation of the sun was used as a calibrator. Usually, in the middle of an observation day, a set of three Dopplergrams at 30 degrees east, center of the disk, and 30 degrees west were made. The velocity calibration constant is calculated from the published solar rotation speed and the Doppler signal in the three Dopplergrams. The magnetic field calibration was obtained by comparing the Doppler shift with the Zeeman shift.

For a 4096-integration, 12-bit memory mode magnetogram, the calibration constant is about 0.5 gauss/pixel unit. This value hardly changes if the system setup remains the same. During the observation run in the middle of October 1985, we had simultaneous Big Bear and Kitt Peak magnetograms of the same region. The calibrations at the two observatories are quite consistent.

The saturation ring correction, i.e. the removal of the contours which are caused by wrapping the signal around to the opposite sign in alternate pattern when the 8-bit memory is filled, is an important step for performing quantitative analysis. After removing the saturation rings and calibrating the images, the pixel value in the map represents the magnetic field strength in gauss.

3. Auto-Correlation Study of the Weak Magnetic Fields

As it was described by Leighton et al. (1962), the auto-correlation function is

defined as

$$AC(u,v) = \frac{1}{A}\int_{-\infty}^{+\infty} T(x,y)T(u+x,v+y)dxdy,$$

where T(x,y) is the intensity of the image, A is a constant. Usually, we set

$$A = \int_{-\infty}^{+\infty} T(x,y)T(x,y)dxdy$$

so that AC(0,0)=1.0.

To simplify the problem, we calculated the one-dimensional auto-correlation function only, i.e.

$$AC(u,0) = \frac{1}{A}\int_{-\infty}^{+\infty} T(x,y)T(u+x,y)dxdy$$

or

$$AC(0,v) = \frac{1}{A}\int_{-\infty}^{+\infty} T(x,y)T(x,v+y)dxdy.$$

In fact, the range of integration is the size of the image rather than infinity. This approximation is valid as long as the size of the image is much larger than the average size of the feature to be studied.

Figure 2(a) is a typical auto-correlation curve for a quiet sun magnetogram with good seeing conditions. The full width at half-maximum (FWHM) provides a measurement of the average linear size of the magnetic elements in the field of view. Since most of the flux is contributed by the network fields in our observing sensitivity, the FWHM gives the information primarily on the network field. The average FWHM from 14 measurements is 5740 ± 340 km. Kömle (1979) measured

the Kitt Peak magnetograms and gave an average size for the magnetic network patches of 4000 to 5000 km.

Figure 2(b) is the auto-correlation curve similar to 2(a), but with all the points in the VMG image replaced with absolute values. So this auto-correlation curve can be compared with the result of CaK image. The secondary maximum (SM) in Figure 2(a) and 2(b) implies some sort of periodicity or a secondary structure. The same kind of periodicity also appears in the auto-correlation curve of Dopplergram (Wang and Zirin, 1987a). An example is given in Figure 2(c). For the Dopplergram, the distance between the first and the second maximum is regarded as the dimension of the supergranule, which has a typical value of 32,000 km (Leighton et al., 1962). However Figure 2(a) shows that this distance is about 15,000 to 20,000 km for the magnetograms. The average distance of SM is 16700 ± 700 km from 15 measurements. Kömle (1979) showed that the distances of SM for different magnetogram data differ strongly. Sykora (1970) plotted the auto-correlation curve for the K_{232} spectroheliogram and found that the distance of SM is about 37400 km, which is about the size of the supergranule. There exists a good correlation between the K line plages and the network magnetic fields (Simon and Leighton, 1964). The magnetic elements located at the boundaries of the supergranule form the magnetic network. The distance between the first and the second maximum could be the average size of magnetic network. It is unclear why this size derived from the VMG data is much smaller than the supergranular scale. One possible reason might be:

In the quiet sun, the network is not well defined by magnetic flux, so its size is not easily defined. The SM of the auto-correlation of the magnetogram might not represent the size of the supergranule.

As mentioned earlier, the quiet sun magnetic fields generally have two categories: the network and IN fields (Zirin, 1985). These two structures could not be separated in the auto-correlation curve shown in Figure 2(a) and 2(b). The reason could be that the IN fields are too weak to appear in the auto-correlation curve, or that the sizes of IN and network elements have a continuous spectrum rather than two discrete components.

In the summer of 1986, we made seeing measurement tests for the VMG system. We found that the smallest detectable elements were about 2" when the seeing was good and did not increase as the number of integrations increased from 16 to 1024. The FWHM of the elements derived from the auto-correlation curve is much bigger than 2", so it represents the real physical size of the network elements; however the filling factor inside the elements is unknown.

To test the results of the auto-correlation study, we measured the size distribution of magnetic flux tubes directly. We found that 20 gauss contours represent the network elements quite well. We measured the sizes of all the elements marked by the 20 gauss contours. The size of individual element is defined as $(d_1 d_2)^{1/2}$, where d_1 and d_2 are lengths of the major and minor axis of the element. There are about 170 network elements in a $300'' \times 200''$ field of view, with an average element

size of 4,200 km. The relative distributions are plotted in Figure 3. The relative number of flux tubes decreases with increasing tube size, but the distribution does not increase rapidly as the size of tube size approaches 0. It is unlike the distribution of the sizes of active regions; the number of regions decreases exponentially with increasing region size (Tang et al., 1984). So the network flux tubes have a characteristic size and the size distribution is within a certain range. An uncertain factor is that the number of small flux tubes may be reduced because they are below the sensitivity threshold. However that should not affect the tubes larger than 2″, which is the seeing size.

Assuming the magnetic flux density of a flux tube has a gaussian profile:

$$B = B_0 \exp(-r^2/{a_0}^2),$$

the FWHM of that flux tube is $1.67a_0$. The average B value inside the 20 G contour is

$$\overline{B} = \frac{2\pi B_0 \int_0^a \exp(-r^2/{a_0}^2) r dr}{\pi a^2} = B_0 {a_0}^2/a^2\{1 - \exp(-a^2/a_0^2)\},$$

where a is the radius of the 20 G contour. We calculated $\overline{B}$ by averaging all the pixels having $B \geq 20$ gauss in the image. We found $\overline{B} = 38.4$ gauss. By definition:

$$20 \text{ gauss} = B_0 \exp(-a^2/a_0^2).$$

From the two equations above, we derived that $a_0 = 0.92a$; we know that $a = 2,100$ km, so that the average FWHM of flux elements is 3250 km, which is substantially smaller than the size derived by auto correlation curve (5740 km).

4. Cross-Correlation Study of Weak Magnetic Fields

4.1. Correlation Time Scale

The cross-correlation is defined as

$$CC(t) = \frac{1}{A}\int_{-\infty}^{+\infty} T(x,y,t_0)T(x,y,t)dxdy,$$

where t_0 is the time in the beginning of the observing sequence. A is defined in section 3.

Because of guiding errors and solar rotation, the images may be shifted and must be re-registered. We have two procedures for this purpose. First we register them manually, i.e. shift image 2, relative to image 1, until they are roughly aligned. Second, we calculate the cross-correlation function

$$CC(u,v,t) = \frac{1}{A}\int_{-\infty}^{+\infty} T(x,y,t_0)T(u+x,v+y,t)dxdy$$

such that a maximum C is found for a value of u and v. Then we shift the second image relative to the first one by u, v pixels in x and y directions respectively.

Figure 4(a) is the cross-correlation curve made from the magnetograms taken on June 22, 1985. The correlation lifetime is defined as the time the correlation drops from unity to $1/e$. Based on June 22, 1985 data, it is about 11 hours in a quiet region of mixed polarity. However, Kömle (1979) gave 8 hours for the Kitt Peak data.

Both the intrinsic change and the motion of magnetic flux tube may cause the correlation to drop. The auto-correlation curve, e.g. Figure 2(a), shows that if the

whole image shifts about 3,000 km, the correlation drops to 0.5; Figure 4(a) shows that the cross-correlation drops to 0.5 after 6 hours. If the reduction of correlation is entirely due to the motion of magnetic elements, the mean velocity would be 3000 km/6 hours, i.e. 0.14 km/s. That gives an upper limit of motion on the the network magnetic elements. However, if the elements did not move, 1/2 of them changed in 6 hours. Velocity measurements (Zirin 1986) give 0.1 km/sec as the mean velocity of the network elements. This result is consistent with ours. The change of the magnetic fields includes the appearance, disappearance, merging and splitting of magnetic flux (Harvey and Martin, 1973; Wang et al., 1985; Martin et al., 1985; Livi et al., 1985; Zirin, 1985, 1987).

This result also can be shown mathematically. Assume the whole VMG image consists of many small elements and the flux density has a Gaussian distribution for the individual elements:

$$B = B_0 \exp(-r^2/\sigma^2),$$

where σ is the average radius of the elements of about 5 arcseconds and r is the distance from the element center.

By the definition, the constant A is

$$A = {B_0}^2 \int_0^{+\infty} \exp(-2r^2/\sigma^2) 2\pi r\, dr$$

or, in Cartesian coordinates,

$$A = {B_0}^2 \int_{-\infty}^{+\infty} \int_{-\infty}^{+\infty} \exp\{-2(x^2+y^2)/\sigma^2\} dx\, dy = \frac{\pi}{2}\sigma^2 {B_0}^2.$$

If the element moves in X direction with a speed v, the distance it moves after time t is $d = vt$.

The cross-correlation is

$$CC(t) = \frac{{B_0}^2}{A} \int_{-\infty}^{+\infty} \int_{-\infty}^{+\infty} \exp\{-2y^2/\sigma^2\} \exp\{-(x^2 + (x-d)^2)/\sigma^2\} dx dy.$$

The result is

$$CC(t) = \exp\{-(vt)^2/2\sigma^2\}.$$

When $vt \ll \sigma$

$$CC(t) = 1 - \frac{(vt)^2}{2\sigma^2}.$$

From this equation and Figure 4(a) with the least square fit technique, we concluded that the average velocity of proper motion of the network magnetic elements is less than 0.14 km/sec.

Figure 4(b) shows of the cross-correlation from the observation made on July 28, 1985. This is an enhanced magnetic network region. The least square fit shows that the correlation lifetime is about 19 hours, longer than that of the mixed polarity quiet region, so the mean speed of the magnetic element motion is less than 0.10 km/s.

We also estimated the effect of differential rotation on the cross-correlation. For a region of size 250″ by 250″ at the solar disk center, the average transverse velocity difference due to differential rotation is about 0.003 km/sec, which is negligible.

4.2. Diffusion Constant

Mosher (1978) constructed a diffusion model of solar magnetic fields based on cross-correlation data. Assuming the image to consist of isolated circular magnetic flux tubes of an average radius r_0, Mosher got

$$(FWHM)_{AC} = 1.6r_0,$$

where $(FWHM)_{AC}$ is the full width at half-maximum of the auto-correlation curve. He also derived the cross-correlation coefficient as

$$CC(t) = 1 - (\sqrt{\pi Dt}/1.7r_0)\mathrm{erf}(1.7\mathrm{r_0}/\sqrt{4\mathrm{Dt}}),$$

where D is the effective diffusion constant and erf is the error function. Fitting K line data (Simon 1963) and H_α data (Rogers 1970) to the above equations, Mosher derived effective diffusion constant of 200 km^2/sec and 300 km^2/sec, respectively.

We can improve on Mosher's work in two aspects: (1). Mosher used the K line and $H\alpha$ data, which represent the chromosphere network, but are indirect indicators of magnetic flux tubes; we used the magnetic data directly. (2). Mosher only estimated the FWHM for the data he used; we have the direct measurements of the FWHM from the magnetograms. The effective diffusion constant is very sensitive to FWHM.

Applying Mosher's technique to our magnetic cross-correlation curve, we obtain an effective diffusion constant of about 150 km^2/sec. In the Figure 5(a), two fits are plotted. The upper one is the fit by the least square method which gives

diffusion constant of 150 km^2/sec; the lower one gives the upper limit for the diffusion constant, since all the points of the observed cross-correlation coefficient are above this fit. This value is 200 km^2/sec.

Figure 5(b) is a fit for the October 15, 1985 data, another quiet region with mixed magnetic polarity. The fit is better than 5(a). The least square value for D is 145 km^2/sec. In the enhanced network region, the correlation drops more slowly than in the mixed polarity region. We estimate that the diffusion constant in the enhanced network region is less than 100 km^2/sec.

As we mentioned in section 4.1, the random walk is not the only reason for the decrease of cross-correlation; the appearance and disappearance of the magnetic flux are other factors which might affect the correlation. Taking these factors into account, it should be noted that we only give an upper limit of the diffusion constant.

One reason that we derived a smaller diffusion constant than Mosher's is that in the Hα images, there are many small-scale structures (e.g. the spicules) having short time scales; they may cause a sharp decrease of the correlation during the first few hours. We could not explain why Mosher's K line data fit also produced a substantially larger diffusion constant than our results. However, we confirm Mosher's conclusion: If the diffusion of magnetic flux is only due to the random motion of magnetic flux tubes by the supergranule, the diffusion constant is much smaller than that required by Leighton's solar cycle model (Leighton, 1969). Marsh (1978) proposed a mechanism which might explain the long-term diffusion of magnetic flux.

When one pole of ephemeral region (ER) is cancelled with the opposite polarity of the network element, the net consequence of this interaction is that small quantities of network flux are transported over distances of the order of the ER pole separation. Marsh concluded that this mechanism gives an effective diffusion constant of 800 km^2/sec.

5. The Statistical Study of the Magnetic Flux in the Quiet Sun

In the papers by Martin (1983), Wang et al. (1985), and Zirin (1985, 1987), the authors concluded that the basic processes for the appearance of flux in the quiet sun are the intranetwork magnetic fields and the ephemeral regions; the disappearance of flux is caused by the cancelling of opposite polarities and fragmentation of magnetic elements. However, Wang and Zirin (1987b) pointed out that although the IN fields are swept to the boundary of supergranules, since IN fields have mixed magnetic polarity, they cannot form new network elements. It has generally been assumed that these processes are all in long-term balance, or else we would not find quiet sun fields all over the sun. Wilson and Simon (1983) studied the flux balance in the active region. They concluded that the changing rates of positive and negative flux are very different.

To test the assumption mentioned above, we need to answer the following questions: In the quiet sun, does the total magnetic flux increase or decrease over a period longer than the lifetime of IN elements? Does the difference between the

total positive flux and the negative flux in a region remain constant? To answer these questions, we use a set of magnetograms observed for a duration of 10 hours taken on June 22, 1985. The field of view is 228" by 165", the area is 2×10^{20} cm^2. Figure 6 plots the distribution of the magnetic flux as a function of flux density; it has a peak around 5-10 gauss and a mean field about 10 gauss. 30% of the total magnetic flux is contributed by the pixels with magnetic flux density $\leq 10G$. A typical ephemeral region or a typical pair of cancelling feature has a total flux of 1.0×10^{19} Mx, including both negative and positive fluxes.

In Figure 7, we plot the mean field vs. time, including only those points with the flux density greater or equal to 3 gauss and discarding the weak ones as noise. Some fluctuation of mean field may be due to changes of the system sensitivity, but there is no tendency of systematic change of mean fields. In Figure 8 we plot the positive and negative flux vs. time. We can conclude from this plot that the difference between the positive and negative magnetic flux does not change in 10 hours, so there is equal amount of positive and negative flux modifying the old magnetic fields.

Finally, we take a look at the flux budget. On June 22, 1985, during 10 hours of observation, 16 ERs emerged in the area of 4.5×10^{10}km^2. It gives an ER birthrate of 0.36/hr/10^{10}km^2, which is consistent with the result of Tang (private communication). The average magnetic flux for these 16 ERs is 1.5×10^{19} Mx which gives a rate of flux emergence of 2.2×10^{15} Mx/sec. The parameters and

the method of measurement were described in a previous paper by Chou and Wang (1987). The same 10 hour data also contained 14 cancelling features. The average flux is 1.3×10^{19} Mx and the rate of flux decrease is 1.2×10^{15} Mx/sec. In summary, the emergence of ERs in the observation region contributed 2.3×10^{20} Mx to the new network flux, and concentration from smaller elements or fluxes below sensitivity threshold contributed 0.3×10^{20} Mx; the magnetic flux decreased by 2.3×10^{20} Mx due to cancelling features, and 0.5×10^{20} Mx due to fragmentation of existing network element. Thus the emergence of ERs and cancelling features are the major sources for the appearance and disappearance of magnetic flux respectively, in the mixed polarity region of quiet sun. The total magnetic flux in the area is 3.2×10^{21} Mx, which gives a mean field of 9.6 gauss. The ERs and cancelling features replace about 1 percent of the network flux every hour. A study of the October 15, 1985 data shows the similar results.

6. Summary

From quantitative study of the Big Bear digital magnetograms, we may draw the following conclusions:

1) In the quiet sun, the mean field strength does not change in 10 hours; the disappearance and the appearance of the flux are in balance. ERs and cancelling features are the major sources for the appearance and disappearance of magnetic flux on quiet sun.

2) The network magnetic flux tubes are discrete with an average size of 5″ to 7″, which is greater than the 2″ seeing size.

3) The correlation time of the magnetograms is about 10 to 20 hours. The correlation lifetime is longer in the enhanced magnetic network region than that in the mixed polarity region. The average speed of network magnetic elements is $\leq$0.14 km/s.

4) The effective magnetic diffusion constant is $\leq$ 150km^2/sec for the mixed polarity quiet region. In the enhanced network region, the diffusion constant is less than 100 km^2/sec.

The relationship between the supergranule and various quiet sun magnetic features (e.g., the relationship between the proper motions of magnetic elements and the supergranule horizontal motion), the location of ephemeral regions, cancelling features respect to the supergranule are interesting problem worth studying. They will be discussed in future papers.

Acknowledgments

I am indebted to Prof. H. Zirin, my thesis advisor, for his supervision, discussion and suggestions. I express my appreciation to the Big Bear staff for assistance in the observations. I am very grateful to Drs. S. Martin and D. Chou for valuable discussions. Also, I thank F. Tang and J. Kaufman for reading the manuscript

and giving me valuable comments. This research is supported by NSF under grant ATM-8513577 and NASA under grant NGL 05 002 034.

References

Chou, D. and Wang, H.: 1987, *Solar Phys.* **110**, 81.

Duvall, T. L.: 1980, *Solar Phys.* **66**, 213.

Harvey, K. and Martin, S. F.: 1973, *Solar Phys.* **32**, 389.

Kömle, N.: 1979, *Solar Phys.* **64**, 213.

Leighton, R. B.: 1957, *Publ. Astron. Soc. Pacific* **69**, 497.

Leighton, R. B.: 1969, *Astrophys. J.* **156**, 1.

Leighton, R. B., Noyes, R. W. and Simon, G. W.: 1962, *Astrophys. J.* **135**, 474.

Livi, S. H. B., Wang, J. and Martin, S. F.: 1985, *Australian Journal of Physics* **38**[6], 855.

Marsh, K. A.: 1978, *Solar Phys.* **59**, 105.

Martin, S. F.: 1983, *BBSO Preprint* **No. 228**.

Martin, S. F., Livi, S. H. B. and Wang, J.: 1985, *Australian Journal of Physics* **38**[6], 929.

Mosher, J. M.: 1976, *BBSO Preprint* **No. 159**.

Mosher, J. M.: 1977, *Ph. D. Thesis*, California Institute of Technology.

Rogers, E. H.: 1970, *Solar Phys.* **13**, 57.

Shi, Z., Wang, J. and Patterson, A.: 1986, *BBSO Preprint* **No. 257**.

Simon, G. W.: 1963, *Ph. D. Thesis*, California Institute of Technology.

Simon, G. W. and Leighton, R. B.: 1964, *Astrophys. J.* **140**, 1120.

Sykora, J.: 1970, *Solar Phys.* **13**, 292.

Tang, F., Howard, R. and Adkins, J. M.: 1984, *Solar Phys.* **91**, 75.

Worden, S. P. and Simon, G. W.: 1976, *Solar Phys.* **46**, 73.

Wang, H. and Zirin, H.: 1987a, in preparation.

Wang, H. and Zirin, H.: 1987b, accepted by *Solar Phys.*

Wang, J., Shi, Z., Martin, S. and Livi, S.H.B.: 1985, submitted to *Solar Phys.*

Wilson, P. and Simon, G. W.: 1983, *Astrophys. J.* **273**, 805.

Zirin, H.: 1985, *Australian Journal of Physics* **38**[**6**], 961.

Zirin, H.: 1987, *Solar Phys.* **110**, 101.

FIGURE CAPTIONS

Fig. 1 A set of magnetograms made on June 22, 1985 in a region near the solar disk center. The data have 4096 integrations with the 12-bit memory mode.

Fig. 2a The auto-correlation curve of a magnetogram observed on June 22, 1985 at 1806UT.

Fig. 2b The auto-correlation curve of a magnetogram observed on the same day as in 2(a). All the pixels which represent the magnetic fields strength are converted to the absolute value.

Fig. 2c The auto-correlation curve of a Dopplergram observed on May 11, 1986 at National Solar Observatory/Kitt Peak.

Fig. 3 The size distribution of magnetic flux tubes in a quiet region on June 22, 1985.

Fig. 4a The cross-correlation curve for the June 22, 1985 data. The straight line was obtained by the linear regression.

Fig. 4b The cross-correlation curve of magnetograms obtained on July 28, 1985. The region is an enhanced magnetic network region with a dominating negative polarity.

Fig. 5a The cross-correlation curve of the June 22, 1985 data. Two fits are included: the upper one, gives least square fit with D=150 km^2/sec; lower one, gives an upper limit that D=200 km^2/sec.

Fig. 5b The cross-correlation curve of the October 15, 1985 data, the least square fit gives D=150 km^2/sec.

Fig. 6 The histogram of the magnetic flux density distribution in the quiet sun.

Fig. 7 The variation of the mean magnetic strength in a 2×10^{20} cm^2 window as a function of time.

Fig. 8 The total positive and negative magnetic fluxes inside the window defined in Figure 7.

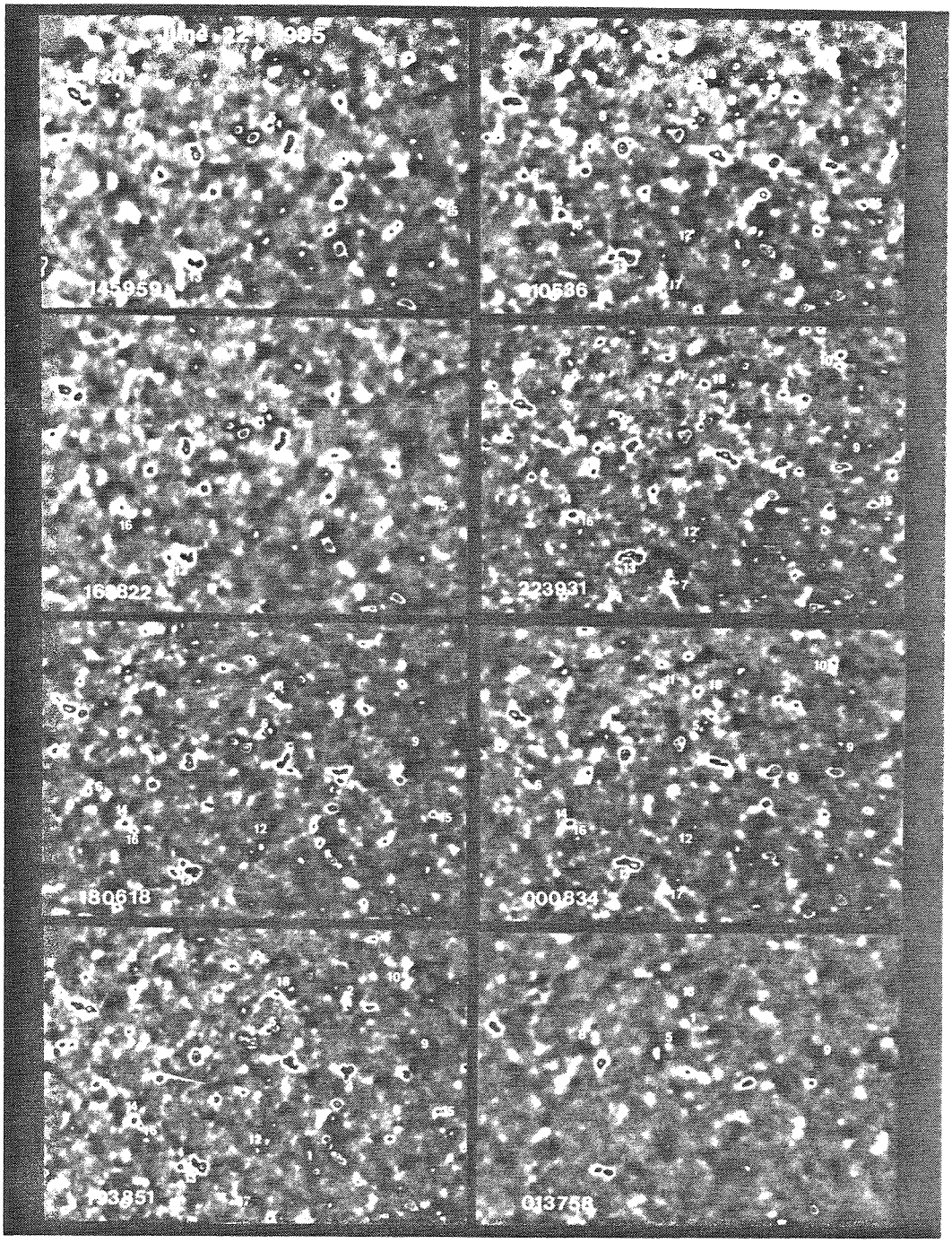

FIGURE 1

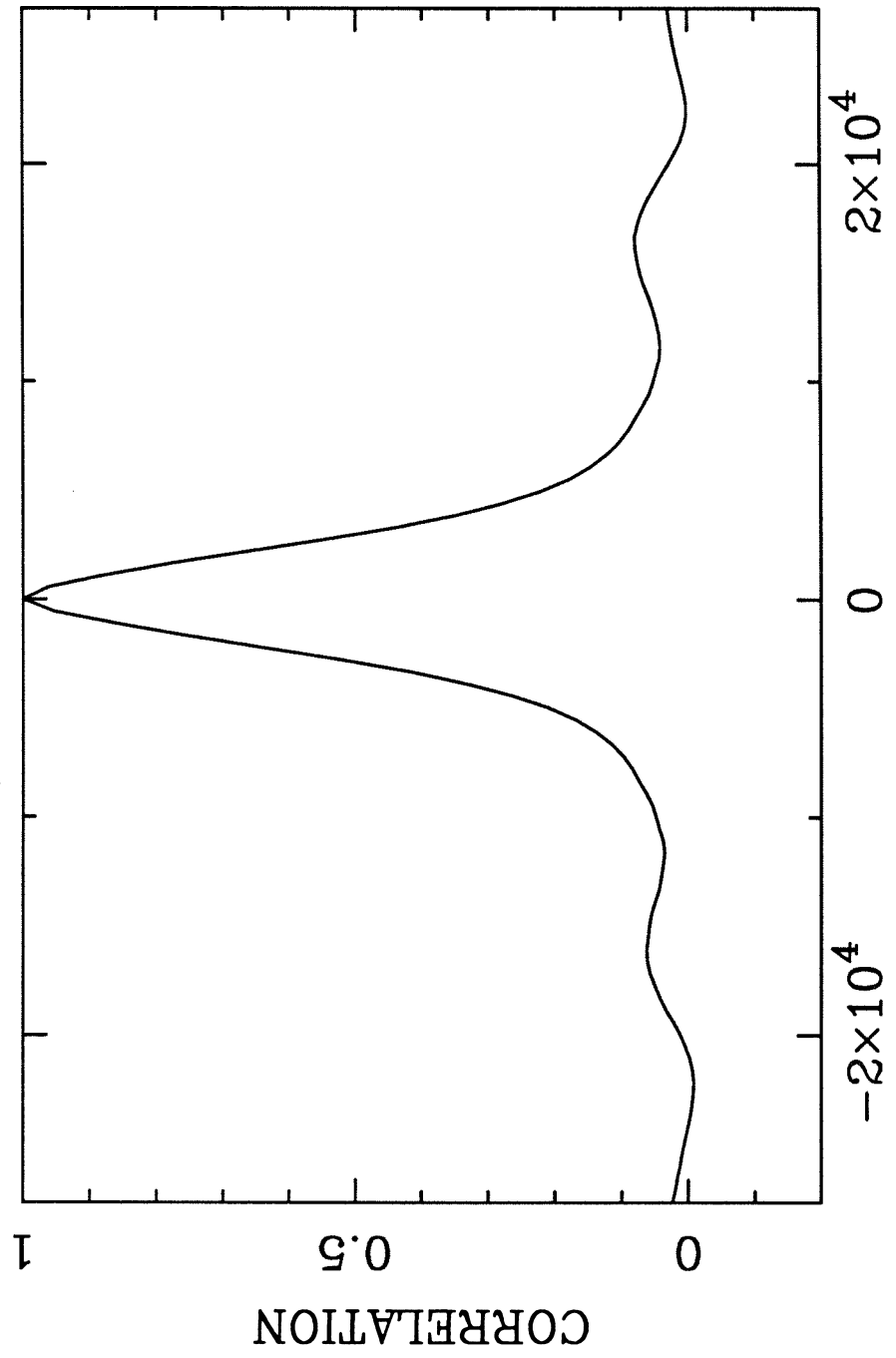

FIGURE 2a

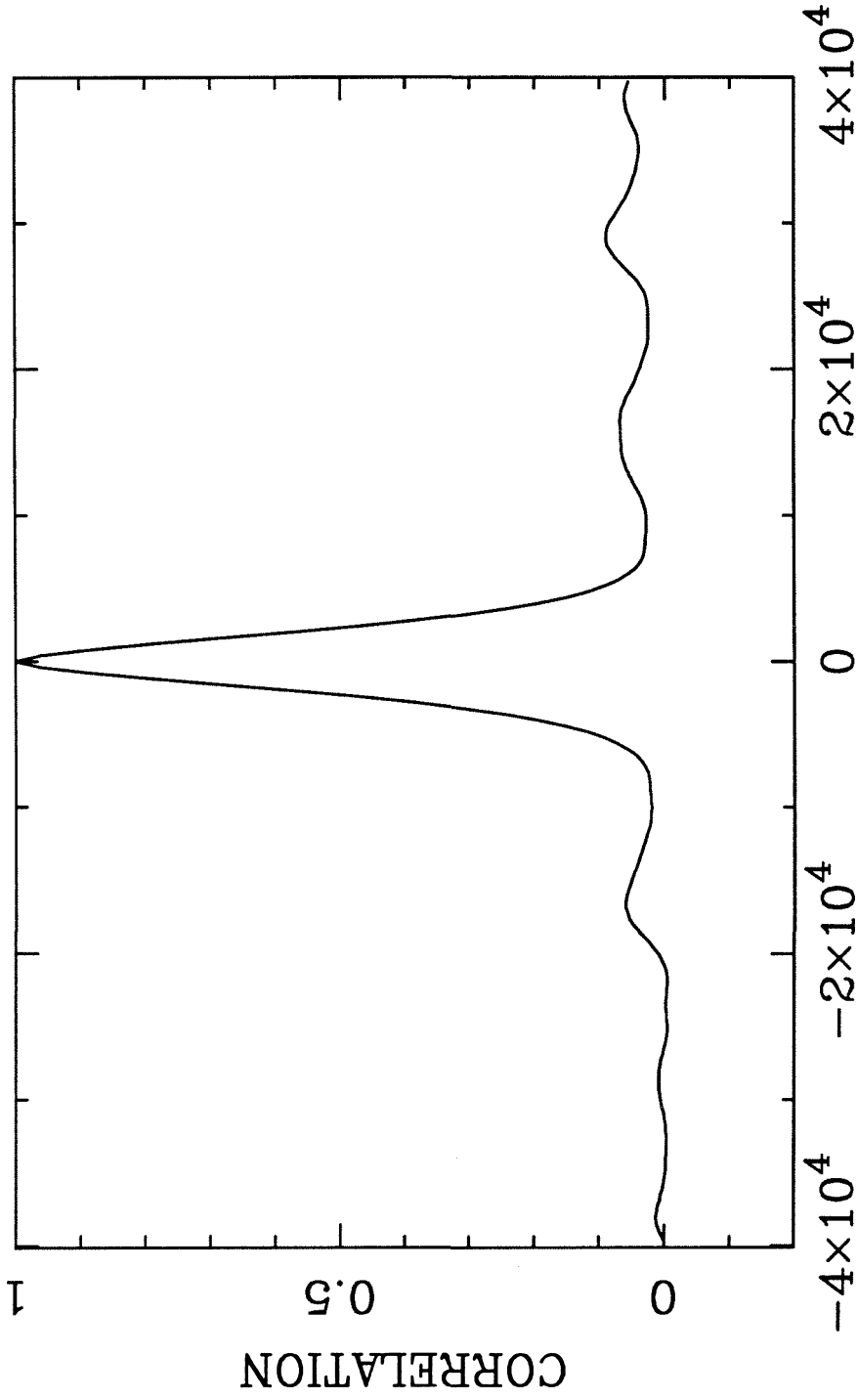
CORRELATION
1
0.5
0
-4×10^4
-2×10^4
0
2×10^4
4×10^4
SHIFT(km)

FIGURE 2b

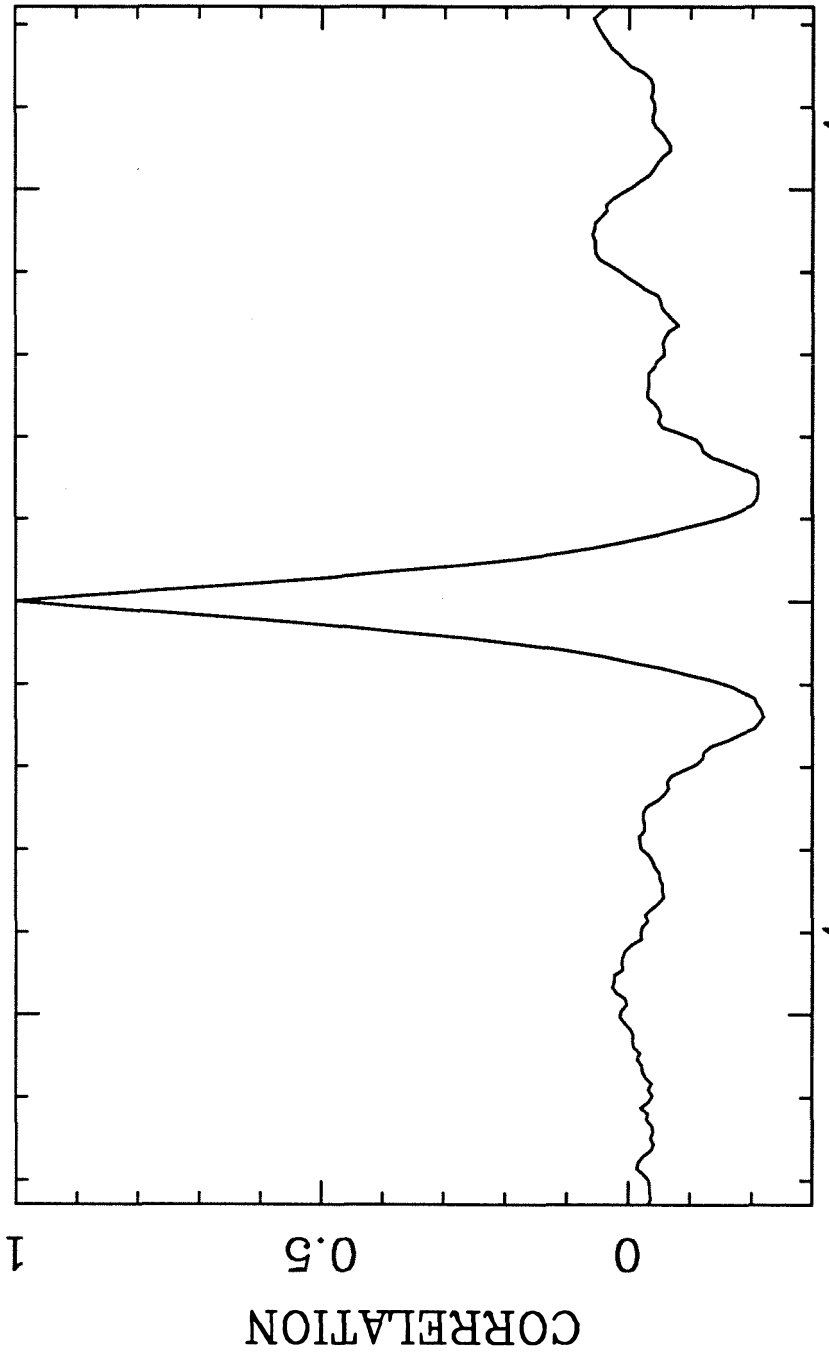

FIGURE 2c

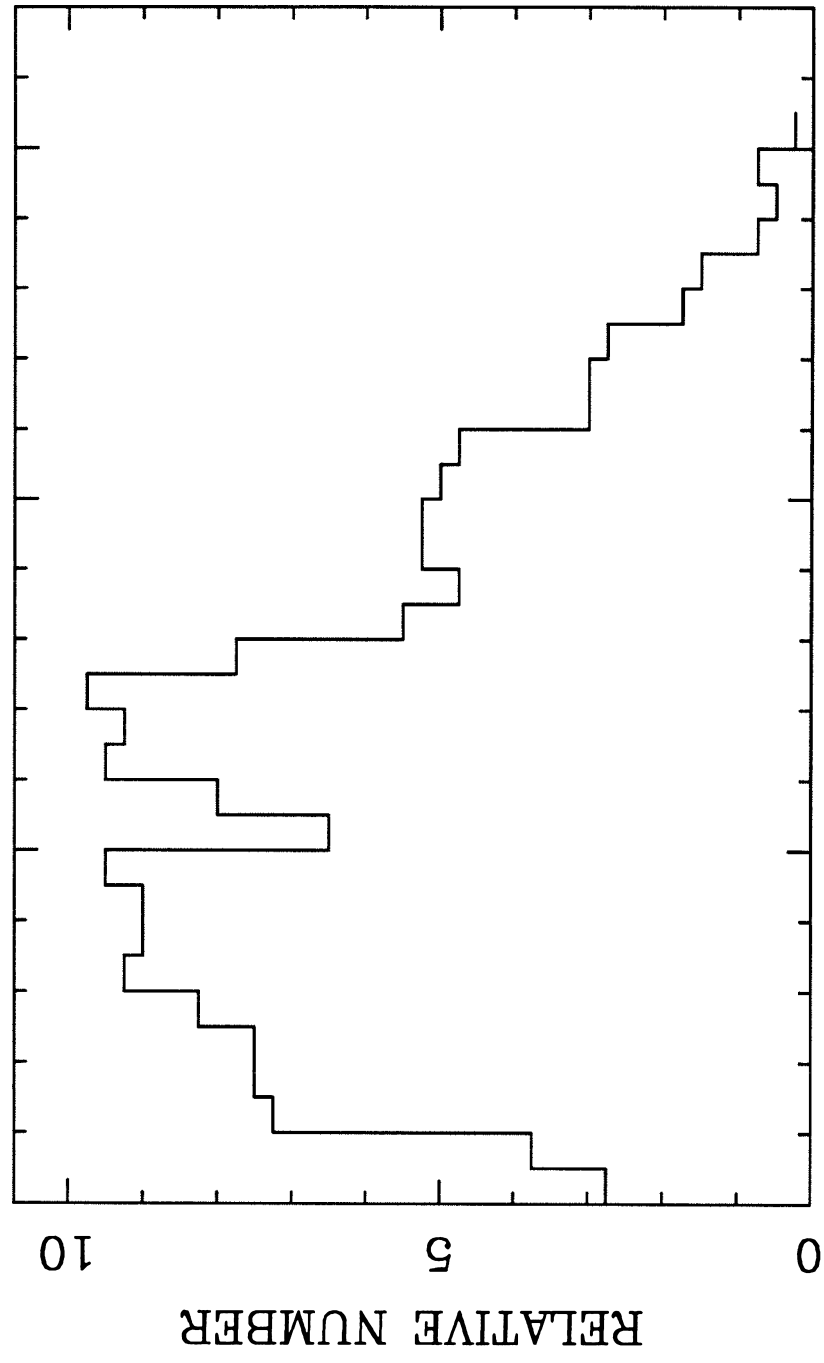

FIGURE 3

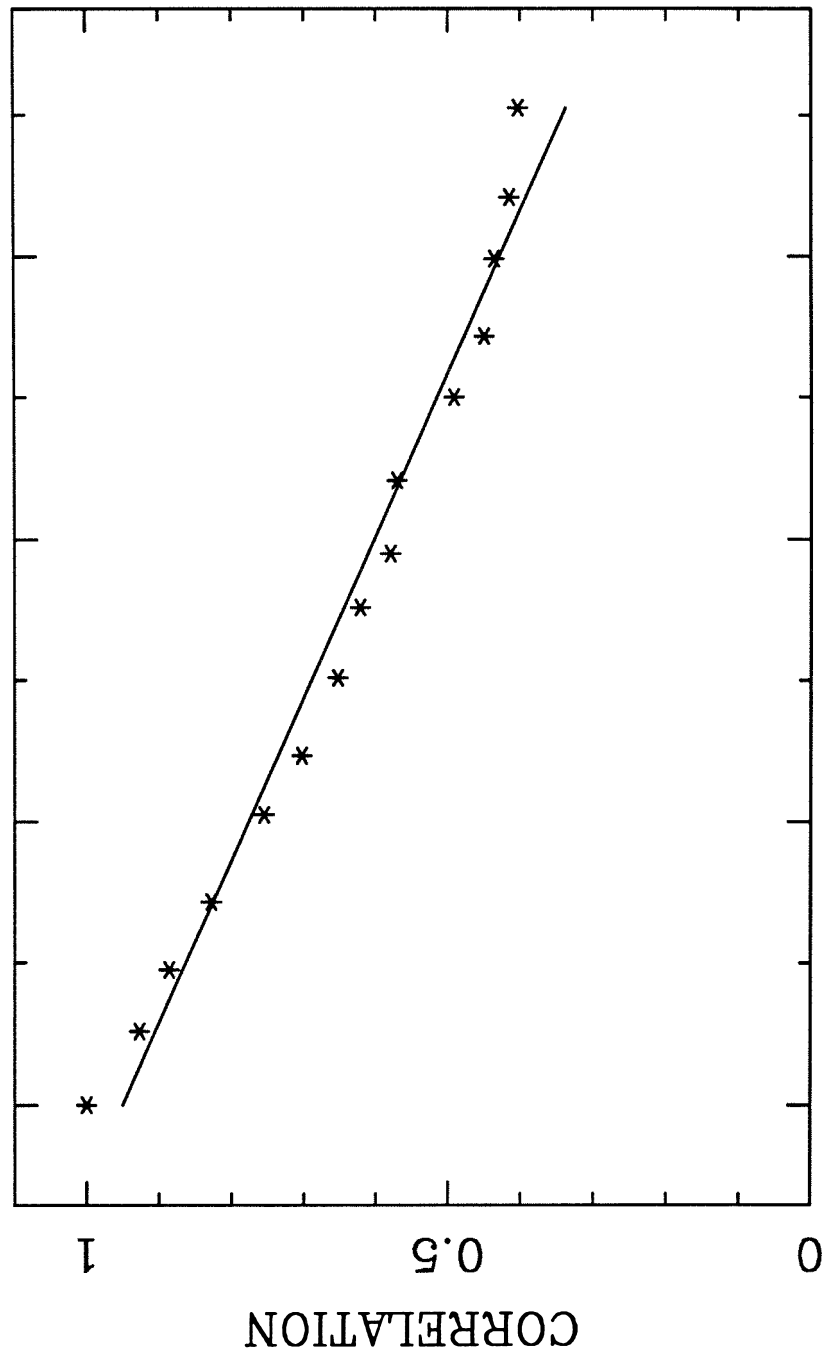

FIGURE 4a

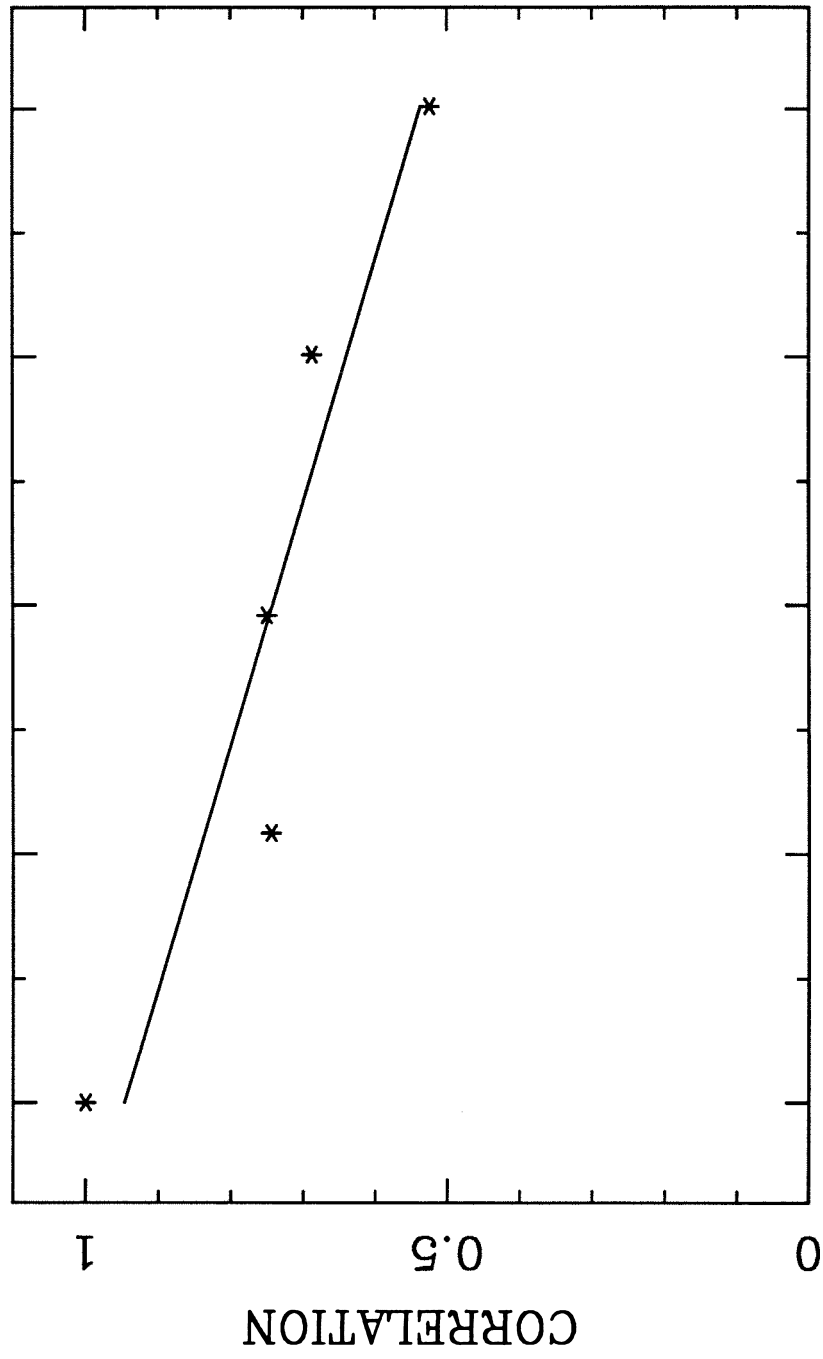

FIGURE 4b

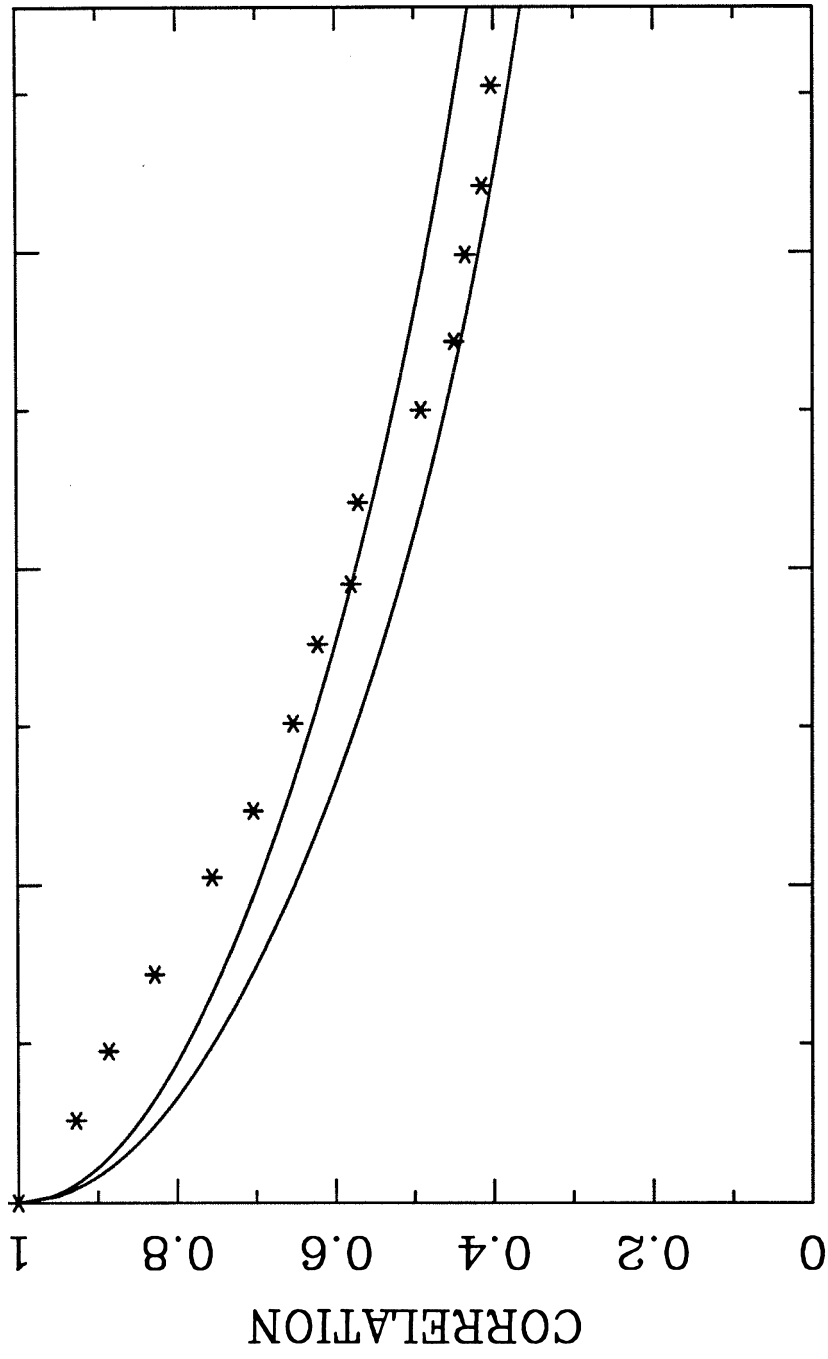

FIGURE 5a

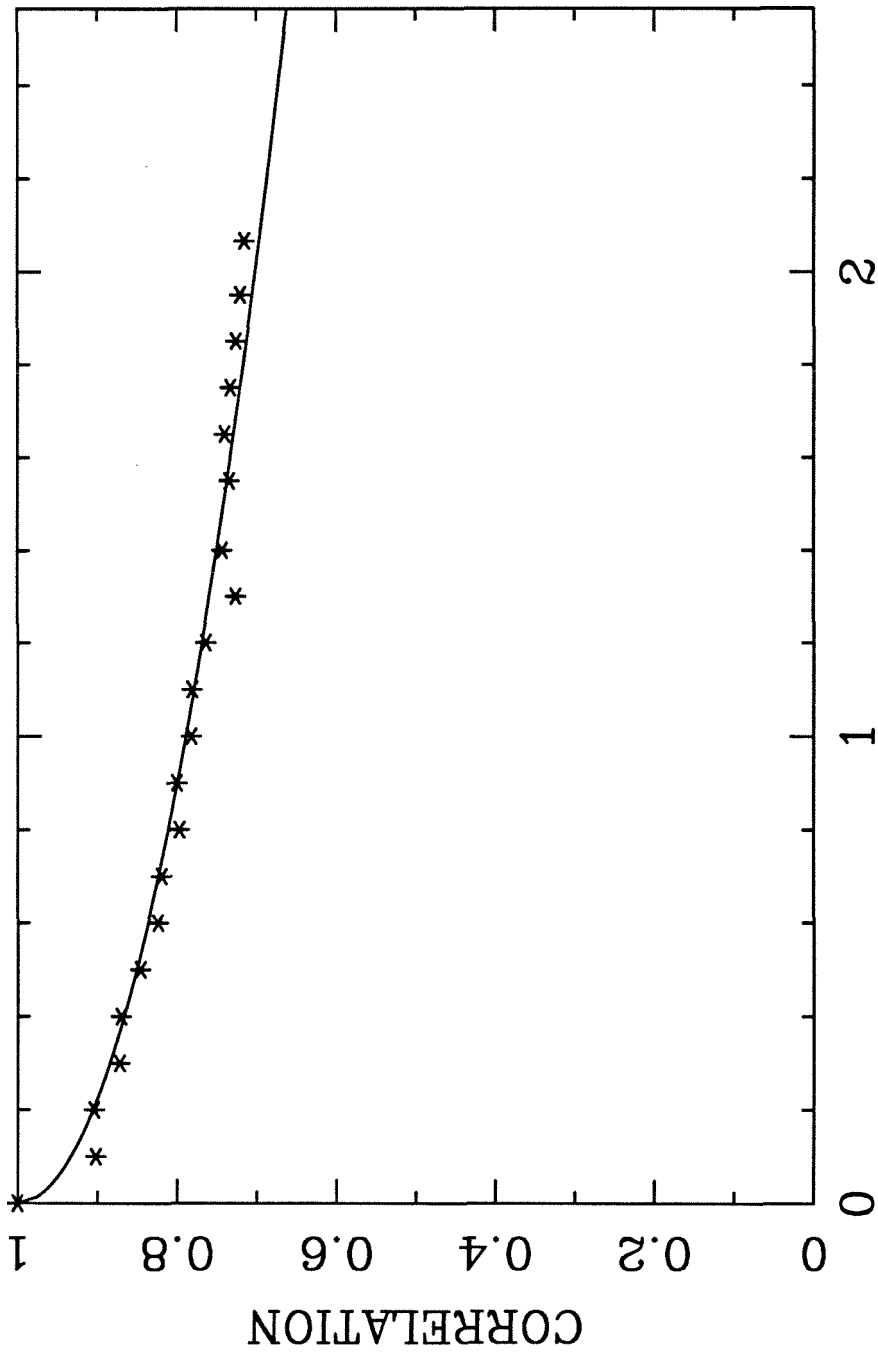

FIGURE 5b

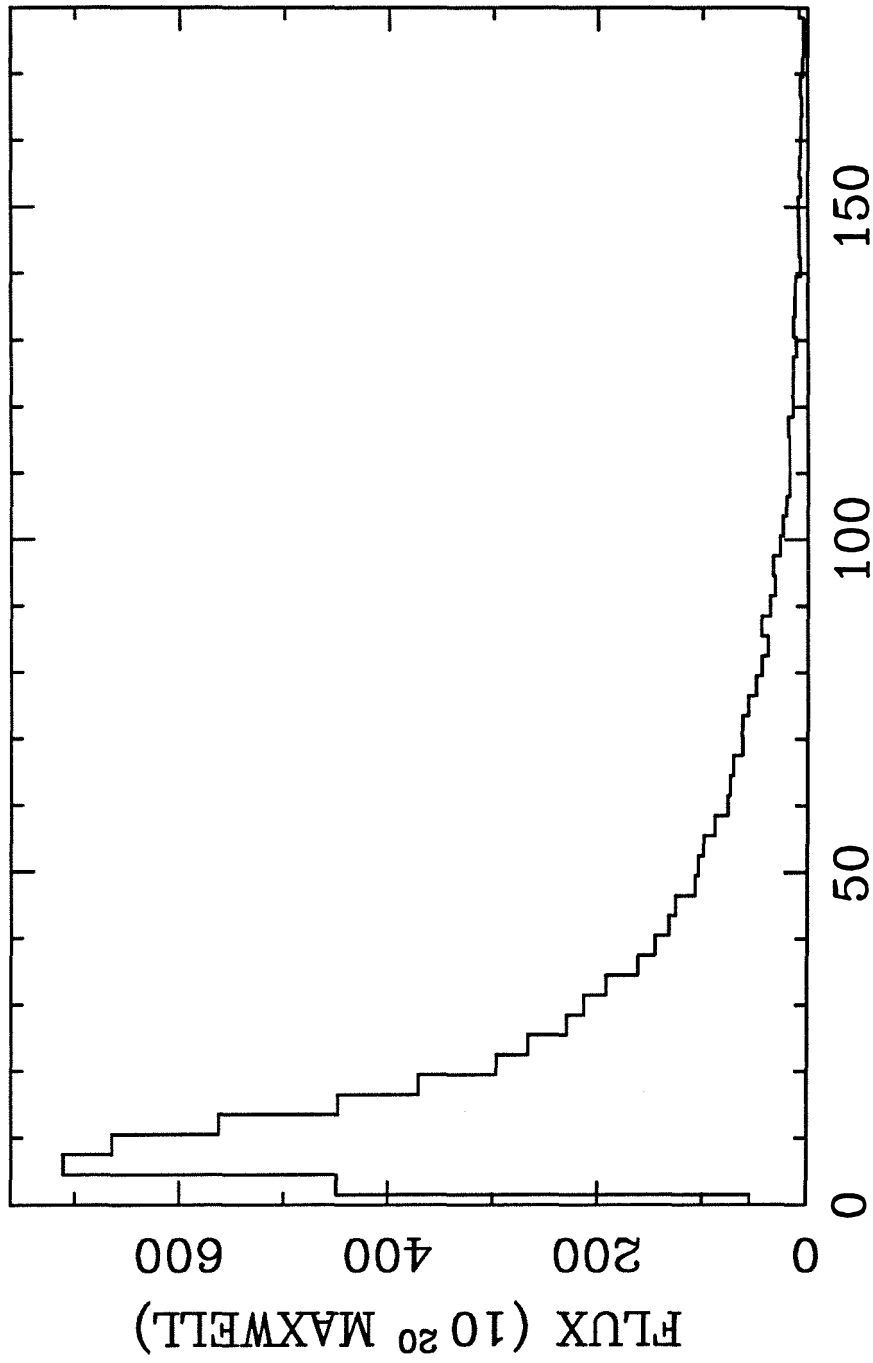

FIGURE 6

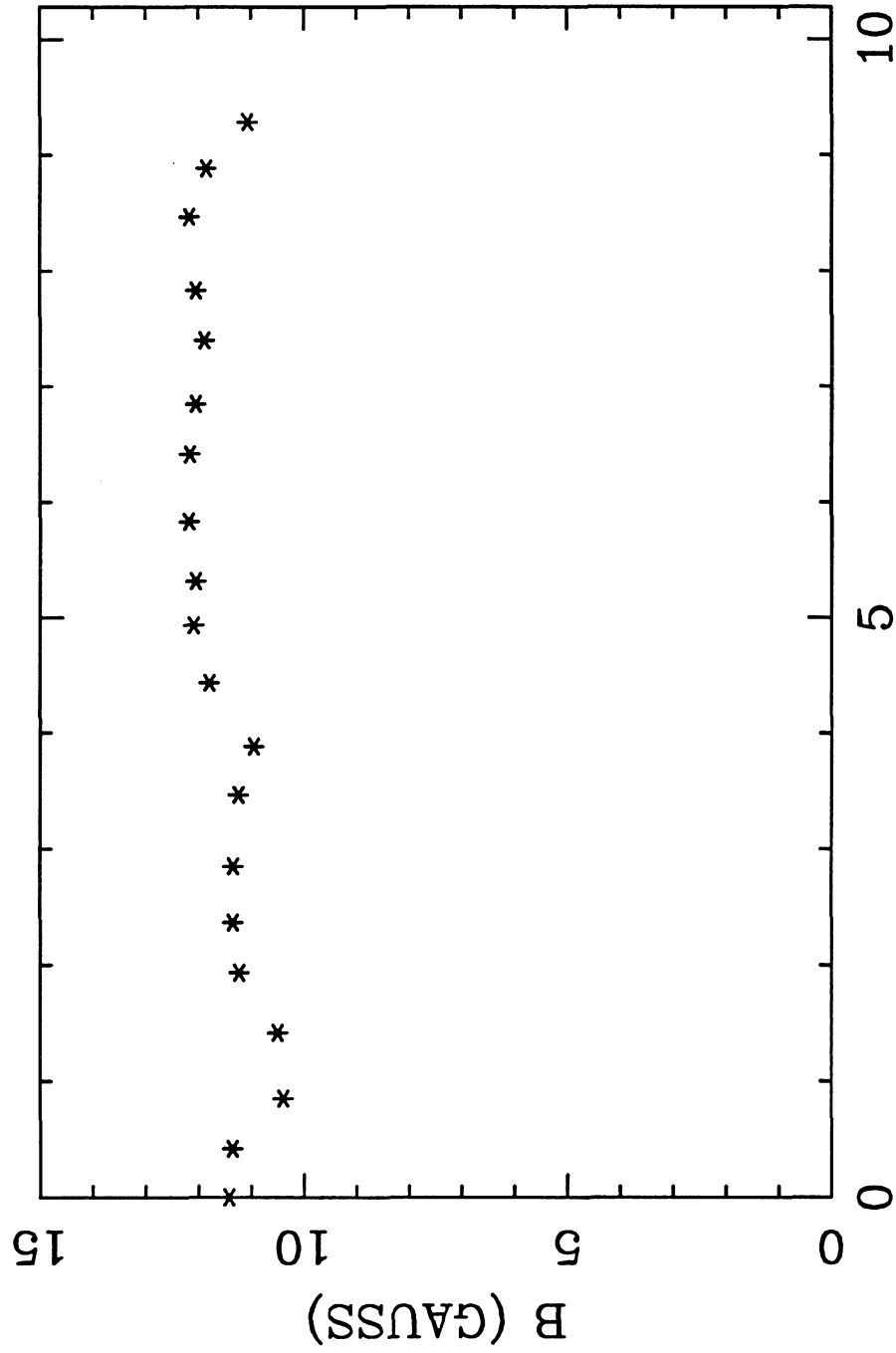

FIGURE 7

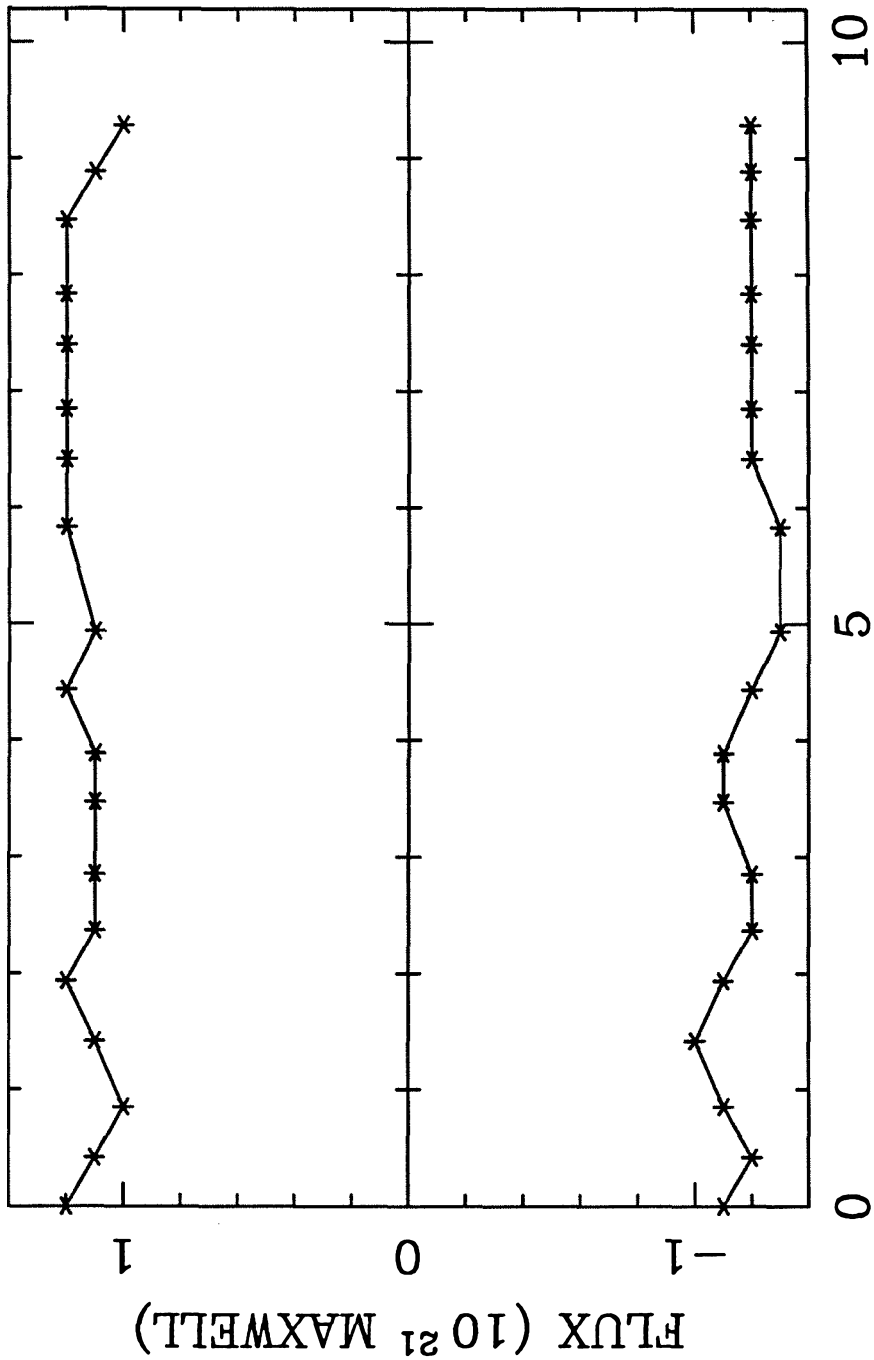

FIGURE 8

Chapter 3

Study of Supergranules

To be submitted to **Solar Physics**

ABSTRACT

Results of a detailed study on supergranule lifetime and velocity fields are presented. There is a linear relationship between the downdraft velocity and the magnetic flux density below B=50 Gauss. Some downdraft velocities can be observed after excluding areas with magnetic flux density $\geq$ 25 Gauss. After excluding these areas, the upper limit of the supergranule vertical speed is 0.1 km/s for both downdraft and updraft, the r.m.s. speed is 0.03 km/s. By observing the evolution of individual supergranules, we find that the average lifetime of supergranules might be $\geq$50 hours. We describe different ways of formation and decay of supergranular cells. New cells usually form in an area containing no pre-existing supergranule velocity fields. Cells may disappear in two ways: fragmentation and fading away.

1. Introduction

The supergranulation velocity field was discovered by Hart (1954,1956). It has been interpreted as a convective flow pattern (Leighton *et al.*, 1962; Simon and Leighton, 1964; Leighton, 1964, 1969). The lifetime of supergranule cells is an important parameter with which the velocity and temperature structure within a cell may be estimated by convective theory (Antia *et al.*, 1981). The lifetime is important for another reason. Leighton (1964, 1969) attributed the observed breakup and dispersion of active region magnetic fields over the solar surface to a random walk process. If supergranules, which are responsible for moving the magnetic field, have a mean lifetime of about 20 hours, then the breakup of magnetic active regions can be explained by Leighton's mechanism.

Studies of supergranule lifetime by Simon and Leighton (1964), based on the cross-correlation calculation of the chromospheric network in the CaK line, gave a lifetime of about 20 hours. Rogers (1970) and Janssens' (1970) correlation analysis of 62 hours continuous $H\alpha$ chromospheric network data from the Arctic showed a similar result. The investigations of Smithson (1973), Worden and Simon (1976) and Duvall (1980), however, found the lifetime to be about 40 hours. Livingston and Orrall (1974) noticed certain magnetic structures (magnetic pukas) persisting for 4 to 7 days. They explained the phenomenon as the existence of very stable supergranule convective cells. Kubicêla (1976) gave evidence that some supergranules have a lifetimes of 72 hours or more in the quiet sun.

The amplitude of the horizontal component of supergranule velocity has been well studied. Its peak speed has been found to be around 0.3 to 0.5 km/sec (Leighton *et al.*, 1962; Worden and Simon, 1976). However, despite numerous studies, the amplitude of the vertical velocity in supergranules is still unclear. Different authors give very different r.m.s. speeds ranging from on the order of 0.01 km/s (Musman and Rust, 1970; Giovanelli, 1980) to about 0.4 km/s (Skumanich *et al.*, 1975; Deubner, 1971). The correlation between downdraft velocity and magnetic flux density is well known (e.g. Frazier, 1970). Studies on the vertical velocity were reviewed and studied further by Giovanelli (1980). His result shows that supergranule vertical velocities have r.m.s. values $\leq$ 0.01 km/sec. Downward velocity $\geq$ 0.1 km/sec in regions of strong magnetic fields are attributed to the motion inside the elements themselves that is unrelated to supergranule motion.

In this paper, we discuss the mean lifetime of supergranule cells by direct study of the evolution of the horizontal component of supergranular velocity fields. We also study the vertical velocity of supergranules and its relationship with the magnetic flux density.

2. Observation

Some of the velocity observations presented here were made with the 512 channel magnetograph (Livingston *et al.*, 1976a) at the Solar Vacuum Telescope of the National Solar Observatory, Kitt Peak (Livingston *et al.*, 1976b). The velocity is

inferred from the difference in intensities in the two wings of the FeI line (8688Å). Magnetograms were obtained at Kitt Peak and Big Bear Solar Observatory simultaneously with the velocity observations. The pixel size in the Kitt Peak data is 1" and the scan area is 256" × 256" for the October 1985 run, and 400" × 256" for the May 1986 run. To remove the five minute oscillation most efficiently, the time interval between images is set at 150 seconds.

Additional velocity and magnetic field observations were made with the Videomagnetograph(VMG) system at Big Bear Solar Observatory during the summers of 1985 and 1986. While the Kitt Peak magnetograph scans the area line by line with the spectrum slit, at Big Bear, a narrow bandpass Zeiss filter obtains two dimensional images instantly. The VMG system at Big Bear was described in detail by Mosher (1976a) and Zirin (1985). CaI 6103Å was used and the VMG and Doppler modes were alternated for the magnetic field and velocity field observations. The pixel size is about 0.5", the area covered is 250" × 250". The duration of each observing day was 7-12 hours and the same regions were usually followed for three consecutive days.

Vertical velocity of supergranules may be observed only in the solar disk center, while the horizontal velocity can be clearly observed when the heliocentric angle is larger than 20°. Thus targets were set at the disk center to study the vertical component of the supergranule velocity, and away from the disk center 27° to 55° to study the horizontal component.

3. Data Reduction

The calibration of magnetic and velocity fields was done by using the solar rotation as the calibrator (Shi *et al.* 1986). The solar rotation and non-uniformity in the images were removed by subtracting a two-dimensional smoothed background image. The five-minute oscillation was removed by averaging 60 images spanning 1 hour.

Since the various velocity phenomena (granulation, horizontal and vertical velocity of supergranulation and five-minute oscillation) have different spatial scales, the information on each of these velocity fields can be separated within the spatial frequency domain of the Fourier transform. Thus, to isolate the horizontal component of supergranular velocity fields, the data are Fourier transformed, and all frequencies representing size scales significantly different from the supergranular scale (32,000km) are removed, then the transform is inverted to produce a filtered picture.

Dopplergram movies were made from the time sequence observation using the Megavision Image Processor system at Caltech. The movies greatly facilitate the detailed study of the evolution of supergranule velocity fields.

4. Vertical Velocity

To study the vertical component of supergranule velocity fields, we averaged

60 center disk Dopplergrams taken at a rate of 1 image/minute. The observations were made on Aug. 21, 1985 and Aug. 17, 1987 at BBSO. Only data with the best seeing were used. On Aug. 17, 1987, several magnetograms were taken immediately before and following the 1 hour Dopplergram observation.

Figure 1a shows a 60-frame averaged Dopplergram on Aug. 21, 1985. A histogram of the distribution of the vertical speed for the Dopplergram shown in Figure 1a is plotted in Figure 2. It shows that 98.4% of the image area is covered by pixels with velocity $\leq$ 0.1 km/s. The r.m.s. velocity is 0.04 km/s. There is a small tail on either side of the histogram representing higher velocity regions. The blue shift tail does not exceed 0.15 km/sec and red shift tail does not exceed 0.20 km/sec. Many dark patches in Figure 1a represent isolated areas of downward motion probably corresponding to network magnetic elements, but there were no corresponding magnetograms available to confirm this. However, simultaneous Hα off band data were obtained. Figure 1b shows a negative print of a Hα -0.5Å filtergram averaged over 60 images spanning the same one-hour time interval as Figure 1a. The correlation coefficient between two images is 0.55. Roughly, the downdraft velocity fields coincide with the Hα network.

To study the relationship between the downdraft and magnetic flux density, we analyzed a set of Dopplergrams and their corresponding magnetograms made on Aug. 17, 1987. Figure 3a shows a Dopplergram averaged over an hour and Figure 3b shows the corresponding magnetogram. In Figure 4a, we plot the average vertical

velocity vs. the magnetic flux density for the data shown in Figure 3a and 3b. For $B = 0$ to $B = 50$ gauss, a linear least square fit gives,

$$V(\text{km/sec}) = -1.2 \times 10^{-3}\text{B(Gauss)} \quad (1)$$

In this regime, our result is consistent with the work by Chou *et al.* (1988). For B greater than 60 Gauss, there are less than 100 sampling points for each bin, so reliable data are restricted to B$\leq$60 gauss. One uncertain factor in our observation is the actual physical size of the downdraft velocity elements. If the elements are concentrated in a small area, the high downdraft velocity would be missed by our observation.

The r.m.s. velocity of the Dopplergram shown in Figure 3a is 0.038 km/s. Following the method used by Giovanelli (1980), we block the areas in the Dopplergram in which the magnetic flux density exceeds 25 Gauss. The blocked Dopplergram is shown in Figure 3c. There are still many dark patches left in this image. The r.m.s. velocity of the blocked Dopplergram is 0.029 km/s. This is 3 times the upper limit given by Giovanelli.

Stenflo *et al.* (1984) used the Fourier Transform Spectrometer at Kitt Peak National Observatory to study the diagnostics of magnetic flux tubes. They concluded that if the Stokes V profiles had not been fully spectrally resolved, the V asymmetry would have caused an apparent redshift of the V profile leading to fictitious downdrafts in the fluxtube. Our study is unable to test their results. However, the V asymmetry could not explain the downdrafts outside the magnetic elements.

As a comparison with the vertical velocity component, in Figure 4b we plot the supergranule horizontal velocity vs. the flux density for a region at a heliocentric angle of 40°. Since strong magnetic elements are located at the boundary of supergranule, therefore, the horizontal velocity is smallest where the average magnetic flux density is greatest - average velocity decreases monotonically with flux density.

5. Lifetime of Supergranules

5.1 Auto-Correlation of Dopplergrams

From the auto-correlation curves of Dopplergrams, Leighton *et al.* (1962) and Simon and Leighton (1964) derived an average supergranule scale of 32,000 km. Averaging 8-day results, we get an average supergranule scale of 31200±2300 km. Our analysis confirms Leighton *et al.*'s early results and ensures that our data contain the real supergranule signal.

5.2 Correlation Lifetime

The lifetime of supergranulation cells have been measured using the cross-correlation function (Simon and Leighton, 1964; Worden and Simon, 1976). The mean lifetime is defined as the time needed for the cross-correlation coefficient to fall to $1/e$. Figure 5 shows cross-correlation coefficients vs. time and the linear fit for the data observed on Oct. 13, 1985. The correlation lifetime derived from the linear fit is 18 hours. Figure 6 shows the result for three days of Doppler data,

Oct. 13 - 15, 1985. An exponential least squares fit gives a lifetime of 23 hours. Our data show less uncertainty in the least squares fit than previous observations. For example, Worden and Simon (1976) gave a correlation lifetime of 36^{+72}_{-24} hours, whereas the standard deviation in our fit is only about 1 to 2 hours.

The correlation lifetime of magnetograms in the quiet region is about 10 hours (Wang, 1988), shorter than that derived from the correlation curve of Dopplergram. This confirms what Smithson (1973) suggested that the shorter supergranular lifetime derived from network studies was misleading due to the manner in which it was derived. Since the network is a "thin" system defining only the cell boundary, not the entire cell, small changes in the shape of a cell can cause a large decrease in cross-correlation coefficients. This may produce a spurious short lifetime compared to the correlation lifetime derived directly from the velocity data.

5.3 The Lifetime of Supergranulation Derived from the Evolution of Supergranules

Does the correlation lifetime represent the real mean lifetime of supergranules? This is a problem we will discuss in this section.

The study of solar granules by Zirin and Wang (1987) shows that the average lifetime of granules is 16 minutes when measured visually, which is twice the value found by many authors using the correlation technique (e.g. Leighton, 1957).

One striking feature shown in supergranule movies is that the basic patterns

of the supergranule velocity hardly change during one observing day. In an area of 256" × 256", there are approximately 30 supergranular cells. If the mean lifetime equals the correlation time, which is about 24 hours as found by us and other authors, then in a 7-10 hour observation, 1/3, or 10, of cells should change substantially, and lose their identity at the end of the observation. We found, however, in 8 days' supergranule movies we examined, it is very hard to find disappearance of more than 3 cells during each observing day.

We express the mean lifetime of supergranules, τ, as:

$$N(t) = N_0 \ \exp(-t/\tau) \tag{2}$$

where N_0 is the number of supergranule cells at the beginning of an observation, $N(t)$ is the number of cells remaining after time t. Figure 7 plots the number of supergranule cells that survived vs. time during the period of October 13 to 15, 1985. The least squares fit to equation (2) gives an average lifetime of 53 hours. We used the same data set to plot Figure 6 and 7.

We analyzed 5 other sets of Doppler data, one observing day for each. Applying equation (2) to these data, we obtained the lifetimes of 50 to 80 hours. We conclude that the average lifetime of of supergranules is $\geq$ 50 hours. The big difference between the correlation lifetime and the lifetime τ defined in equation (2) may be due to the fact that it is possible for a cell to change its shape without losing its identity.

6. Evolution of Supergranules

The use of supergranule movies is helpful in studying the short term evolution of supergranules. Unfortunately, since the average lifetime of supergranules is longer than 50 hours, a movie covering 7-10 hours of observation does not show long term evolution. However, a few cases of growth and decay of supergranule cells are observed. Some examples are shown in Figure 8. It appears that most of the new cells form in a blank area, containing no pre-existing velocity fields. Figure 8a shows an example of growing cell. The new cell is labeled as G1. The cell grows to a size of the normal supergranule in less than 2 two hours. A cell may disappear by either fading away or by fragmentation. Figure 8b and 8c shows two examples of decaying cells. In Figure 8b, there are several features, labeled D1 through D3, faded away. They left a blank space at the end of the observation. Figure 8c shows a case of cell fragmentation. A white velocity component(F1) fragmented first, then all the fragments faded away. A black element(F2), which belongs to another cell, starts to fragment at 2200UT. We did not find a single case in which a cell formed and disappeared during a 7-10 hour period. Our observation suggests that the the supergranules have relatively short growing and decaying phase of about 3 to 6 hours for each, and a long mature phase. However, the sampling from our 8 days of data is small, the results are not statistically significant.

To study the evolution of the magnetic network during the process of appearing and disappearing supergranular velocity fields, superposed magnetograms and

Dopplergrams are used. Unfortunately, the changes in magnetic fields during the appearance and disappearance of a supergranule velocity cell are difficult to detect. In a few cases the network expands when the velocity cell is growing. An example is shown in Figure 9a: while a new cell(G2) is forming, it pushes a magnetic element of positive polarity to the right. However, the network does not appear to contract when the cell is decaying. The network magnetic elements of an old cell may become the elements of new cells. We give an example of a decaying velocity cell with its network fields, labeled D4, in Figure 9b.

7. Conclusion and Discussion

From 8 days of observations made at Big Bear and Kitt Peak, we conclude that the mean lifetime of supergranules is much longer than 20 hours. Our results show that this lifetime is ≥ 50 hours. The shape change of supergranules may reduce the cross-correlation coefficient leading to a spurious short correlation lifetime. This conclusion is coincident with the study of evolution of the magnetic network by S. Martin (Personal Communication). A longer lifetime of supergranules means a slower diffusion of solar magnetic fields (Worden and Simon, 1976). This implies that other mechanisms such as meridional flow (Mosher, 1976b) and Marsh's mechanism (Marsh, 1978) of interaction between ERs and network elements must share a larger burden of transporting the magnetic flux.

It was generally believed that the network originates from the sweeping of

intranetwork (IN) fields to the boundaries of the supergranule. Although the IN fields move under the control of the supergranule velocity fields (Martin, 1988; Wang and Zirin, 1988), since they have mixed polarities, the net flux accumulated from such a large amount of mixed polarity flux could be small. In our observations of mixed polarity quiet regions, we have not observed that the supergranule velocity fields accumulate sufficient IN flux of the same polarity to form the network.

An upper limit for supergranule vertical velocity is found to be 0.1 km/sec. The linear relationship between the downdraft velocity and the magnetic flux density is good when the flux density is less than 60 gauss. There are a few questions that remain unanswered. 1). Is the downdraft real or it is due to the V asymmetry, as discussed by Stenflo *et al.*(1984)? 2). What is the filling factor of the down draft elements? 3). Do the downdraft areas outside magnetic elements represent real supergranule downdraft velocity?

Reference

Antia, H.M., Chitre, S.M. and Pandey, S.K. 1981, *Solar Physics* **70**, 67.

Chou, D., LaBonte, B.J., Braun, D.C. and Duvall, T.L. 1988, in preparation.

Deubner, F.L. 1971, *Solar Physics* **17**, 6.

Duvall, T.L. 1980, *Solar Physics* **66**, 213.

Frazier, E.N. 1970, *Solar Physics* **14**, 89.

Giovanelli, G.R. 1980, *Solar Physics* **67**, 211.

Hart, A.B. 1954, *Monthly Notice of Roy. Astro. Soc.* **114**, 2.

Hart, A.B. 1956, *Monthly Notice of Roy. Astro. Soc.* **116**, 38.

Janssens, T.J. 1970, *Solar Physics* **11**, 222.

Kubicêla, A. 1976, *Solar Physics* **47**, 551.

Leighton, R.B. 1957, *Publ. Astron. Soc. Pacific* **69**, 497.

Leighton, R.B. 1964, *Ap. J.* **140**, 1547.

Leighton, R.B. 1969, *Ap. J.* **156**, 1.

Leighton, R.B., Noyes, R.W. and Simon, G.W. 1962, *Ap. J.* **135**, 474.

Livingston, W.C. and Orrall, F.Q. 1974, *Solar Physics* **39**, 301.

Livingston, W.C., Harvey, J., Pierce, A.K., Schrage, D., Gillespie, B., Simmons, J. and Slaughter, C. 1976a, *Applied Optics* **15**, 33.

Livingston, W.C., Harvey, J., Slaughter, C. and Trumbo, D. 1976b, *Applied Optics* **15**, 40.

Marsh, K. A. 1978, *Solar Physics* **59**, 105.

Martin, S.F. 1988, accepted by Solar Physics.

Mosher, J. 1976a, *BBSO Preprint* **No. 159**.

Mosher, J. 1976b, *Ph.D. Thesis, California Institute of Technology.*

Musman, S. and Rust, D.M. 1970, *Solar Physics* **13**, 261.

Rogers, E.H. 1970, *Solar Physics* **13**, 57.

Shi, Z., Wang, J. and Patterson, A. 1986, *BBSO Preprint* **No. 257**.

Skumanich, A., Smythe, C., and Frazier, E.N. 1975, *Ap. J.* **200**, 747.

Simon, G.W. and Leighton, R.B. 1964, *Ap. J.* **140**, 1120.

Smithson, R.C. 1973, *Solar Physics* **29**, 365.

Stenflo, J.O., Harvey, J.W., Brault, J.W. and Solanki S. 1974, *Astron. Astrophys.* **131**, 333.

Wang, H. and Zirin, H. 1987, accepted by Solar Physics.

Wang, H. 1987, accepted by Solar Physics.

Worden, S.P. and Simon, G.W. 1976, *Solar Physics* **46**, 73.

Zirin, H. and Wang, H. 1987, Presentation in AAS Solar Physics Division Meeting, May 13-15, 1987, Honolulu.

Figure Captions

Fig. 1a A Dopplergram made on Aug. 21, 1985, after one-hour averaging and two-dimensional smoothing.

Fig. 1b An averaged Hα-0.5Å negative image corresponding to Figure 1a.

Fig. 2 A histogram to show the distribution of the vertical velocity fields for the Dopplergram shown in Figure 1a.

Fig. 3a A Dopplergram made on Aug. 17, 1987, after one-hour average and 2-D smoothing. It is observed in the disk center.

Fig. 3b A corresponding magnetogram of Figure 3a.

Fig. 3c The Dopplergram after blocking areas with B$\geq$25 Gauss.

Fig. 4a Average vertical velocity vs. magnetic flux density for the data shown in Figure 3a and 3b. The bin size is 2 gauss.

Fig. 4b Average horizontal velocity vs. magnetic flux density. The observation was made on May 11, 1986. The target was 40°off the disk center.

Fig. 5 The cross-correlation curve of the Dopplergrams made on Oct-13-1985.

Fig. 6 The cross-correlation curve combined 3-day observation, from Oct. 13 to Oct. 15, 1985.

Fig. 7 The number of supergranule cells survived as a function of time, for the period from Oct. 13 to Oct. 15, 1985. The least square fit gives a mean supergranule lifetime of 53 hours.

Fig. 8 Several examples of the supergranule evolution. (a) A new cell forms. (b) A cell fades away. (c) A cell disappears by fragmentation. All the pictures in Figure 8 and 9 have the same scale as marked in Figure 8a. White is receding motion, and black, approaching. Solar limb is toward the right of the image. A supergranule cell is represented by a structure which has a white element in the right and a black one in the left.

Fig. 9 Two examples showing the magnetic fields associated the growing and decaying of supergranule cells. (a) A growing cell. (b) A decaying cell.

FIGURE 1a

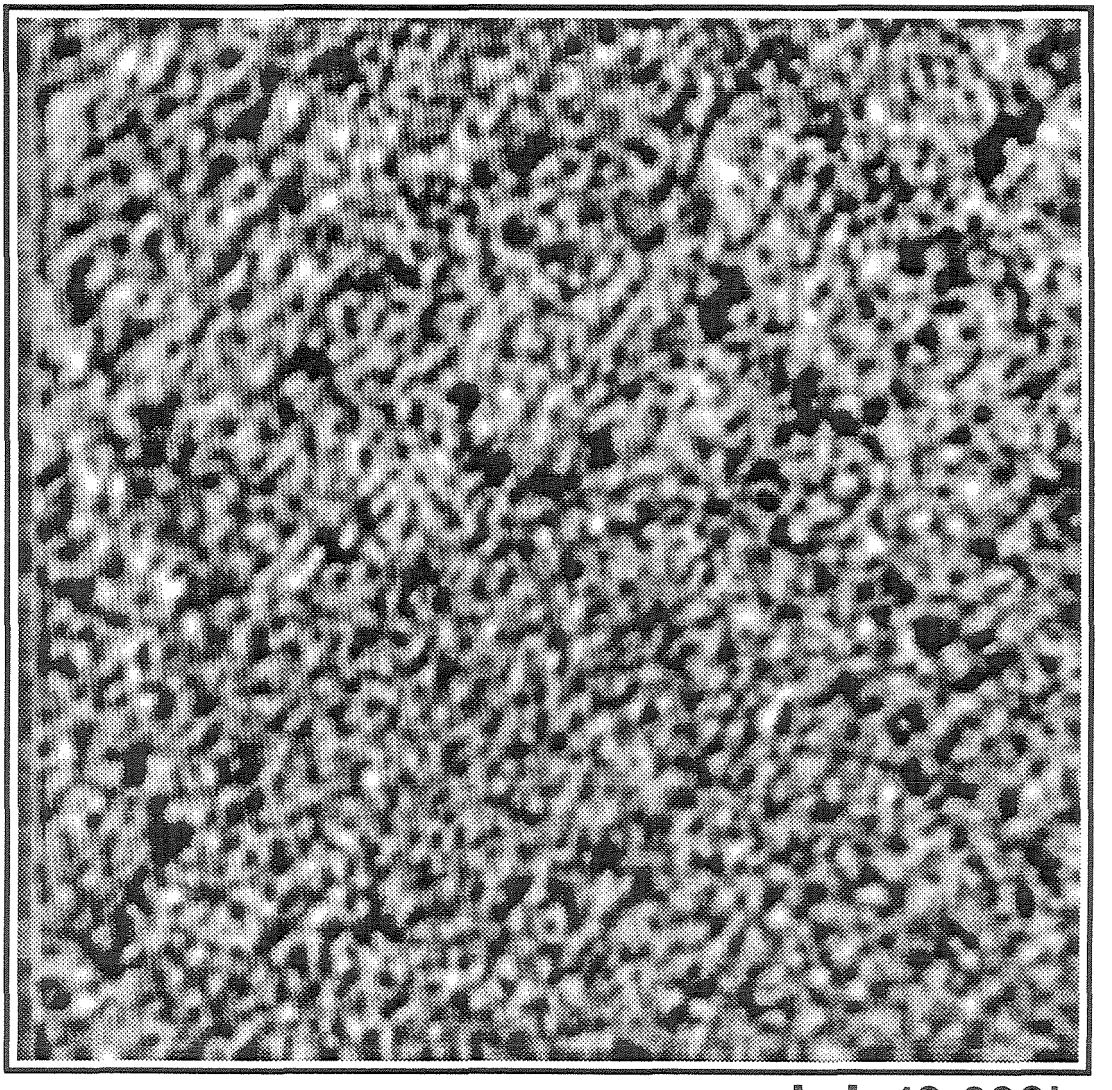

10,000km

FIGURE 1b

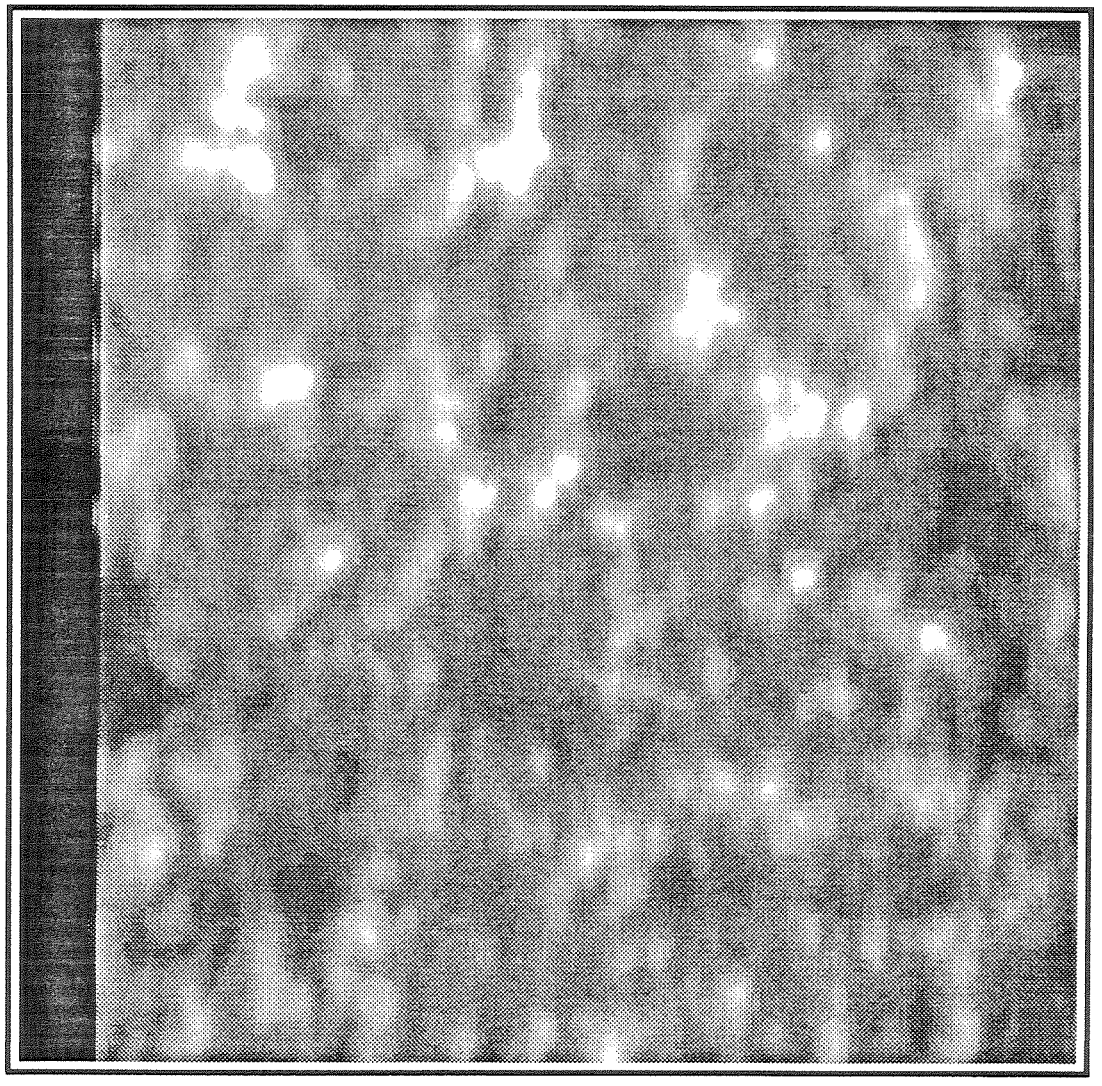

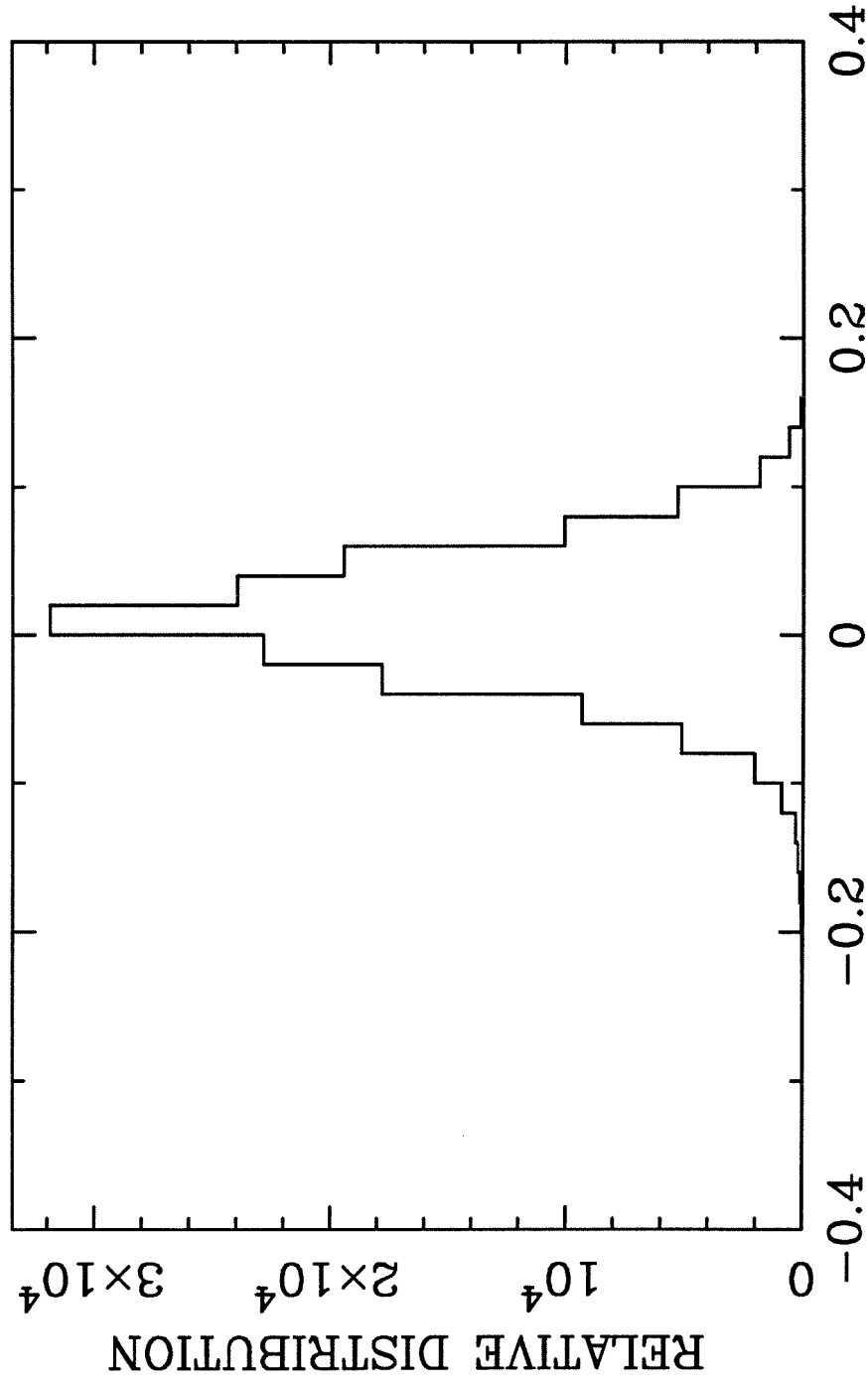
RELATIVE DISTRIBUTION
0
10⁴
2×10⁴
3×10⁴
−0.4
−0.2
0
0.2
0.4
VELOCITY(KM/S)

FIGURE 2

FIGURE 3a

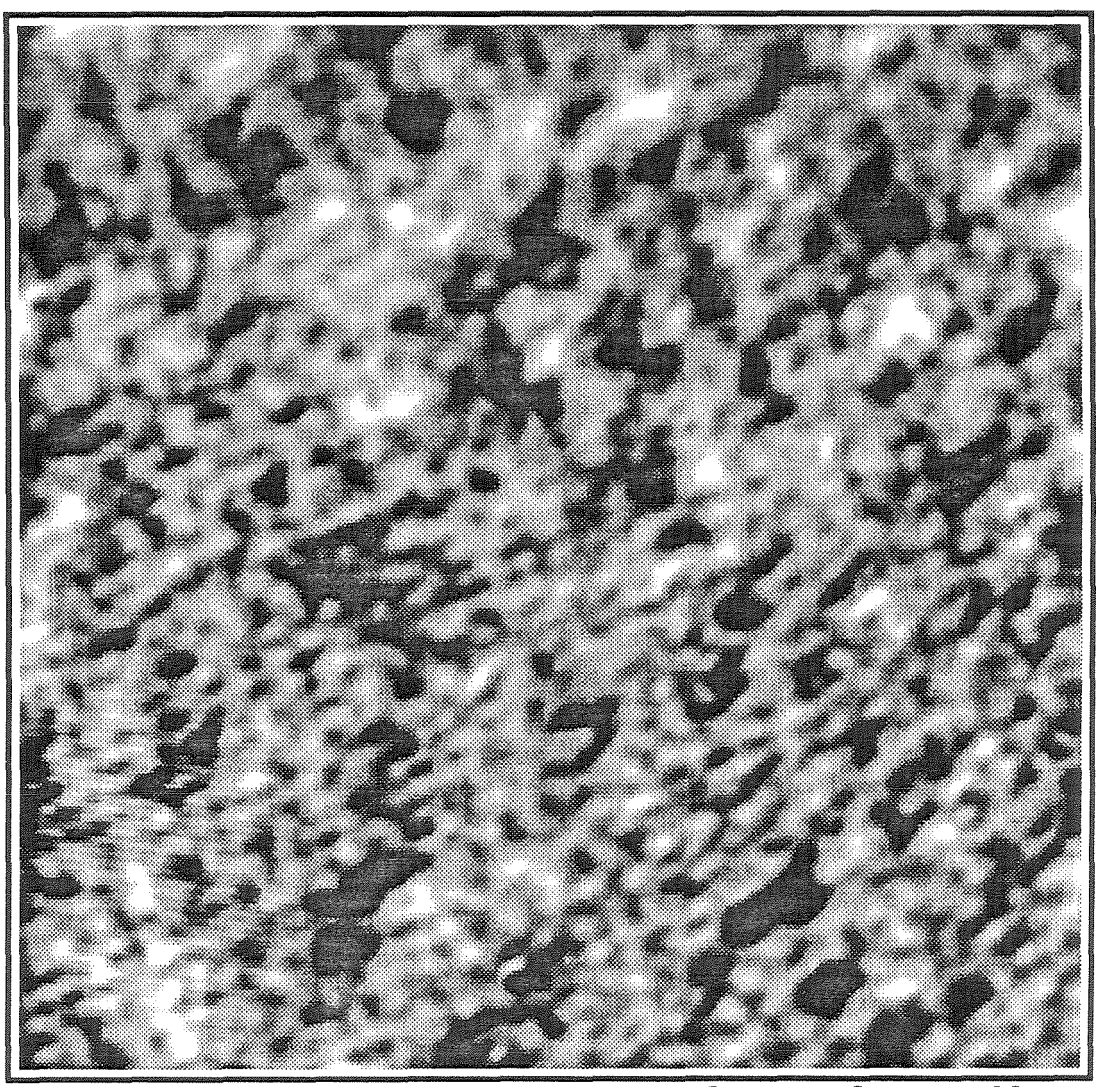

FIGURE 3b

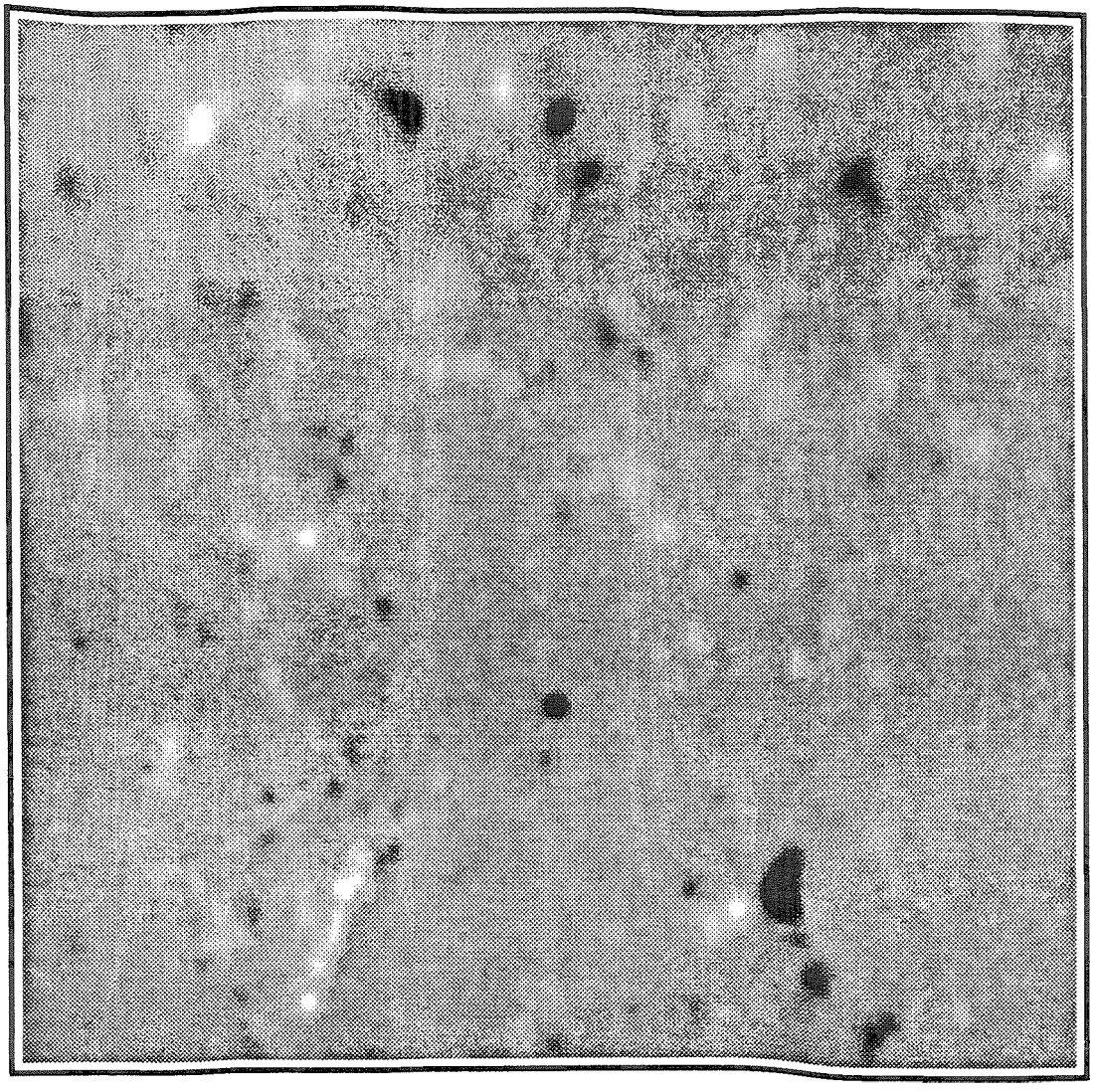

FIGURE 3c

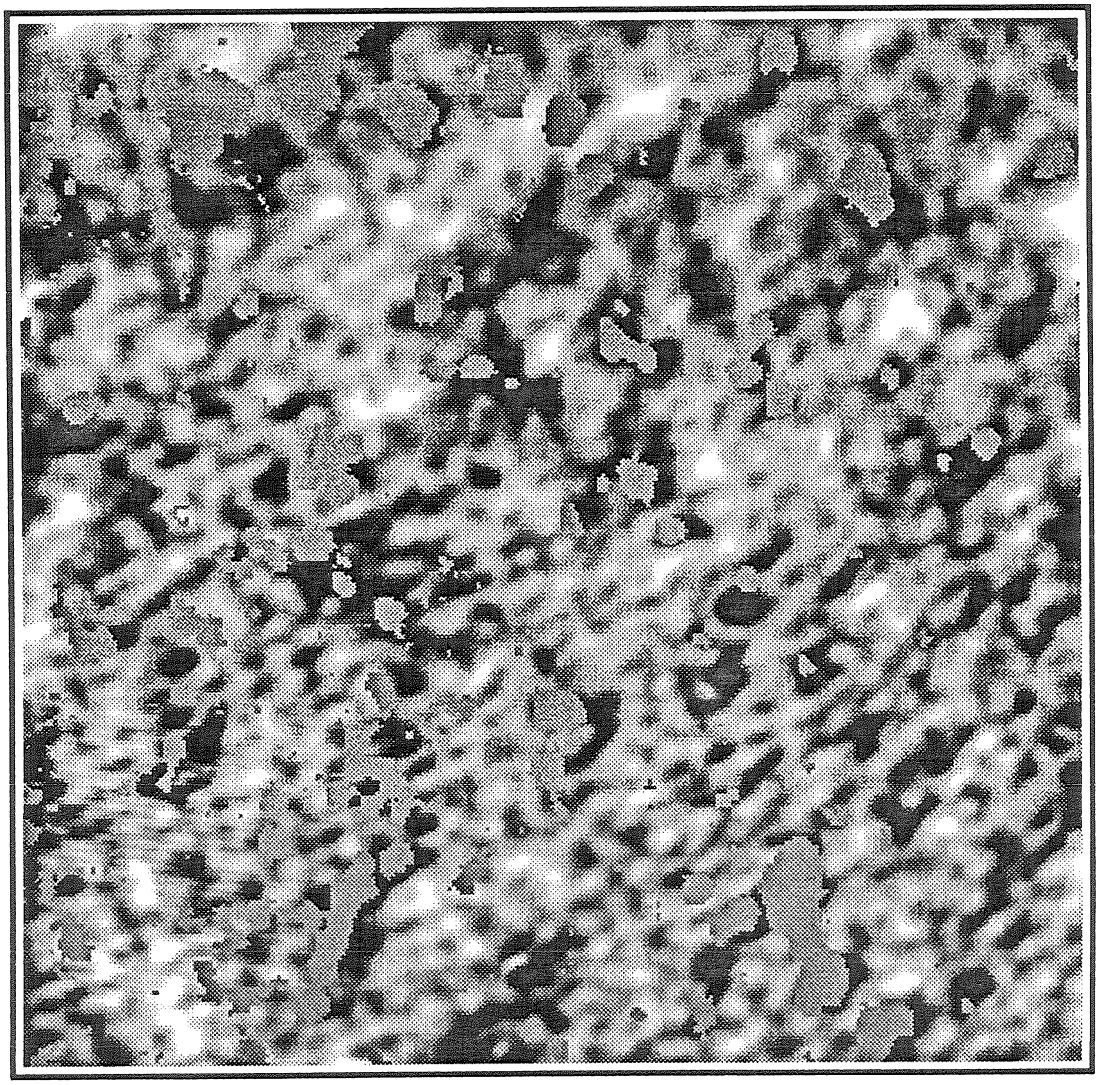

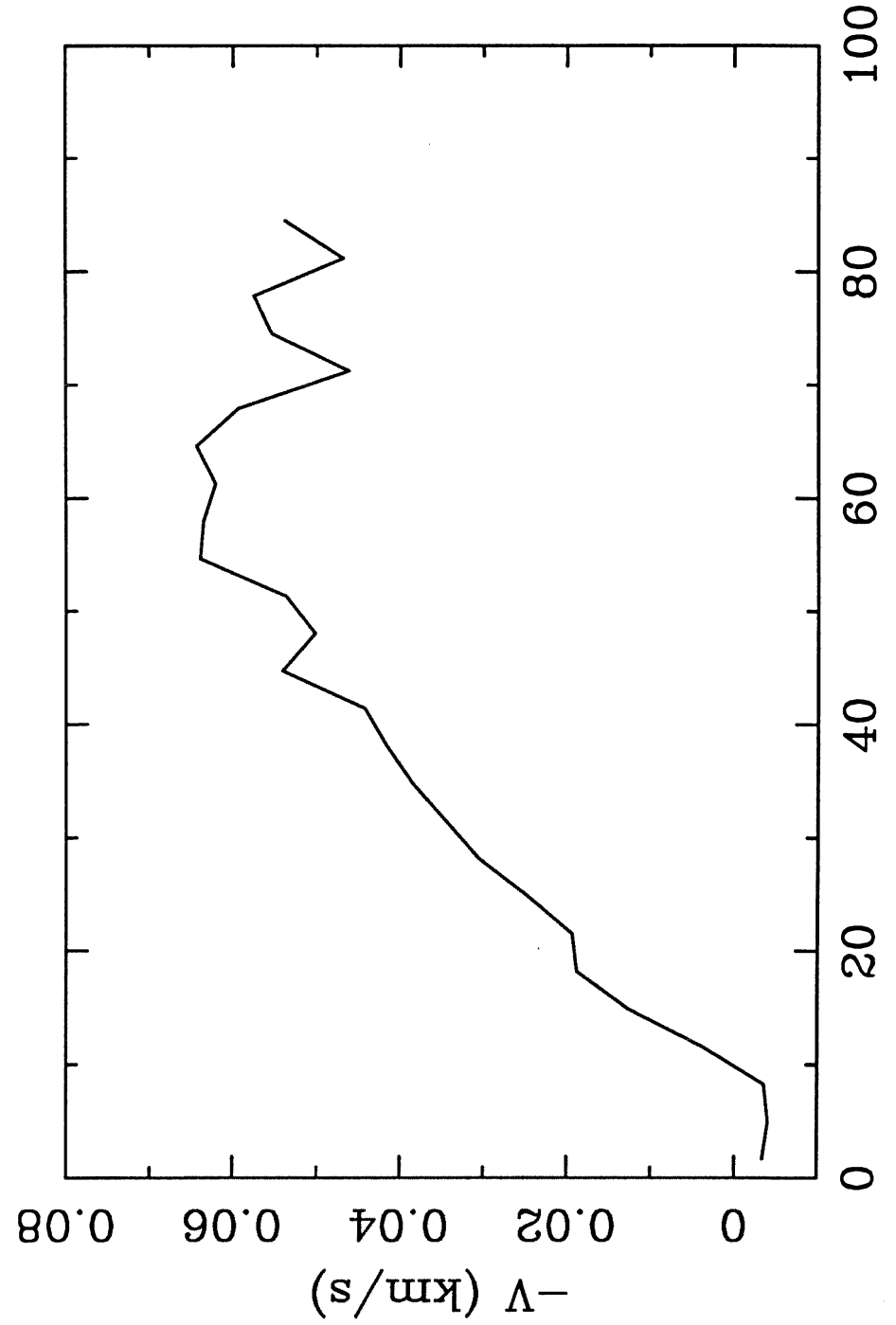

FIGURE 4a

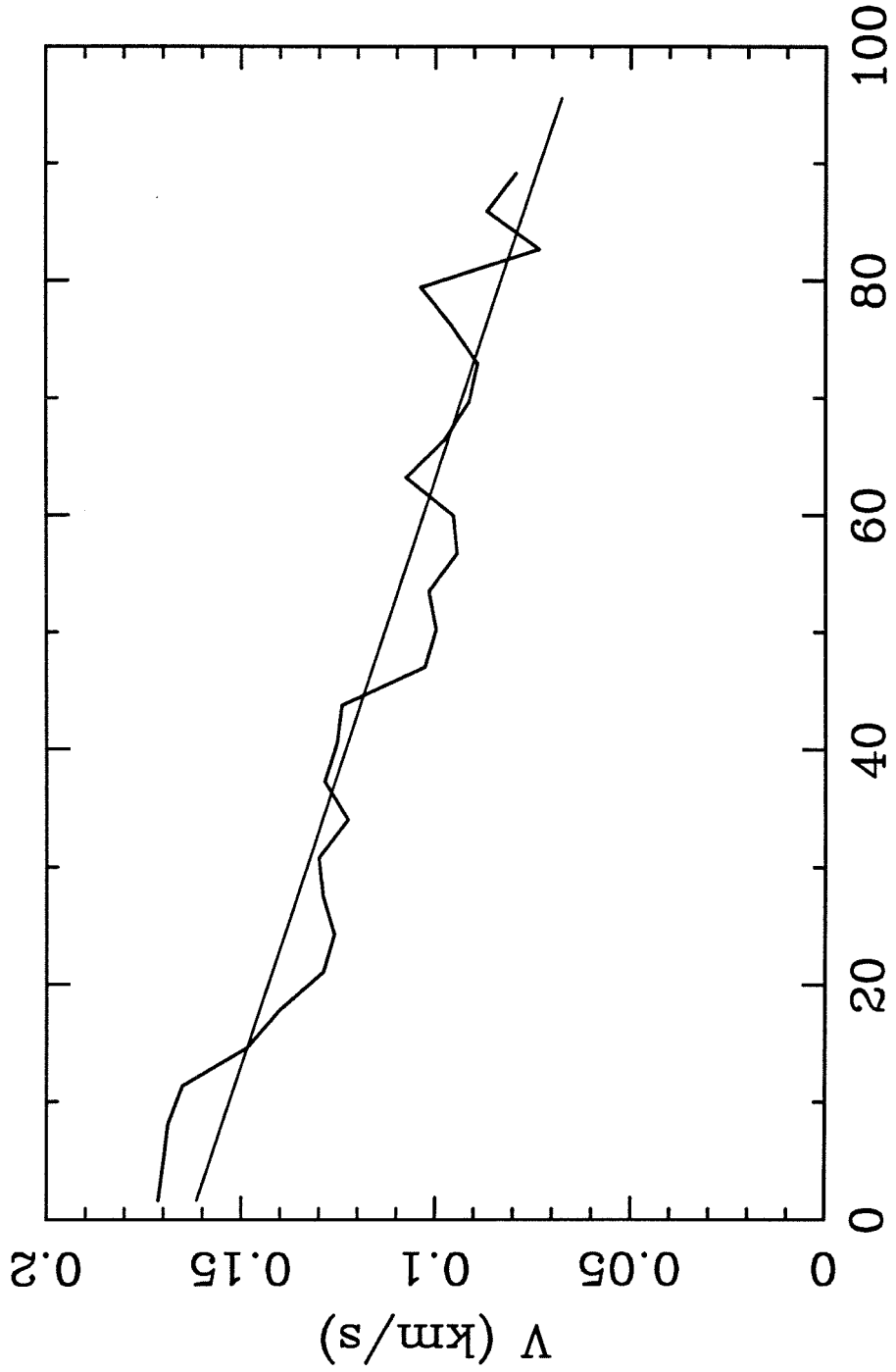

FIGURE 4b

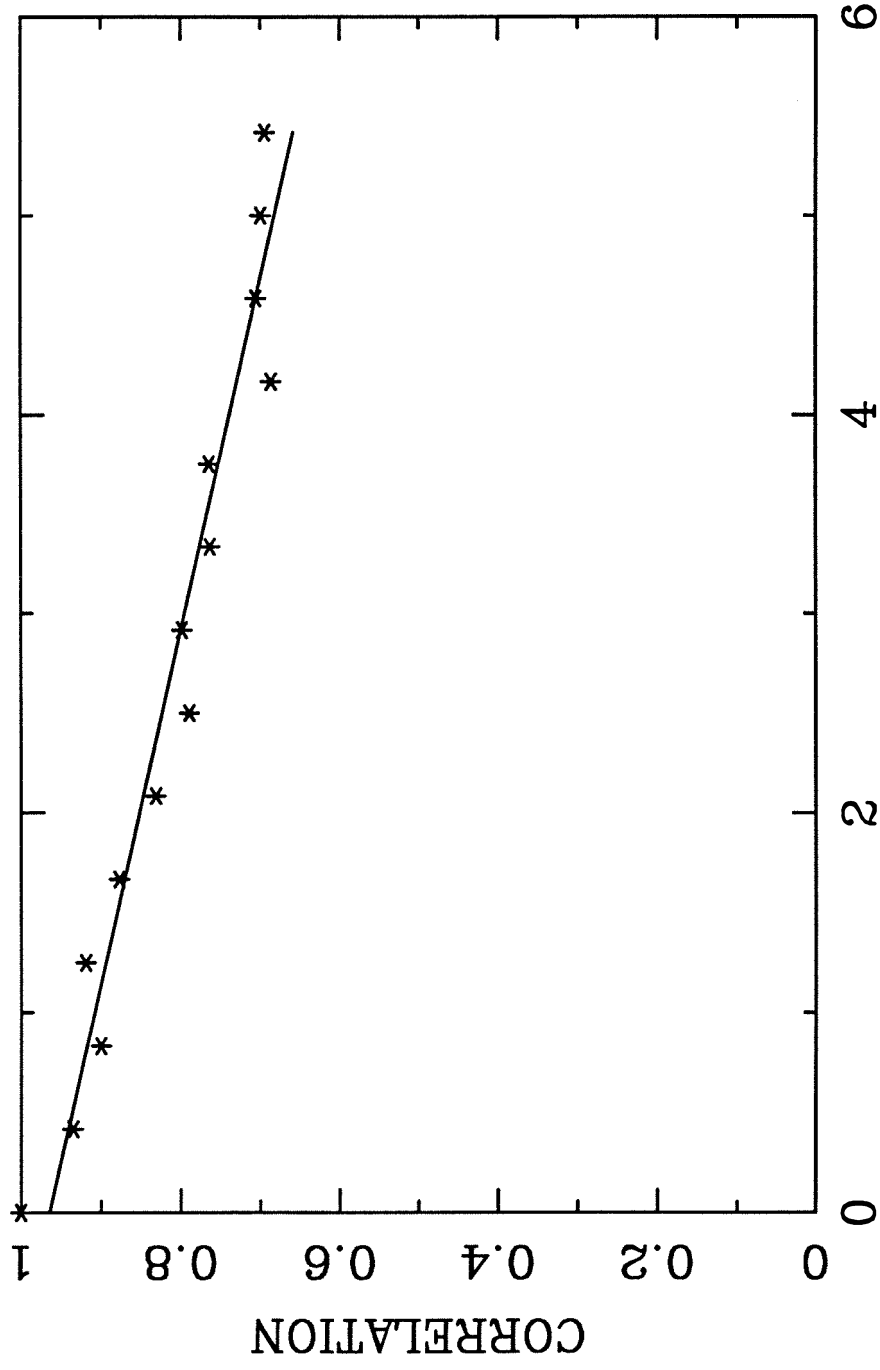

FIGURE 5

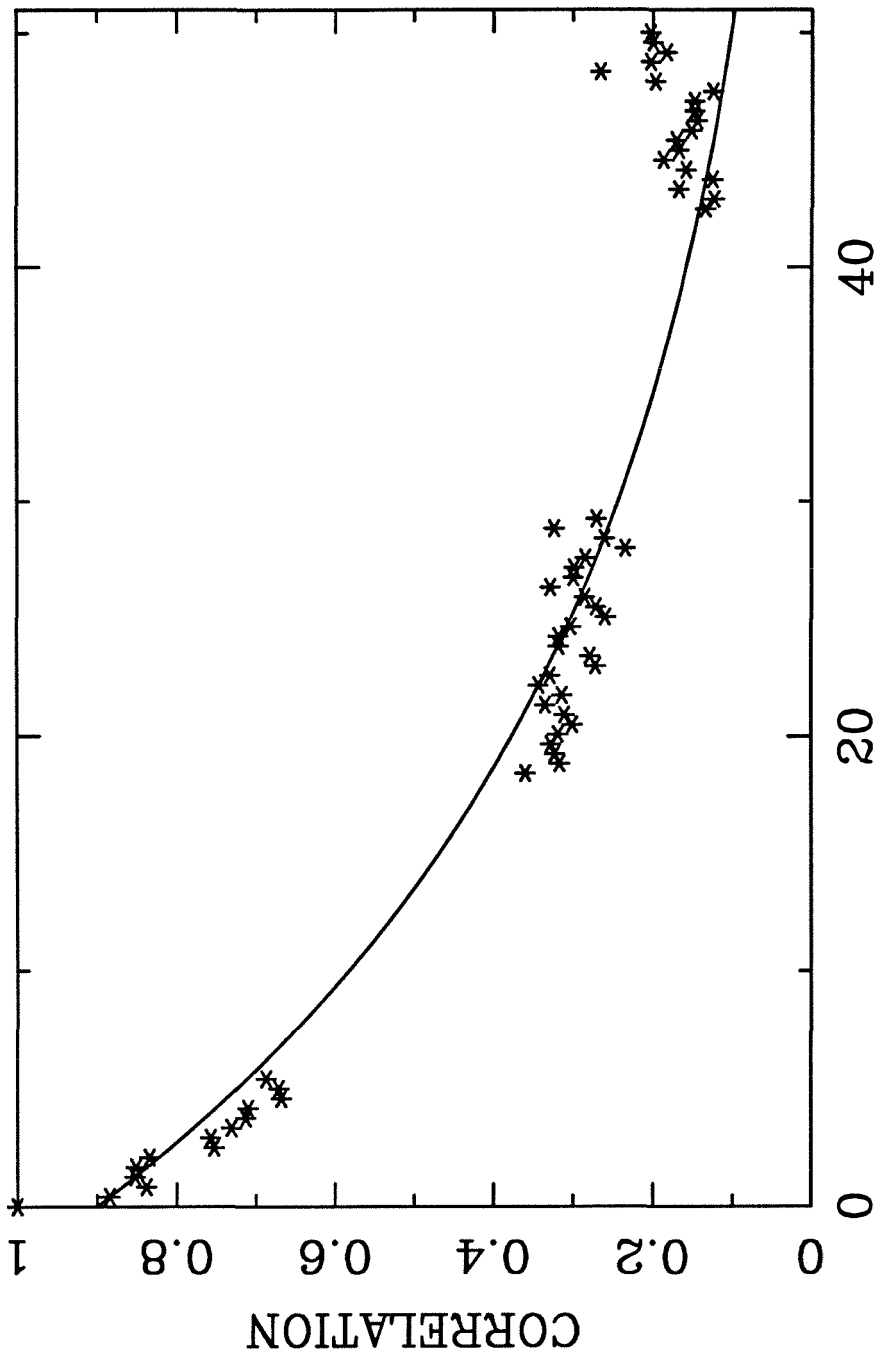

FIGURE 6

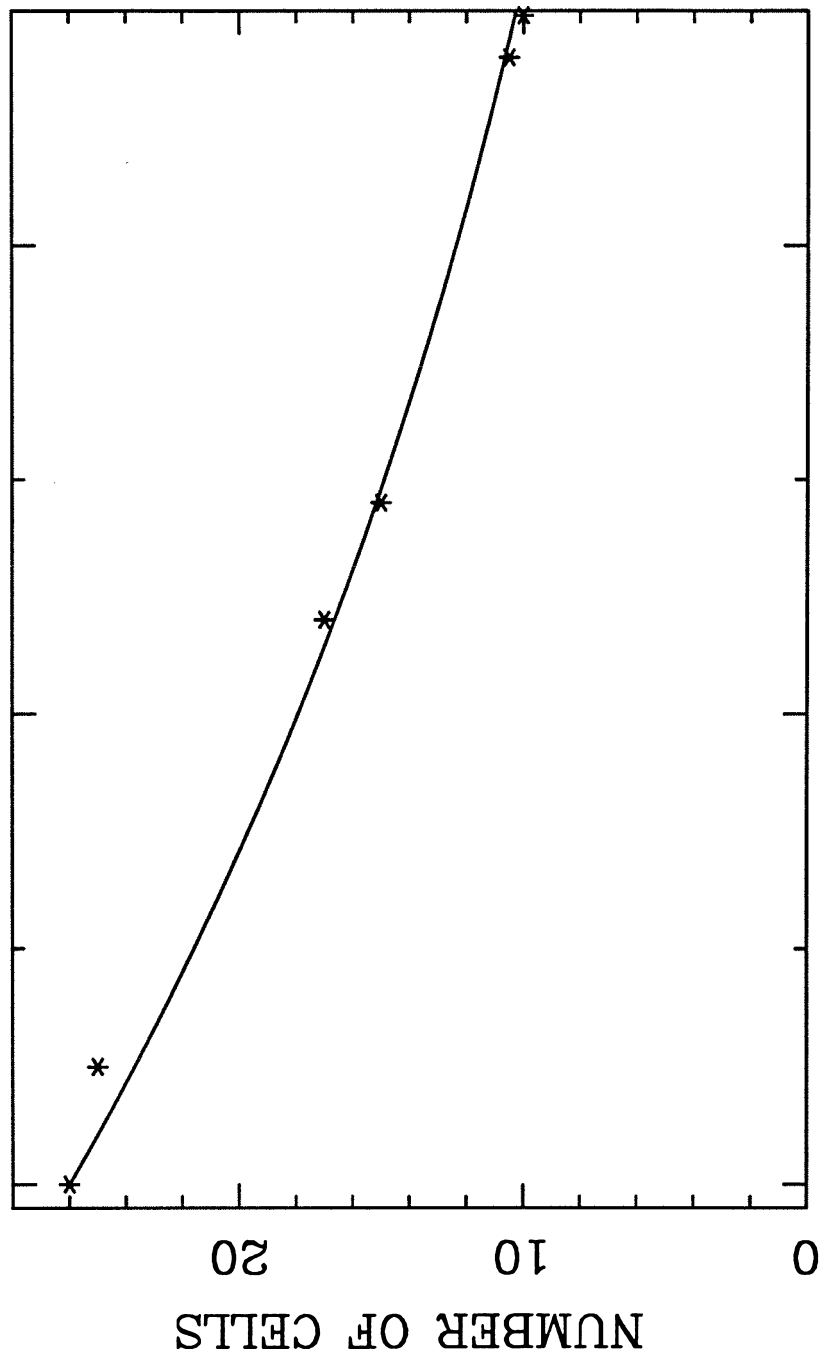

FIGURE 7

FIGURE 8a

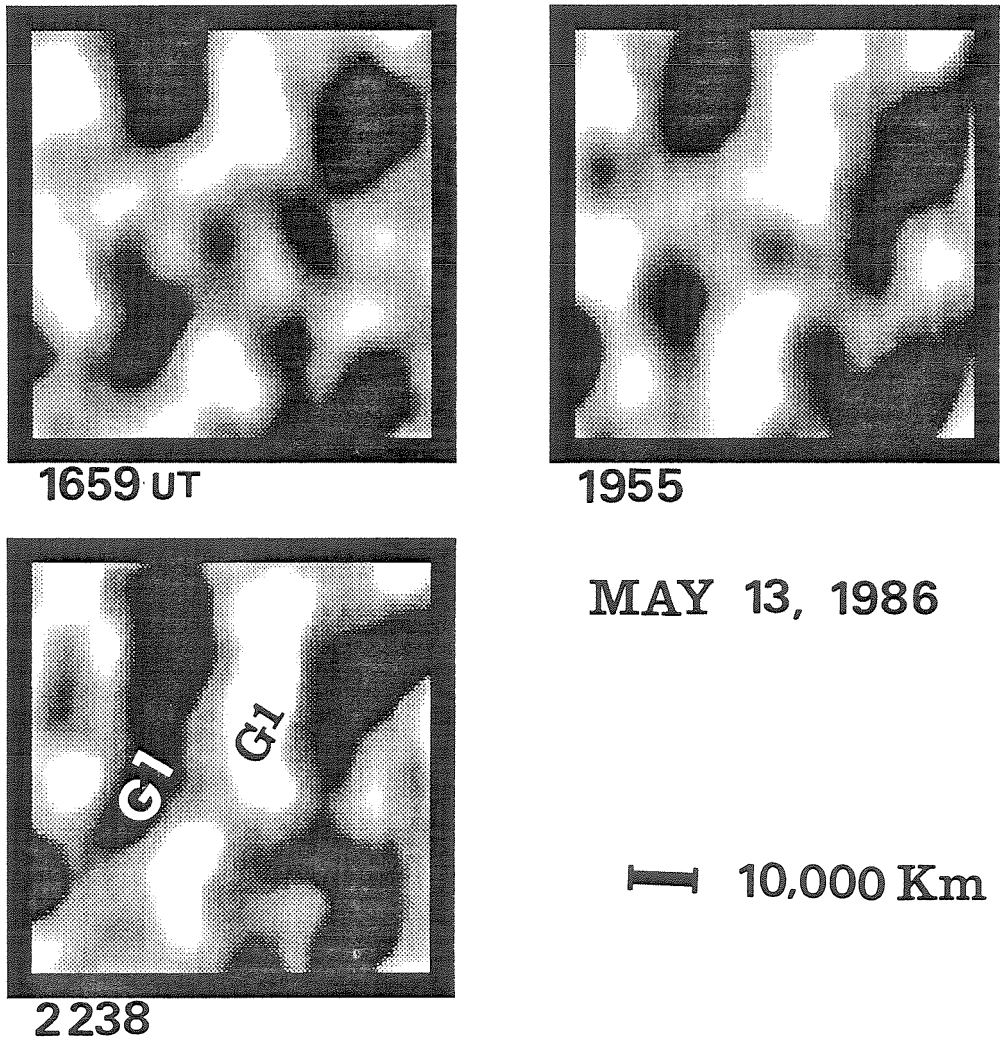

FIGURE 8b

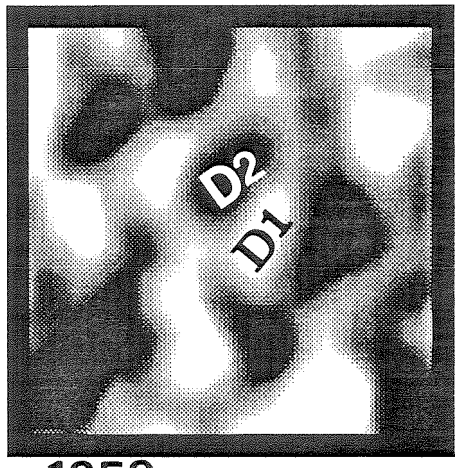

1659

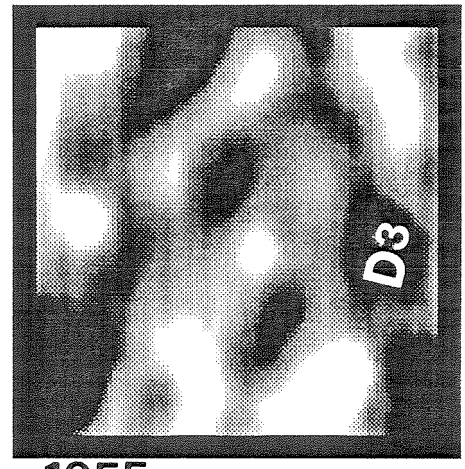

1955

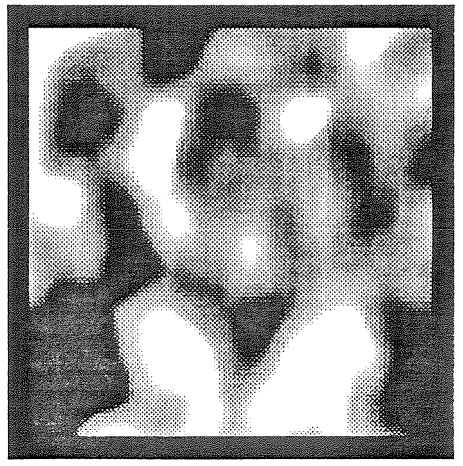

2238

MAY 13, 1986

FIGURE 8c

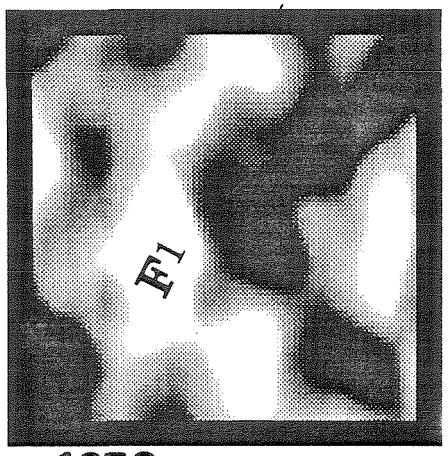

1659

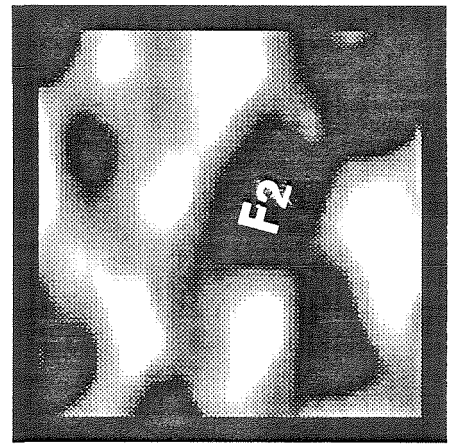

1955

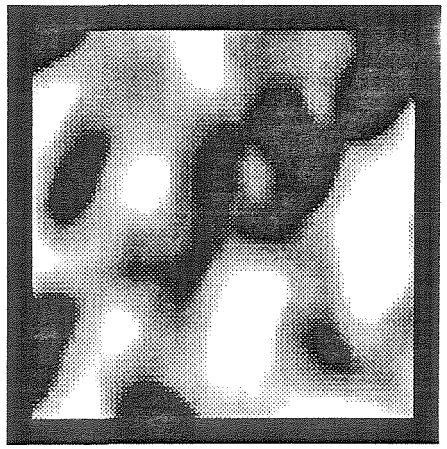

2238

MAY 13, 1986

FIGURE 9a

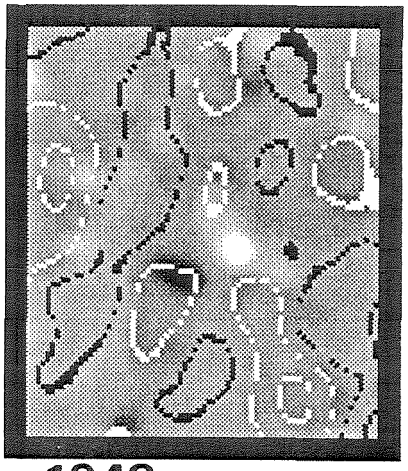

1948

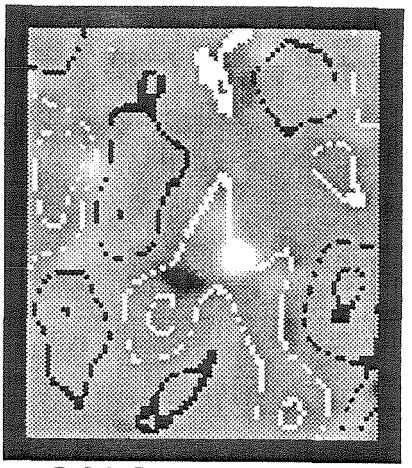

2103

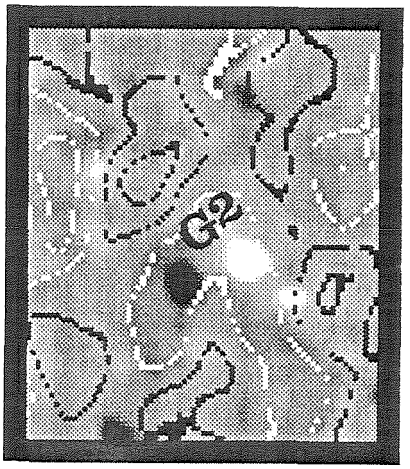

2312

MAY 11, 1986

FIGURE 9b

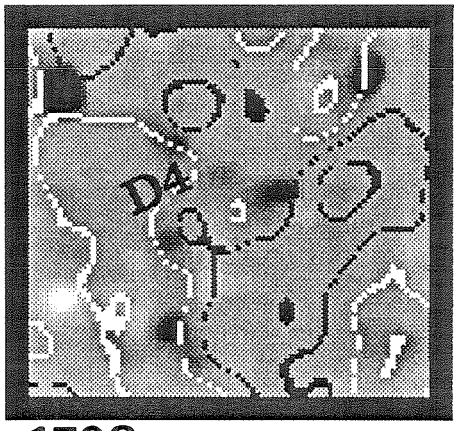

1708

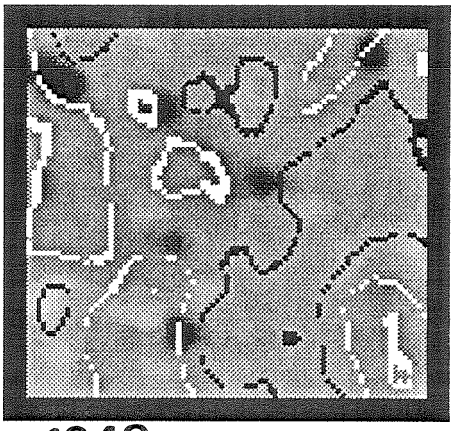

1948

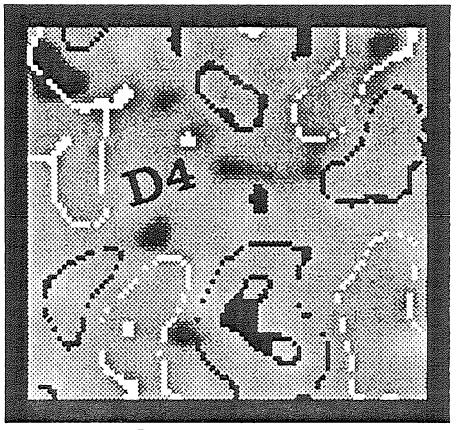

2312

MAY 11, 1986

Chapter 4

Contrast of Faculae Near the Solar Limb

Solar Physics, Vol. 110

ABSTRACT

We have measured the contrast of solar faculae near the limb on direct digital video images made with the 65 cm vacuum reflector at the Big Bear Solar Observatory. We used six broad band filters with different wavelengths from red to violet. The range of heliocentric angle covered in our measurements is $0.05 < \mu = cos\theta < 0.4(\theta = 87° - 66°)$. About 300 images were measured from observations made during the summers of 1983 and 1985. Over 20000 faculae were measured.

By averaging the contrasts of faculae and plotting them vs. heliocentric angle, we found that contrast increases monotonically towards the limb for the shorter wavelengths; however, for longer wavelengths, contrast has a tendency to peak around μ=0.15, and then decrease towards the extreme limb. The contrast increases as wavelength decreases.

1. Introduction

Faculae are regions of enhanced magnetic field observed in the continuum. It is well known that the contrast of the facula to the photosphere increases toward the limb (Muller, 1975). But the exact behavior of the contrast function near the extreme limb has been a matter of some dispute. The question was especially active in discussions of measurements of the solar oblateness (Ingersoll and Chapman, 1975), but the center–limb variation of facular brightness is important evidence on the physical nature of faculae. Why the presence of enhanced magnetic field produces these increases is a mystery.

The variation in measurements made by various authors (Muller, 1975; Hirayama, 1978; Chapman and Klabunde, 1982; Libbrecht and Kuhn, 1984, 1985) is summarized in figure 1 (copied from Libbrecht and Kuhn) where we have included our results. Some of those measurements are from high resolution observation (with the resolution 1" or so, Muller, 1975; Hirayama, 1978), they can be used to derive models of magnetic flux tubes. Others are from the low resolution observation (Muller, 1975; Chapman and Klabunde, 1982; Libbrecht and Kuhn, 1984, 1985), they can be used to estimate the brightness excess of facular area in oblateness measurements or in the sunspot deficit problem. Our measurement is from the high resolution observation. Almost all the previous measurements are indirect, i. e. all the faculae within a range were measured, and the area estimated. The wavelength range of the previous data is also limited. The data of Chapman and Klabunde

are based on integrated observations of bands of constant μ while that of Muller is based on photographic observations in a single wavelength on four days. There have been no previous digital photometric measurements of individual facular points; this would appear to be the most direct and simple way of measuring the contrast when resolution is adequate. This method also permits us to approach closer to the limb than most of previous data. Our data go to $\theta = 87°$, 1.2 arc sec from the limb.

Two kinds of theoretical models which attempt to explain the excess continuum emission of the faculae over the quiet photosphere: (1) The 'Hot Wall' model (Spruit, 1976). (2) The 'Hot Cloud' model (Chapman, 1970; Ingersoll and Chapman, 1975; Schatten et al., 1986). The 'Hot Wall' model predicts that the contrast of facula peaks at a heliocentric angle of $\cos\theta$=0.2 then decreases rapidly. The 'Hot Cloud' model predicts a rapid increase of the facular contrast when $\mu < 0.2$. The measurement of the center-to-limb variation in facular contrast gives an important test of those models.

2. Instrument and Data Collection

For the present work we used a RCA camera with Newvicon vidicon tube on the 65 cm reflector at Big Bear. Frames were digitized with eight–bit accuracy on the Quantex or Eyecom video image processors. Usually four successive frames were averaged to reduce video noise. The total exposure is thus 1/8 second. A photograph of one of the plage regions is given in Fig. 3. The resolution in the

BBSO in the summer is usually about 1 arcsec. A rotating filter wheel made possible rapid change of the wavelength observed. The video image processors make possible the direct measurement of intensities within small polygons on the images.

Measurements of step wedges showed our system to be linear within a few per cent. For the small contrast of facula to photosphere this is adequate. We placed a small piece of neutral filter with a transmittance around 50-80 percent in front of the TV camera for gain calibration.

We checked scattered light by measuring the scattered light off the limb. For most images it was below the Newvicon threshold, or less than a few percent . As a check, we obtained limb darkening curves for 3862Åand 5250Åwhich are presented in figure 2. They are compared with the limb darkening curves from the parameters in Allen's Astrophysical Quantities. Our observed curves coincide within 5 percent with Allen's curve except at $\mu = 0$. That means scattered light is not significant and we made no scattered light correction. A filter wheel was used to shift rapidly from one to another of six wavelengths; neutral filters were used to keep the images within the range of the vidicon. The accuracy and repeatability of a single measurement with this system is about one per cent, but the accuracy for a facular point is somewhat less because of calibration and position registration errors.

The video image in figure 3 was obtained on May 4, 1983 at 3862Åand 7140Å, they are the results after averaging four successive frames. The scale size of the faculae is marked. We see that the plage is an array of small points or strings

of points, many of which are about one arc sec. Due to the 1" resolution, they are either some large isolated facular points or some unresolved clusters of small adjacent facular points.

3. Data Analysis

Our measurements were obtained in the summer of 1983 and 1985 on about 35 active regions on 25 days. The broad band filters used were 3470Å, 3862Å, 4642Å, 5250Å, 5700Å and 7150Å for 1983; and 3862Å, 4642Å, 5250Å, 5700Å, for 1985.

We used two different analysis methods to reduce our data.

(a) For the 1983 data, we randomly selected many faculae, averaged the peak contrast of every facula within bins of $\delta\mu$=0.05, then plotted the contrast vs. μ. We used about 150 images, 10 to 20 points in each.

(b) For 1985 data, in order to get rid of any bias in selecting faculae, we used a more automatic technique. We plotted a profile parallel to the limb of the sun and found the average intensity and noise (i.e. standard deviation) along this line. Any point on this line with contrast larger than 3 times the noise level, was chosen as a facula. We repeated this procedure for about 130 images in 4 wavelengths. On the average, about 2000 faculae are identified in each image. Finally, we averaged the contrast within bins of $\delta\mu$=0.05, and then plotted contrast vs. μ. There is one problem in this method, ie. the ratio noise/average intensity increases as μ

decreases, which removes the low contrast faculae from our sample. This tends to increase the contrast measured close to the limb. In order to solve this problem, we did the following and we call this procedure *normalization*:

Suppose the facular contrast has the Gaussian distribution:

$$n(I) = ae^{-bI^2} \tag{1}$$

a,b are constants, and I is the contrast.

The total observed number of faculae within the bin i is:

$$N_i = a_i \int_{3S_i}^{\infty} e^{-b_i I^2} dI \tag{2}$$

S_i is the average noise/photosphere signal in given μ bin. The observed average contrast within the bin is :

$$\overline{I}_i = \frac{\int_{3S_i}^{\infty} Ie^{-b_i I^2} dI}{\int_{3S_i}^{\infty} e^{-b_i I^2} dI} \tag{3}$$

Combining equation (2) and (3), b_i can be found. Finally, we set noise/intensity=S_0 for all the bins, so that the normalized average contrast is:

$$(\overline{I}_i)_0 = \frac{\int_{3S_0}^{\infty} Ie^{-b_i I^2} dI}{\int_{3S_0}^{\infty} e^{-b_i I^2} dI} \tag{4}$$

The effect of the *normalization* will be discussed in the next section.

4. Results

Our results are given in the figures. Figure 1 shows those for 5250$\mathring{A}$ compared to those of other authors. Our results, shown by circles, show neither the sharp dropoff deduced by Libbrecht and Kuhn (1984) nor the sharp increase found by Chapman and Klabunde (1982). Instead the slowly rising contrast reaches a maximum near $\mu = 0.15$.

The contrast vs. $\cos\theta$ is plotted in Figure 4 for 1983's observations. The facular contrast increases monotonically towards the limb at shorter wavelengths. At longer wavelength, the contrast increases towards a maximum around cosθ=0.15 to 0.10, then decreases limbwards.

In Figure 5, we include the μ and contrast relation for 3 different situations. (1) Before the normalization; (2) After the normalization, set $S_0 = 0.0$; (3) After the normalization, set S_0 = average noise/intensity over the all the bins.

The normalization increased the number of weaker facular points in our sample as $\cos\theta$ approaches the limb. We can see that after the normalization, the qualitative behavior of the contrast is independent of the choice of S_0, i.e. the facular contrast increases monotonically towards the limb at shorter wavelengths. At longer wavelength, the contrast increases towards a maximum around cosθ=0.15 to 0.10, then decreases limbwards. It is same as the conclusion we got from 1983's data. However, if the smaller S_0, is chosen, the facular contrast is reduced systematically. The normalization has a significant effect only at the two bluest wavelengths.

The contrast of the facula as a function of wavelength is plotted in figure 6. From figure 4, 5 and 6 , it is obvious that the contrast increases as wavelength decreases at the same $\cos\theta$.

The method we used supposes that with a large sample the distribution of facular brightness at any position angle to be independent of time. One might think a better way would be to measure the change in individual faculae in the course of a full day's observations. We did this in three cases, obtaining seven-hour sequences covering $\mu = 0.2$ to $\mu = 0.15$. While we had no difficulty identifying the faculae in these sequences, the curve of the contrast turned out to be the diurnal seeing curve, the contrast peaking at noon when the seeing was best. We also tried to measure the same facula from day to day, but found it impossible to identify more than a few faculae from one day to the next. Those results are therefore not significant and not included here.

The statistical analysis appears the most practical way to find how the contrast varies with the heliocentric angle. The average brightness of all the points appears to be a stable and repeatable measurement.

5. Error Analysis

There are several sources of error in this data, as follows:

(a) The limb fit: The points which have maximum pixel value gradient in an

image were chosen as the locus of the limb. The error arising from this limb fit could be about 3-5 pixels. So when $\mu > 0.1$, the error for μ is less then 10 percent .

(b) Calibration: The system is slightly nonlinear (D. Chou and Z. Shi, personal communication). If the contrast is less that 30 percent, the error from nonlinearity is less then 5 percent. So the nonlinearity is more important for large sunspots then for faculae.

(c) Selection effect for 1983 observation. i.e. the tendency to miss weak faculae near the extreme limb, increases the average contrast of those points measured near the extreme limb.

(d) Because many of the points are unresolved, the true contrast of the facular points must be greater than that measured. But since brightness is averaged over pixels, the total brightness of the facular point is unaffected.

The difficulty involved in obtaining accurate measures of facular intensity is obvious. The faculae may change in intensity from day to day. The seeing may change. Because of the variations in faculae, we felt that a large sample (in this case, about 20000 faculae) would give a reasonable representation of the run of facular brightness. The relatively low scatter of the results suggests that it does.

6. Discussion

Our statistical measurements of a large number of faculae show that they behave as one would expect from cursory examination of a high resolution photo. At a given $\cos\theta$, the contrast increases with wavelength. For shorter wavelengths, the facular contrast increases monotonically limbwards; for longer wavelengths the facular contrast shows less change with position and at 7150Å peaks around μ=0.1 to 0.15, and then decreases slightly towards the limb. We find no great deviation near the extreme limb; the facular contrast neither dives nor skyrockets, as has been suggested by various indirect measurements.

Our results do not show the high contrast near the extreme limb, as obtained by Chapman and Klabunde, since we observed all the faculae directly, there is no way in which objects of such high contrast could have been missed.

Another important result lies in the fact that we make an integral brightness measurement in several wavelengths. It has been suggested by Stenflo (1976) and others that the magnetic elements involved in faculae are extremely small, rather strong (1000 gauss or more) and unresolved by magnetograms. If the bright faculae correspond to these magnetic elements and also fill only a small fraction of our resolution element, high temperatures and large blue enhancements would be required. We find the color curve we observed is fitted by a black body curve at 5900 degrees. This gives a brightness increase of about 15% at 4000Åand fits the other data shown. If the bright elements were very small they would have to be much hotter and bluer than observed.

While some of the added contrast in the blue is explained by Planck curve effects, the enhanced contrast may be the result of enhanced line absorption; spectroheliograms in blue windows near the CN band head by Sheeley (unpublished) show no faculae at disk center, while those in the band head are well–marked. Similarly, pictures in the UV (Foing and Bonnet, 1984) show strong facular contrast at 1600Å.

The peak in contrast at $\mu = 0.1$ in the near IR may be due to surface roughness. Roughness of the order 20 km in the granule tops would provide such a flattening if the facula is slightly depressed.

Acknowledgements

We are grateful to Dr. S. Robinson for collecting 1983's data at BBSO and some valuable suggestions. We also wish to thank the BBSO staff for help in observation. This work was supported by NASA grant NGL 05 002 034 and NSF grant ATM-8513577.

References

Allen C.W.: 1976, *Astrophysical Quantities,* 3d ed.(London: Athlone).

Chapman G.A. and N.R. Sheeley: 1968, *Solar Physics* **5**, 442.

Chapman G.A.: 1970, *Solar Physics* **14**, 315.

Chapman G.A. and Klabunde D.P.: 1982, *Ap. J.* **261**, 389.

Foing B. and Bonnet R.M.: 1984, *Ap. J.* **279**, 848.

Hirayama T.: 1978, *Pub. Astr. Soc. Japan.* **30**, 337.

Ingersoll A.P. and Chapman G.A.: 1975, *Solar Physics* **42**, 279.

Libbrecht K.G. and Kuhn J.R.: 1984, *Ap. J.* **277**, 889.

Libbrecht K.G. and Kuhn J.R.: 1985, *Ap. J.* **299**, 1047.

Muller R.: 1975, *Solar Physics* **45**, 105.

Schatten K.H., Mayr H.G., Omidvar K. and Maier E.: 1986, *Ap. J.* **311**, 460.

Spruit H.C.: 1976, *Solar Physics* **50**, 269.

Stenflo J.O.: 1976, *IAU Symp.* **71**, 69.

Volkhanskaya N.F.: 1966, *Soviet Astron.* **10**, 325.

Figure Captions

Fig. 1 The facula contrast vs. $cos\theta$. All the measurements are at 5250Å. Bold solid line is deduced by Libbrecht and Kuhn; lighter solid line is Spruit's theoretical curve assuming a 2000 Gauss magnetic field; the dotted curve is the measurement of Muller; the dot-dashed curve gives the measurement of Hirayama; the dashed curve represents the measurement of Chapman and Klabunde, it is normalized to contrast=0.2 when $cos\theta = 0.2$; the circles show our 1985's measurements normalized to contrast=0.2 when $cos\theta = 0.2$.

Fig. 2 Limb darkening curves for 3862Åand 5250Å. Solid lines represent theoretical limb darkening curve by using the parameters from Allen's 'Astrophysical Quantities.' The circles show our measurement on May 4, 1983. Because the solar disk center is not covered in our images, we assume the intensity at $\cos\theta$=0.25 equals to the theoretical value ($\cos\theta$=0.25 located in the middle of the images) and intensity at other $\cos\theta$ is scaled by it.

Fig. 3 Photograph of the video image at the solar west limb at 20:15 UT in May 4, 1983. Observed at 3862Åand 7140Åwith the 65cm vacuum telescope. The obscured at lower left is a neutral density filter.

Fig. 4a-4f The averaged facula contrast vs. $\cos\theta$ for 1983.

Fig. 5a-5d The averaged facula contrast vs. $\cos\theta$ for 1985. Circles are from the data before normalization; triangles represent the data after normalization by setting

$S_0 = 0$; stars represent the data after normalization by setting S_0=average noise/intensity, 0.068 for 3862Å, 0.029 for 4642Å, 0.025 for 5250Å, 0.017 for 5700Å.

Fig. 6a-6c The averaged contrasts of faculae as a function of wavelength. It was averaged for 1983's data.

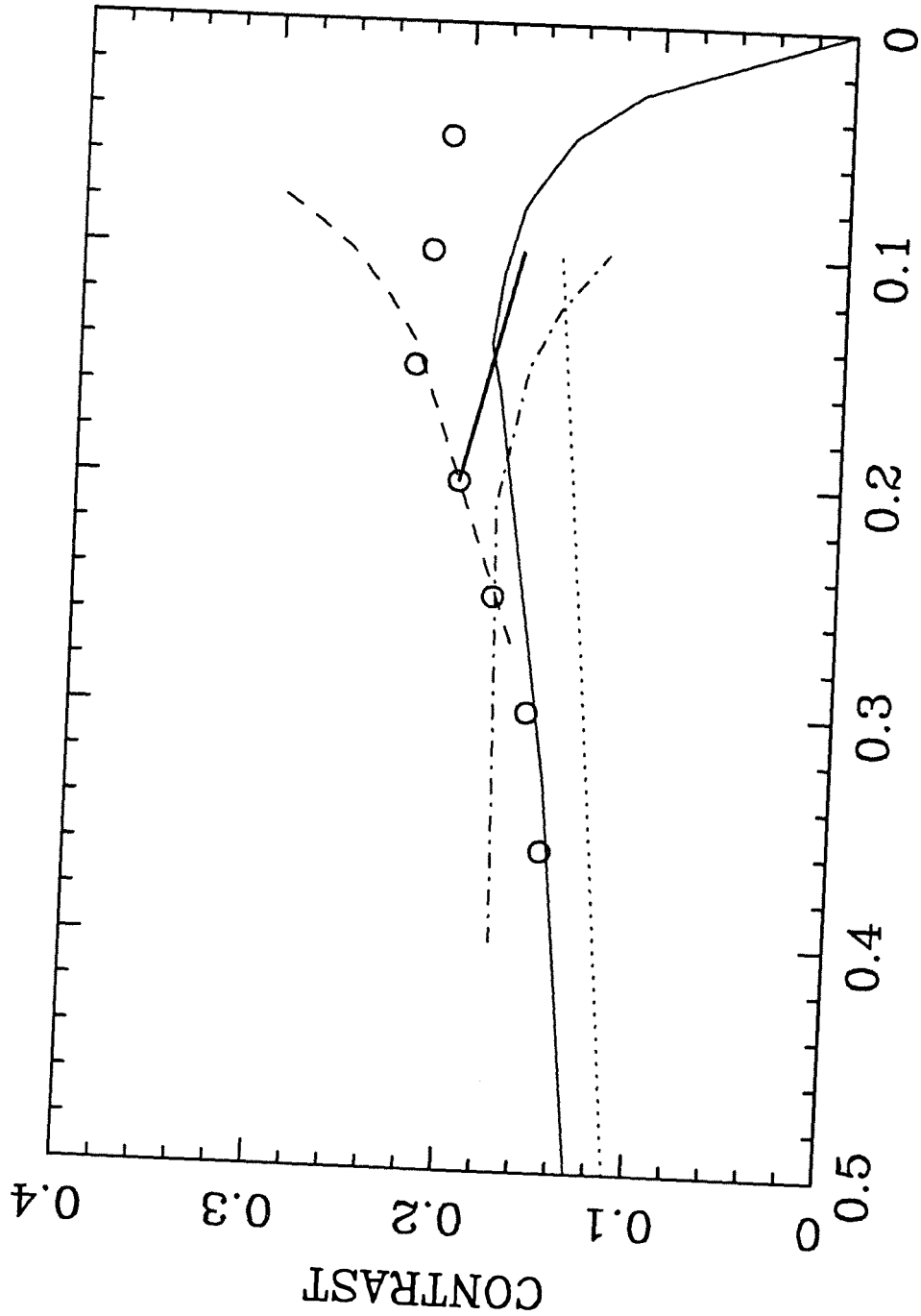

FIGURE 1

Figure 2a

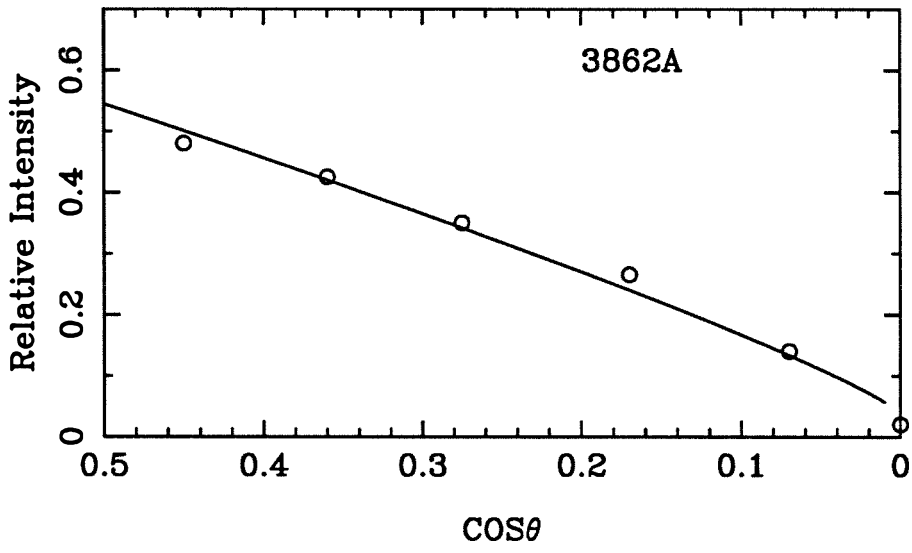

Figure 2b

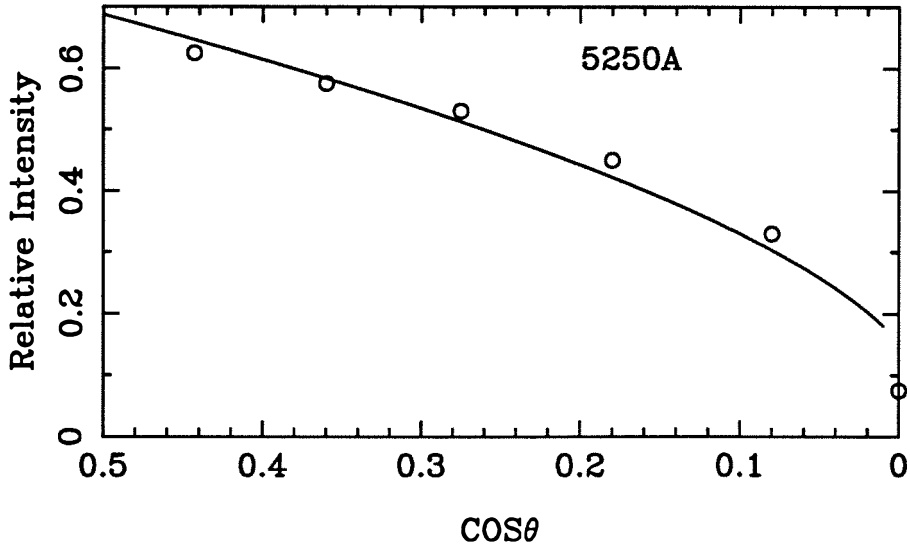

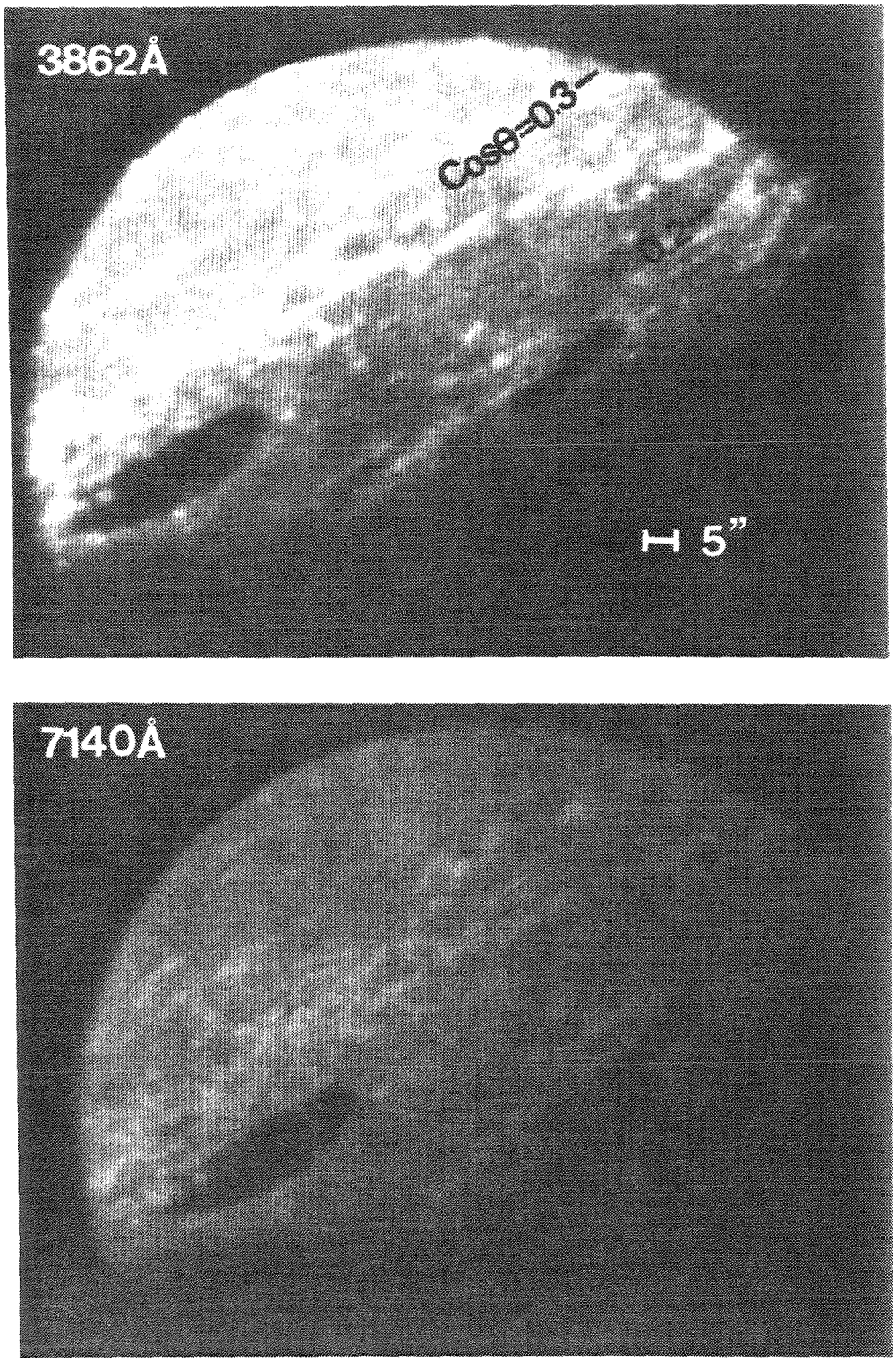

FIGURE 3

Figure 4a

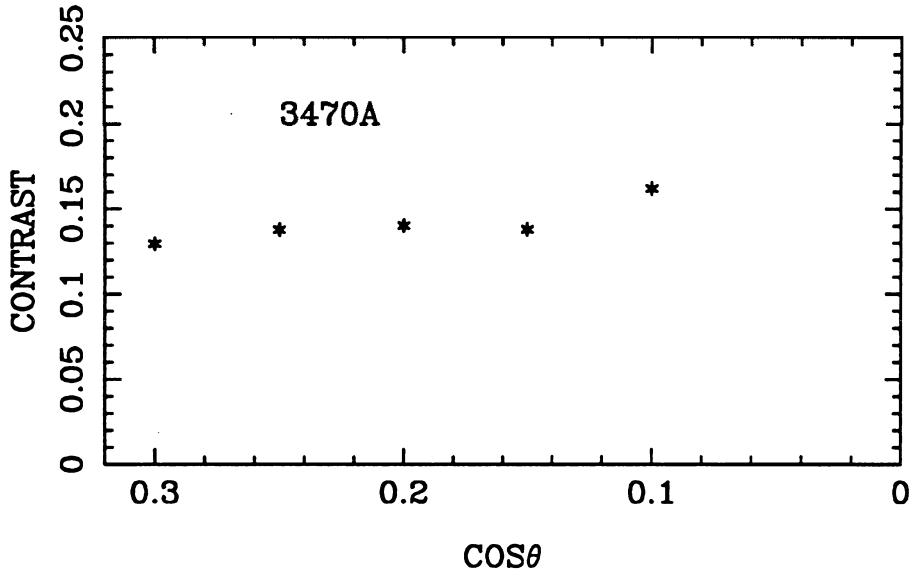

Figure 4b

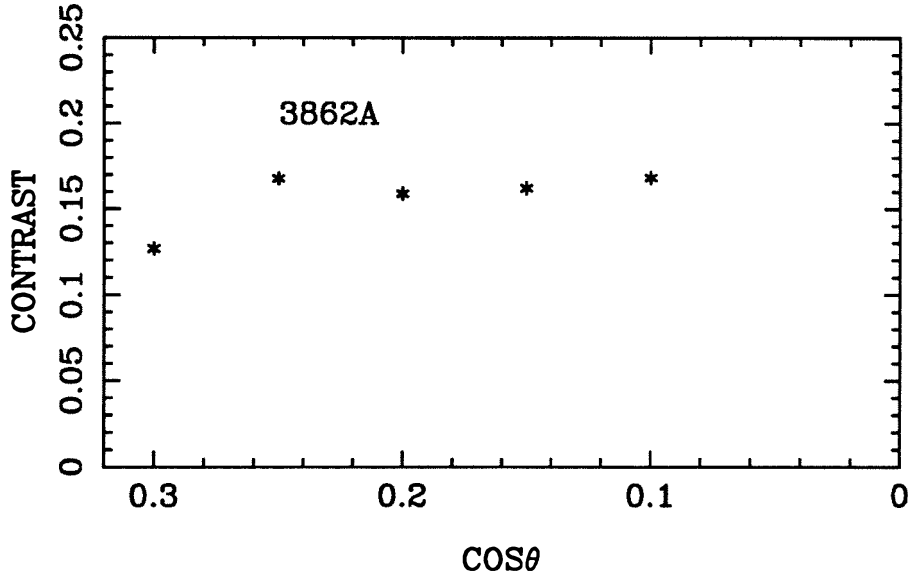

Figure 4c

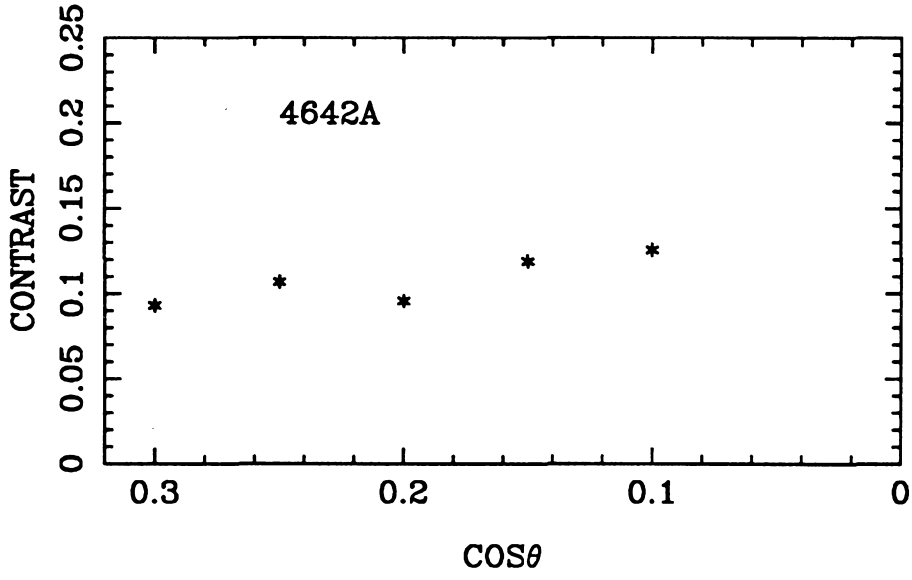

Figure 4d

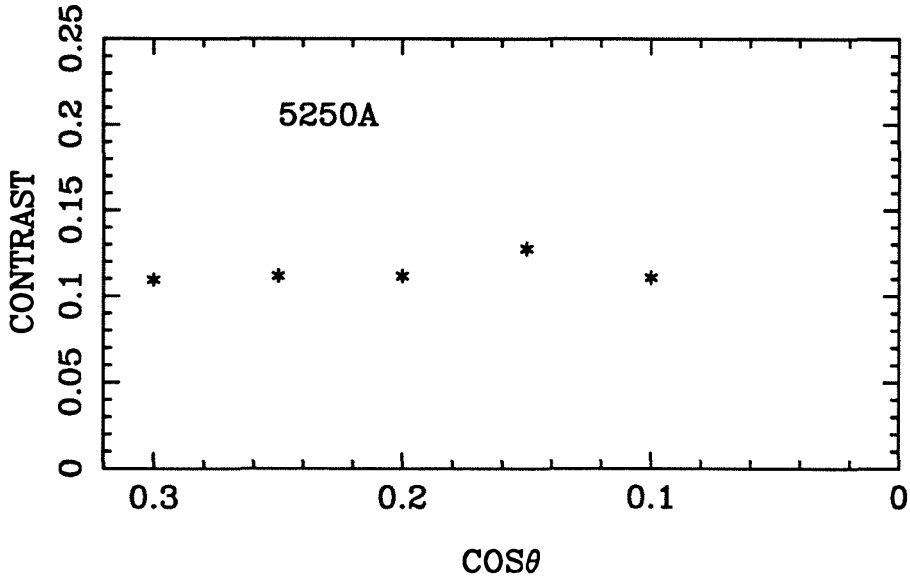

Figure 4e

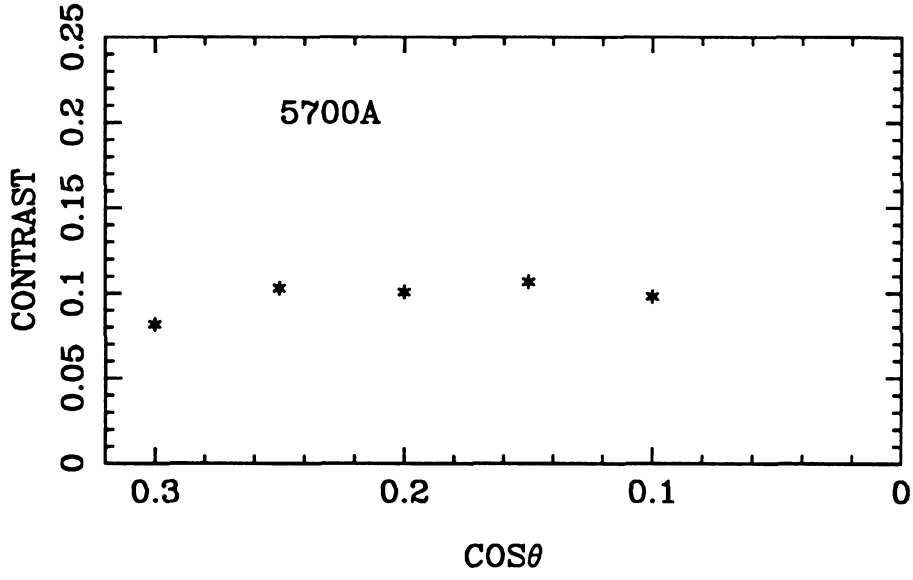

Figure 4f

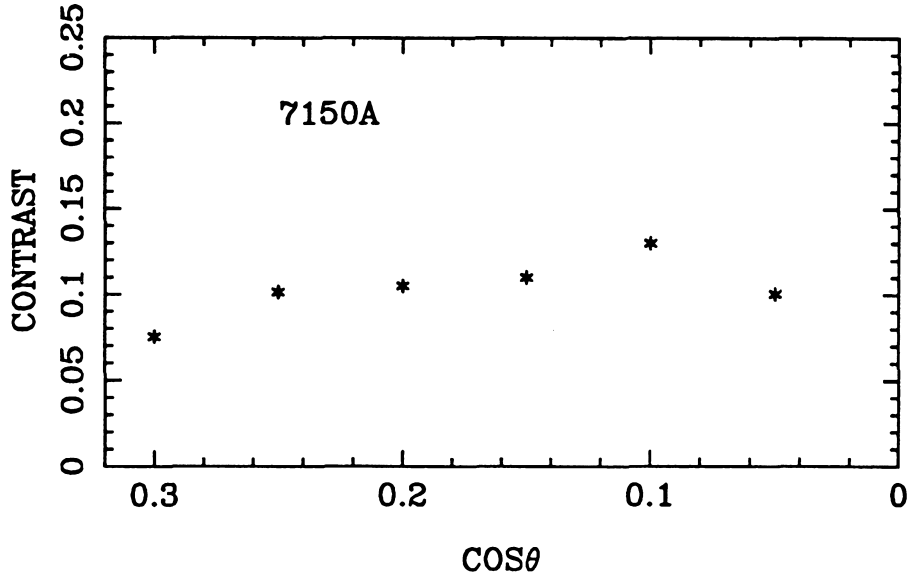

Figure 5a

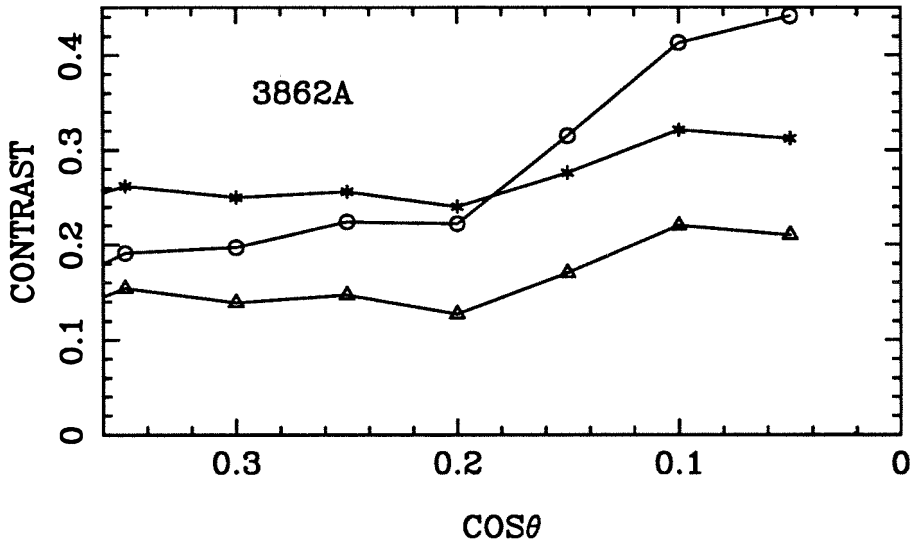

Figure 5b

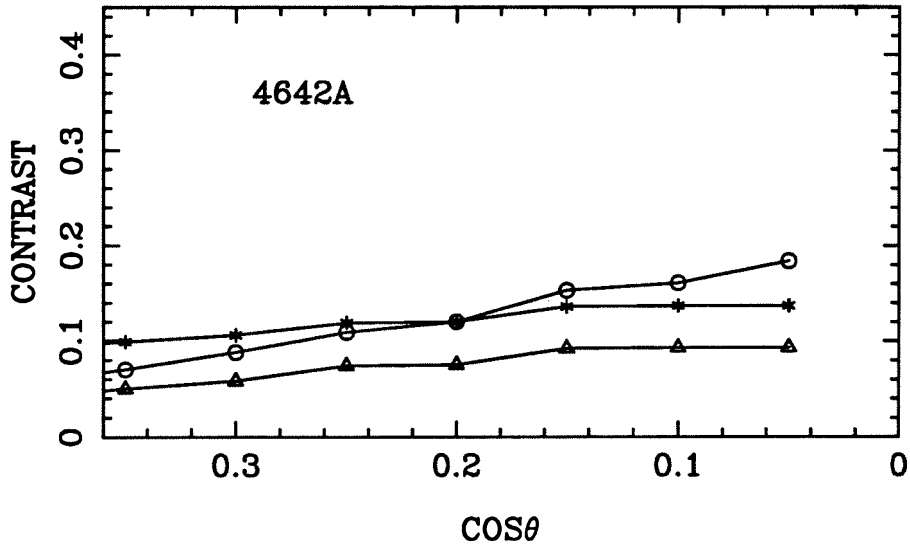

Figure 5c

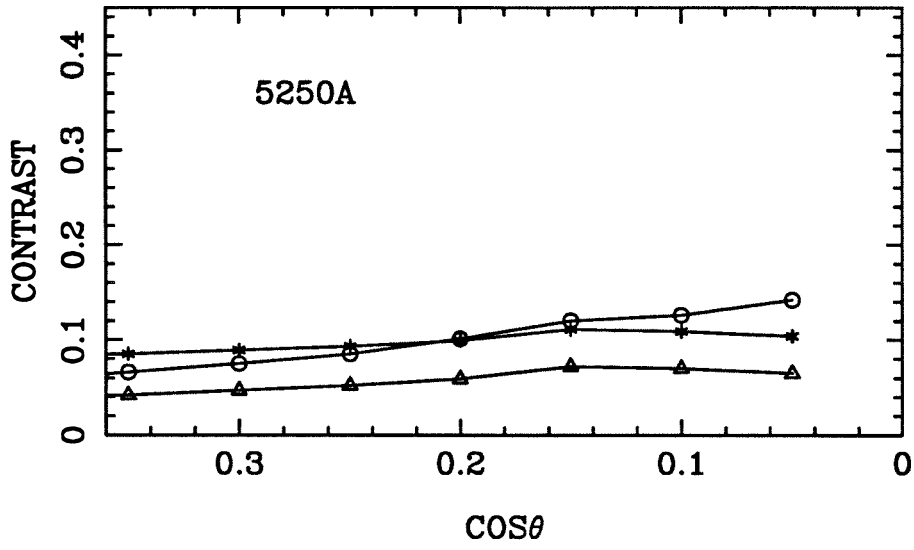

Figure 5d

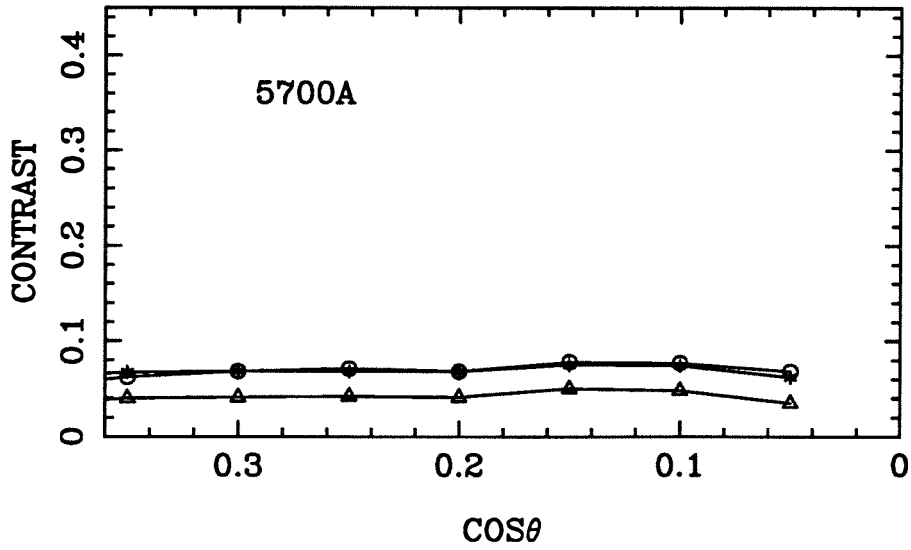

Figure 6a

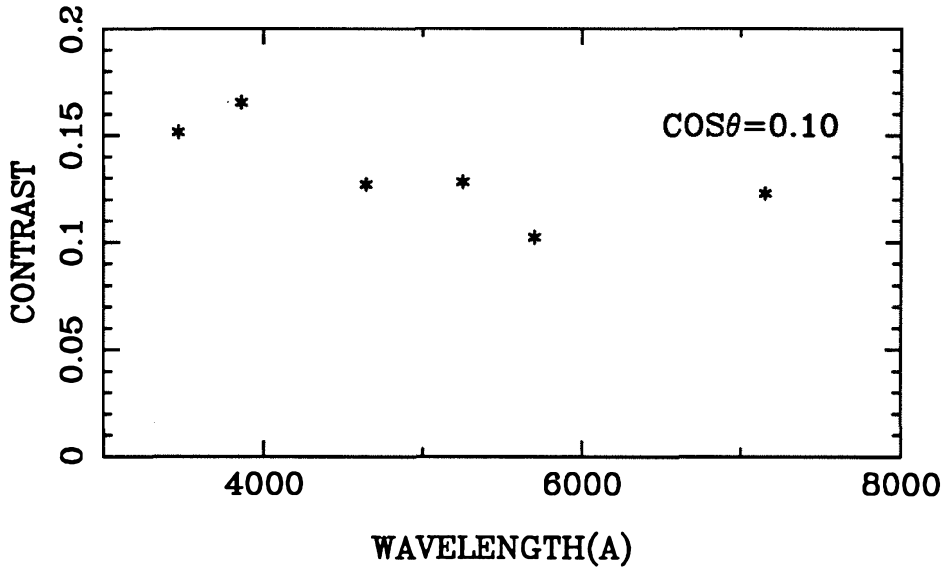

Figure 6b

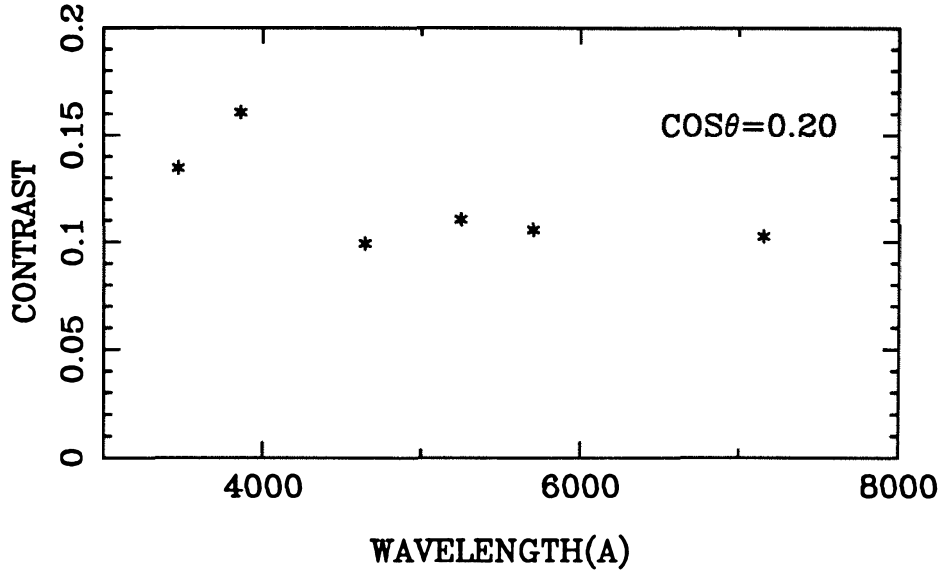

Figure 6c

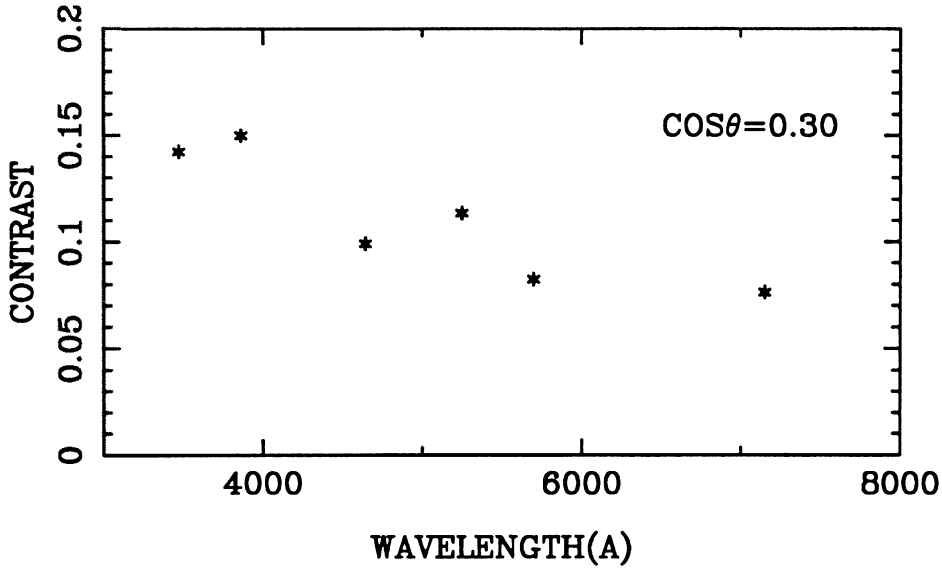

Chapter 5

The Separation Velocity of Emerging Magnetic Flux

Solar Physics, Vol. 110

Abstract

We measure the separation velocity of opposite poles from 24 new bipoles on the sun. We find that the measured velocities range from about 0.2 to 1 km/s. The fluxes of the bipoles range over more than two orders of magnitude, and the mean field strength and the sizes range over one order of magnitude. The measured separation velocity is not correlated with the flux and the mean field strength of the bipole. The separation velocity predicted by the present theory of magnetic buoyancy is between $7.4\,B\,a^{-1/4}\,cot\theta$ and $13\,cot\theta$ km/s, where θ is the elevation angle of the flux tube at the photosphere (see Figure 9), B is the mean field strength, and a is the radius of the observed bipole. The rising velocity of the top of flux tubes predicted by the theory of magnetic buoyancy is between $3.7\,B\,a^{-1/4}$ and 6.5 km/s. The predicted separation velocity is about one order of magnitude higher than those measured, or else the flux tubes are almost vertical at the photosphere. There is no correlation between the measured separation velocity and the theoretical value, $7.4\,B\,a^{-1/4}$. The predicted rising velocity is also higher than the vertical velocity near the line of inversion in emerging flux regions observed by other authors.

1. Introduction

Observations have shown that some magnetic fields on the sun emerge from below the photosphere. The mechanism responsible for bringing magnetic fields to the solar surface has long been believed to be magnetic buoyancy, which was first introduced by Parker (1955). Since then, many theoreticians (Parker 1975, 1979; Unno and Ribes 1976; Schüssler 1977, 1979; Tsinganos 1980; van Ballegooijen 1982; Moreno-Insertis 1983; Schmidt et al. 1985) have contributed to this hypothesis. But few observations have been made to provide information for testing the theory. Kawaguchi and Kitai (1976) report: " We have not observed the single blue shift of Fraunhofer lines in the region corresponding to dark lanes in between the developing sunspot pores; we expect that the velocity of rising loops is not larger than the mean errors (0.2 km/s) of our measurements of radial velocities." However, Brants (1985) reports that an upward velocity of about 1 km/s is found near the line of inversion in emerging flux regions. Other authors (Harvey and Martin 1973; Born 1974) measure the separation velocities of opposite poles of ephemeral regions and emerging flux regions.

In this paper, we measure the separation velocities and magnetic fluxes of 24 emerging bipoles, and compare them with the values estimated from the present theory of magnetic buoyancy to provide preliminary information on the emerging mechanism. In section 2, we discuss the measurements of the separation velocities and other quantities of 24 emerging bipoles. In sections 3 and 4, we discuss the

present theory of magnetic buoyancy and the buoyant velocity. In section 5, we compare the theoretical values with the observed ones and discuss other possible theories.

2. Observations and Results

Emerging magnetic fields on the sun always appear as new bipoles, with the opposite polarities moving apart during the growth phase. The new regions have a broad spectrum of size, flux and lifetime. Some of these new regions are designated as emerging flux regions (EFR), which are defined as the first stage of active regions (Zirin 1972). They might develop into large active regions with flux of about 10^{22} Maxwell, and last for several solar rotations. Some of these new regions are ephemeral regions (Harvey and Martin 1973; Martin *et al.* 1984) with flux of only 10^{18} Maxwell, and last for only a few hours. Even though ephemeral regions may have some properties (for example, flux, size, numbers and distribution) different from emerging flux regions, in this paper we consider them as the same entity. We classify them only by the amount of flux they develop.

We have observed 24 new bipoles with the high sensitivity videomagnetograph and the 1/4 $\AA$ Hα Zeiss filter at the Big Bear Solar Observatory. The videomagnetograph has been described by Martin (1983), Zirin (1985) and Shi (1986). The digital magnetograms are taken at rates of about 10 to 30 per hour, depending on integration time. The high spatial resolution Hα pictures are taken at a rate of

about about 4 per minute. The observed quantities of these new bipoles are listed in Table 1, and explained as follows:

(1) Separations

We define two different separations of the opposite poles of a new bipole. The first one, the separation of maxima, is the distance between the maxima of the opposite polarity fields. The second one, the separation of borders, is the distance between the outer borders of two poles. The separation of maxima can be measured more accurately than the separation of borders, but the latter has better physical meaning, because the position of the maxima might be affected by the development of a new stronger pole. The velocities derived from the two different separations will be discussed in (2). The geometric projection has been corrected such that all regions are transformed to the center of the solar disk for comparison on the same base. Most regions we observed are within 20° off the disk center. Two regions have the heliocentric angle about 40°. Plots of the separations of maxima *versus* time of two typical new bipoles are shown in Figures 1a and 2a. For some regions (e.g. Figure 2a), the position of the emerging flux is difficult to define at a very early stage and the measured separation has a larger error. Otherwise, the error is about 1 to 2 arcsec.

(2) Separation Velocities

The separation increases nearly linearly with time over a certain period. Usually, the slope of the curve decreases with time. We define the separation velocity

as the slope of a linear fit of the *steepest* portion of the curve (as shown in Figures 1a and 2a). The choice of the steepest portion is made by eye. The variation in the beginning of Figure 2a is caused by the uncertainty in defining the position of the emerging flux upon first appearance. This portion of the curve is not included in the determination of the separation velocity. Because of the high temporal resolution, the velocity can be determined accurately. The error caused by the choice of the steepest portion of the curve is usually less than 30%. Both the separation velocity of maxima (v_m) and the separation velocity of borders (v_b) are measured and shown in Table 1. A plot of v_b *versus* v_m is shown in Figure 3. They are nearly the same. Hereinafter, we use the "separation velocity" to refer to the separation velocity of maxima. The separation velocity *versus* the magnetic flux (defined in (4)) and the mean field strength (defined in (8)) are plotted in Figures 4 and 5 respectively. Figures 4 and 5 show that the separation velocity is not correlated with the flux and the mean field strength of the region. From the theory of magnetic buoyancy, the emerging velocity, which is related to the separation velocity, is a function of magnetic field strength and cross section of the flux tube. The measured velocities fall in a narrow range of about 0.2 to 1 km/s. In contrast, the fluxes of the bipoles range over more than two orders of the magnitude, and the mean field strength and the sizes range over one order of the magnitude. We will discuss the theory of magnetic buoyancy in Section 3 and 4.

Some of the bipoles are observed from birth, but we do not find the separation

velocity to be as high as 2 km/s reported by Born (1974), and 5 km/s by Harvey and Martin (1973). We argue that first, as the bipole first emerges, the position of the emerging flux can not be accurately defined; secondly, high temporal resolution is required to accurately measure the separation velocity in the first few minutes because of the error in the position measurement. Frazier (1972) reports transverse velocities of 0.1 to 0.4 km/s of 26 magnetic knots in an active region. These correspond to separation velocities of 0.2 to 0.8 km/s, which are consistent with our results.

(3) Initial Separations and Mean Separations

The initial separation is the separation of maxima we first observe for the bipole. For the regions that we observe from the very beginning of emergence, we define the initial separation as when we first can identify the bipolar feature. For those in which we miss the very beginning of emergence, we simply define the initial separation as the first observed one. The initial separation indicates how early we start observing the new bipole. The mean separation is the separation of maxima averaged over the period in which the separation velocity is defined. Both are shown in Table 1. There is no apparent correlation between separation velocity, v_m, and mean separation and initial separation.

(4) Magnetic Flux

For some new bipoles, the fluxes of two poles are not equal. The same phenomenon is also reported by other authors (Topka and Tarbell 1983; Wilson and

Simon 1983; Simon and Wilson 1985). The possible explanations are geometry of the fields, the position of the regions on the sun, instrumental limitations and effects, seeing effects, the surface dynamo (Akasofu 1984; Simon and Wilson 1985; Wilson 1986), and the cancellation of the flux coincident with its first appearance (Livi *et al* 1985). Plots of the fluxes of both poles *versus* time for the two regions are shown in Figures 1b and 2b. We define mean flux in Table 1 as an average over the period in which the separation velocity is defined for each polarity, and then take the average of two opposite polarities.

(5) Arch Filaments

Some regions show arch filament systems in $H\alpha$ filtergrams. Table 1 shows that there is a threshold flux for an arch filament system, which is about $0.5 \times 10^{20} - 1.0 \times 10^{20}$ Maxwell. Harvey and Martin (1973) suggest that a threshold of about 0.75×10^{20} Maxwell is needed to support an arch filament system.

(6) Pores

Some regions have visible pores or sunspots in white-light pictures or off-band Hα filtergrams during the observing period. Table 1 shows that a minimum flux of about 10^{20} Maxwell is found for a pore. Since the visibility of pores very much depends on the seeing, there is the possibility that we miss them in some cases. A minimum flux of 0.25×10^{20} Maxwell for a pore has been reported by other authors (Zwaan 1978).

(7) Radii

We define the radius as the average of major and minor axes of the 40 Gauss field strength contour of each polarity, then we take the average of two opposite polarities. The geometric projection has also been corrected such that all regions are transformed to the center of the solar disk. There is no apparent correlation between separation velocity, v_m, and radius.

(8) Mean Field Strength

The line-of-sight component of mean field strength, $B_{//}^{(mean)}$, is defined as observed flux divided by observed area.

3. Buoyant Forces

In this section, we review some points of magnetic buoyancy relevant to our discussion. In Section 4, we calculate the buoyant velocity at the photosphere.

Magnetic buoyancy brings azimuthal fields to the surface of the sun. For the deep part of the convective zone, the radius of flux tubes is much less than the pressure scale height, and therefore, the variations of pressure, density and temperature across the radius can be ignored. But as a flux tube approaches the surface, it expands rapidly while the scale height decreases at the same time (Schüssler 1979). In the upper part of the convective zone, the radius of the tube can be greater than the scale height. For example, at the photosphere, the scale height is only about 200 km, while the cross section of an emerging bipole can be few thousand km. Therefore, we can not ignore the variations of pressure, density and temperature

across the tube. In the following discussion, we consider two limits: the radius (a) much less than the scale height (Λ) and $a \gg \Lambda$.

3.1 $a \ll \Lambda$

For a horizontal flux tube, the buoyant force per unit length is proportional to the difference between external density and internal density:

$$F_b = \pi a^2 g (\rho_e - \rho_i), \tag{1}$$

where subscripts e and i refer to external and internal, respectively. For a flux tube of radius a, pressure equilibrium between the flux tube and its surroundings is established on a time scale, $a/(V_A^2 + c_s^2)^{1/2}$, where V_A and c_s are Alfven speed and sound speed, respectively. For $a \ll \Lambda$, $a/(V_A^2 + c_s^2)^{1/2} \ll \Lambda/v$, where v is the upward velocity of the flux tube, which is less than c_s and V_A. Therefore, we can assume that at all times the flux tube is in pressure equilibrium with its surroundings:

$$p_e = p_i + \frac{B^2}{8\pi}. \tag{2}$$

By using the ideal gas law, equation (1) can be written as:

$$F_b = \pi a^2 g \rho_e \{1 - \frac{T_e}{T_e + \Delta T} \cdot (1 - \frac{B^2/8\pi}{p_e})\}, \tag{3}$$

where $\Delta T = T_i - T_e$.

If the flux tube is in thermal equilibrium with its surroundings, that is, $\Delta T = 0$, then the buoyant force is

$$F_b = \pi \frac{a^2}{\Lambda} \frac{B^2}{8\pi}. \tag{4}$$

If the flux tube moves adiabatically, the temperature difference, ΔT, is (Parker 1979)

$$\Delta T(z) = \int_{z_o}^{z} \{(\frac{dT_i}{dz'}) - (\frac{dT_e}{dz'})\}\, dz' + \Delta T(z_o)$$

$$= \frac{m_H\, g}{k_B} \int_{z_o}^{z} \{\mu_e(z')\, \nabla(z') - \mu_i(z')\, \nabla_{ad}(z')\}\, dz' + \Delta T(z_o), \qquad (5)$$

where $\nabla = \partial \ln T_e / \partial \ln p_e$, $\nabla|_{ad} = \partial \ln T / \partial \ln p|_{ad}$, and μ_e and μ_i are external and internal mean molecular weights, respectively. Since the effect of pressure and temperature on mean molecular weight is small, we assume $\mu = \mu_e = \mu_i$. If we further assume that the initial temperature difference, $\Delta T(z_o)$, is zero,

$$\Delta T(z) = \frac{m_H\, g\, \mu}{k_B} \int_{z_o}^{z} \delta(z')\, dz', \qquad (6)$$

where $\delta = \nabla - \nabla_{ad}$. The temperature difference, $\Delta T(z)$, can be computed from a model of the convective zone (e.g. Spruit 1974). Since δ is negligibly small in the deep convective zone, ΔT is not sensitive to the choice of the initial position, z_o. Using the convection zone model of Spruit and choosing $z_0 = -5000km$, we calculate $\Delta T(z)$; it is plotted in Figure 6.

In equation (3), both the temperature difference and magnetic field contribute to the buoyant force. The buoyant force caused by the temperature difference is just the ordinary convective buoyancy; the buoyant force caused by the magnetic field is the magnetic buoyancy. From Figure 6, $\Delta T \simeq 3000K$ at the photosphere, and $T_e/(T_e + \Delta T) \simeq 0.6$ in equation (3); at a depth of 300 km, $\Delta T \simeq 900K$, and $T_e/(T_e + \Delta T) \simeq 0.93$ in equation (3). Thus, the buoyant force caused by the

temperature difference is negligible compared with that caused by the magnetic field, except at the photosphere. But, at the photosphere, the tube is no longer thermally isolated, because energy transport by radiation becomes efficient. Therefore, the buoyant force caused by the temperature difference can be ignored. In the following calculation, we set $\Delta T = 0$ for all z.

3.2 $a \gg \Lambda$

Schüssler (1979) shows that, if (i) there is hydrostatic equilibrium inside and outside the tube, respectively, (ii) the magnetic field is uniform inside the tube, (iii) $T_i(z) = T_e(z) =$ constant, and (iv) there is pressure balance at the bottom of the horizontal tube, then the buoyant force per unit length is

$$F_b = \frac{1}{4} B^2 a \, exp(\frac{-a}{\Lambda}) \, I_1(\frac{a}{\Lambda}), \tag{7}$$

where I_1 is the modified Bessel function of order 1. In the limit $a \ll \Lambda$, equation (7) reduces to equation (4). In the limit $\Lambda \ll a$,

$$F_b \simeq \frac{B^2}{4 \, (2\pi)^{1/2}} \, (a \, \Lambda)^{1/2} \tag{8}$$

Schüssler (1979) shows that equation (4) can be used if $a < 0.5\Lambda$, equation (8) if $a > 5\Lambda$.

If the flux tube moves adiabatically, $T_i \neq T_e$. Equation (7) is modified to

$$F_b = \frac{1}{4} B^2 a \, exp(\frac{-a}{\Lambda_i}) \, I_1(\frac{a}{\Lambda_i}) + 2\pi a p_{eo} \{exp(\frac{-a}{\Lambda_e}) \, I_1(\frac{a}{\Lambda_e}) - exp(\frac{-a}{\Lambda_i}) \, I_1(\frac{a}{\Lambda_i})\}, \tag{9}$$

where $\Lambda_i = kT_i/\mu m_H g$, $\Lambda_e = kT_e/\mu m_H g$, and p_{eo} is the external pressure at the bottom of the horizontal tube. In the limit $a \ll \Lambda_i$ *and* Λ_e, equation (9) reduces to equation (3). In the limit $a \gg \Lambda_i$ *and* Λ_e,

$$F_b \simeq \frac{B^2}{4\,(2\pi)^{1/2}}(a\,\Lambda_i)^{1/2} + (2\,\pi)^{1/2}\,p_{eo}\,(a\,\Lambda_i)^{1/2}\{(\frac{T_e}{T_i})^{1/2} - 1\}. \qquad (10)$$

4. Buoyant Velocity

The velocity of a horizontal tube is determined by the buoyant and drag forces. The drag force per unit length of a cylinder can be written as

$$F_d = \frac{1}{2}\,\rho_e\,v^2\,C_d \cdot 2\,a, \qquad (11)$$

where C_d is the drag coefficient, which is well known from experiments for Reynolds numbers, $R_e = 2av/\nu$, between 10^{-1} and 10^6 (Tritton 1977). If the Reynolds number is much less than 1, the drag force can be expressed analytically as (Landau and Lifshitz 1959)

$$F_d = \frac{4\pi\,\rho_e\,\nu\,v}{0.5 - \gamma - \ln(a\,v/4\nu)}, \qquad (12)$$

where $\gamma \simeq 0.577$. Therefore, first we have to determine the value of the Reynolds number.

In the turbulent convection zone, the effective turbulent kinematic viscosity, ν_t, can be approximated by $v_t l/3$, where v_t is the characteristic velocity of turbulence, and l is the characteristic length scale of turbulence (Parker 1979). Since the molecular kinematic viscosity is much smaller than the effective turbulent kinematic

viscosity in the solar convective zone and atmosphere, we can ignore the molecular kinematic viscosity. The characteristic length scale, l, is different for different sizes of the tube. We define a_c and v_c as the size and velocity of the largest eddies, which are granules. From observations, $a_c \simeq 1000km > \Lambda$, $v_c \simeq 1km/s$.

4.1 $a < \Lambda < a_c$

Since eddies of size comparable to the cross section of the tube are the most effective in braking the motion, we set l equal to a (Moreno-Insertis 1983). From Kolmogorov's law, we can relate the characteristic velocity to the velocity of the largest eddies,

$$v_t = v_c(\frac{a}{a_c})^{1/3}. \tag{13}$$

The Reynolds number is

$$R_e \simeq 6 \cdot \frac{v}{v_c} \cdot (\frac{a_c}{a})^{1/3}. \tag{14}$$

From observations, $v \simeq 1km/s$, $v_c \simeq 1km/s$, and $a_c \simeq 1000km \simeq 5\Lambda$ at the photosphere. For $a < \Lambda$, $Re > 10$. The drag force is expressed by equation (11). From experiments (Tritton 1977), C_d is about 1. From equations (4) and (11),

$$v = V_A \cdot (\frac{\pi}{2\,C_d})^{1/2} \cdot (\frac{a}{\Lambda})^{1/2}, \tag{15}$$

where $V_A = B/(4\pi\rho_e)^{1/2}$.

4.2 $a > a_c > \Lambda$

If a is greater than the size of the largest eddies, a_c, and scale height, Λ, then $l \simeq a_c$ and $v_t \simeq v_c$. The Reynolds number is

$$R_e \simeq 6\frac{v}{v_c}\frac{a}{a_c}. \tag{16}$$

For $a > a_c$ and $v \simeq v_c$, $R_e > 6$. The drag force is expressed by equation (11), and C_d is of order 1. From equations (8) and (11),

$$v = V_A \cdot (\frac{\pi}{2\,C_d^2})^{1/4} \cdot (\frac{\Lambda}{a})^{1/4}. \tag{17}$$

In the above discussions, we consider the tube to be horizontal. If the tube is curved, the buoyant force is balanced by the magnetic tension and the drag force. But the magnetic tension F_t is negligible compared with the the buoyant force, which can be shown as follows. The magnetic tension is

$$F_t = \pi\, a^2 \cdot \frac{B^2}{4\pi\, R}, \tag{18}$$

where R is the radius of the curvature of the tube. From equations (4), (8), and (18), the ratios of the magnetic tension to the buoyant force are Λ/R and $(2\pi)^{1/2}(a/\Lambda)^{1/2}(a/R)$ for $a \ll \Lambda$ and $a \gg \Lambda$, respectively. In general, Λ and a are much less than R. Therefore, we can ignore the magnetic tension, and consider that the tube is straight locally. The effect of magnetic tension will be discussed in section 5. If a tube has an elevation angle, θ, at the photosphere instead of being horizontal (see Figure 9), the apparent separation velocity of two poles at the photosphere is different from equations (15) and (17) by a factor $2 \cdot cot\theta$ (shown in the Appendix). The apparent separation velocity of two poles is

$$v = 2\,cot\theta \cdot V_A \cdot (\frac{\pi}{2\,C_d})^{1/2} \cdot (\frac{a}{\Lambda})^{1/2}, \tag{19}$$

if $a < \Lambda$; and

$$v = 2\,cot\theta \cdot V_A \cdot (\frac{\pi}{2\,C_d^2})^{1/4} \cdot (\frac{\Lambda}{a})^{1/4}, \tag{20}$$

if $a > \Lambda$.

5. Discussion

From Table 1, the measured separation velocities fall in a narrow range of about 0.2 to 1 km/s, while the fluxes of the bipoles range over more than two orders of magnitude, and the mean field strength and the sizes range over one order of magnitude.

It is widely held that all magnetic fields in active regions are concentrated in small kilogauss flux tubes. We assume that each observed bipole consists of a bundle of small flux tubes of radius about 100 km, and field strength about 1500 Gauss at the photosphere. If the filling factor is much less than 1, each flux tube moves independently. Since the radius of these small tubes is less than the scale height, each flux tube has a separation velocity about $v \simeq 13 cot\theta$ km/s at the photosphere from equation (19), assuming that $\Lambda = 200$ km and $C_d = 1$.

If the filling factor is close to 1, the material in between the tubes also moves with the tubes, with the observed bipole behaving like a single tube. The effective field strength is the mean field strength of the bipole, and the radius of the tube is the radius of the observed bipole, which is usually much greater than a_c and Λ. The separation velocity of the two poles is expressed by equation (20). If we choose that $C_d = 1$, $\Lambda = 200$ km, and $\rho_e = 3.2 \times 10^{-7}$, then from equation (20) the

separation velocity is

$$v = 7.4\, B\, a^{-1/4}\, cot\theta \;\; km/s, \tag{21}$$

where B is in units of kilogauss, a is in units of 1000 km, and θ is the elevation angle of the tube at the photosphere. The observed $B_{//}^{(mean)}$ in Table 1 is only the line-of-sight component, which is smaller than the real mean field strength. The observed a in Table 1 is greater than the real radius of the tube because of the geometric projection factor (The geometric projection has been corrected for a such that all regions are transformed to the center of the solar disk). Altogether, if we use the observed values of $B_{//}^{(mean)}$ and a in equation (21), this would give a lower limit for v. The value of $7.4\, B_{//}^{(mean)}\, a^{-1/4}$, defined as v_o, is shown in the fifth column of Table 1. A plot of v_m *versus* v_o is shown in Figure 7. There is no apparent correlation between v_m and v_o.

The angle calculated by equation (21) with observed values of v_m and v_o gives a lower limit for the elevation angle, θ,

$$\theta \geq tan^{-1}(\frac{v_o}{v_m}). \tag{22}$$

The value of $tan^{-1}(v_o/v_m)$, defined as θ_{min}, is shown in Table 1. There is no apparent correlation between θ_{min} and mean separation as shown in Figure 8.

From the measured mean field strength in Table 1, for most of the regions, the filling factor is about 0.1 to 0.6, which is between the two extremes discussed above. The separation velocity would be between $7.4\, B\, a^{-1/4}\, cot\theta$ and $13\, cot\theta$ km/s; and the elevation angle of the tube at the photosphere would be larger than θ_{min}.

Compared with the observed values of velocity in Table 1 (columns 3 and 4), the theoretical values (column 5) seem too large; or else the tubes must be almost vertical at the photosphere for most of the regions. This seems unlikely because observations show that arch filaments, which trace out flux tubes, are flat in the chromosphere and the corona (Roberts 1970). Nevertheless, it is possible that flux tubes are almost vertical at the photosphere, and turn horizontal in the chromosphere. Furthermore, Kawaguchi and Kitai (1976) report that the velocity of rising loops is less than 0.2 km/s; and Brants (1985) reports that the upward velocity near the line of inversion in emerging flux regions, where flux tubes are horizontal, is about 1 km/s. These are lower than the theoretical values, which lie between $3.7\,B\,a^{-1/4}$ and 6.5 km/s. Altogether, the observed values are lower than the values predicted by the present theory of magnetic buoyancy.

The possible resolutions for the discrepancy between the theoretical and the observed values are as follows: (i) The magnetic tension might be important and partially balances the buoyant force. The magnetic tension can be ignored for $a \ll \Lambda$ because the ratio of magnetic tension to buoyant force, Λ/R, usually is much less than 1. However, the magnetic tension might be comparable to the buoyant force for $a \gg \Lambda$, if the radius of curvature, R, is not much greater than $(2\pi)^{1/2}(a/\Lambda)^{1/2}a$. Thus, for the case that the filling factor is much less than 1, the predicted velocity, $13\,cot\theta$ km/s, is not changed. But, for the case that the filling factor is close to 1, the predicted velocity, $7.4\,B\,a^{-1/4}\,cot\theta$, could be overestimated,

that is, the theoretical lower limit of separation velocity could be smaller than $7.4\,B\,a^{-1/4}\,cot\theta$. This might explain the discrepancy between the predicted and the observed velocities for the case that the filling factor is close to 1, because the predicted velocity is close to the theoretical lower limit, which could be less than $7.4\,B\,a^{-1/4}\,cot\theta$. However, this fails to explain the discrepancy for the case that the filling factor is much less than 1, because the predicted velocity is close to the theoretical upper limit, which is $13\,cot\theta$ km/s and which is much greater than the observed values. (ii) The drag coefficient, C_d, might be greater than 1, which is adopted above. The Reynolds number estimated in Section 4, which is based on the mixing length theory, might be too large. This would cause an underestimate of the value of C_d. For example, if the Reynolds number is 10, $C_d \simeq 3$, and the theoretical value of the velocity decreases by a factor of about 1.7; if the Reynolds number is 1, $C_d \simeq 10$, and the theoretical value of the velocity decreases by a factor of about 3. (iii) The drag force in equation (11), based on the laboratory data, might not be applicable in the case that the radius of the flux tube is comparable to the pressure scale height. (iv) The above calculation is based on the assumption of a circular cross section, whereas in fact the cross section may be deformed (Parker 1979; Schüssler 1979; Tsinganos 1980). The deformation may cause an increase of drag force, that is, the rising velocity may be reduced. (v) The magnetic buoyant force discussed in Section 3 (equations (3) and (10)) might not be applicable to flux tubes near the surface of the sun. For example, the assumptions made in deriving

equation (10) might not be valid for flux tubes near the surface of the sun. A better theoretical calculation is required.

van Ballegooijen (1982) estimates the horizontal drift velocity of an adiabatic flux tube by assuming that the flux tube is rooted in the stable layer below the convective zone. Our measurements do not agree with his results on two points: (i) his results show that the horizontal drift velocity is highly dependent on the flux and the field strength of the flux tube; (ii) his estimated values are smaller than our measured ones by more than one order of magnitude.

The other possible mechanism to carry magnetic flux to the solar surface is the motion of supergranulation (Frazier 1972). The horizontal velocity of supergranulation is about 0.3 to 0.5 km/s (Simon and Leighton 1964; Wang 1987). If emerging bipoles are moved by supergranular flow and originate at the center of upwelling of flow, the separation velocity would be twice the horizontal velocity of supergranulation, which is 0.6 to 1.0 km/s. This agrees with the observed values. But this mechanism fails to explain the following. (i) For some regions, the opposite poles move apart more than the size of a supergranule, while supergranules can carry magnetic fields only a distance less than their sizes. (ii) In six of eight bipoles, which are simultaneously observed with the Dopplergraph, the new flux first appears at the boundary of supergranules. Since the flow is downward at the boundary of supergranules, it seems unlikely that magnetic field is moved by supergranular flow.

It is important to mention that preceding spots usually move much faster than following spots (Kiepenheuer 1953). Following spots usually are motionless relative to surroundings, or they move very slowly (Zirin 1986). This implies that something else also controls the rise of flux tubes. A complete model for the emerging mechanism has to be able to explain the asymmetry of motion of preceding and following spots.

This work only provides very preliminary information on the emerging mechanism. The sample of 24 regions may not be enough to allow any statistical conclusion. More direct observations of the vertical velocity field in between opposite polarities, and better theoretical calculations, such as more accurate buoyant force and drag force for an expanding flux tube of radius comparable to or greater than the pressure scale height near the surface for different filling factors, are needed to test the model of magnetic buoyancy.

6. Summary

(1) The measured separation velocities of 24 bipoles range from about 0.2 to 1 km/s. The fluxes of the bipoles range over more than two orders of magnitude, and the mean field strength and the sizes range over one order of magnitude. The measured separation velocity is not correlated with the flux and the mean field strength of the bipole, nor is it with any other observed quantity in Table 1.

(2) The separation velocity predicted by the present theory of magnetic buoyancy

is between $7.4\,B\,a^{-1/4}\,cot\theta$ and $13\,cot\theta$ km/s, where θ is the elevation angle of the flux tube at the photosphere. The rising velocity of the top of flux tubes predicted by the theory of magnetic buoyancy is between $3.7\,B\,a^{-1/4}$ and 6.5 km/s.

(3) The predicted separation velocities are about one order of magnitude greater than the observed velocities, or else the flux tubes are almost vertical for most regions. There is no correlation between the measured separation velocity, v_m, and the theoretical value, v_o ($7.4\,B\,a^{-1/4}$), as shown in Figure 7.

(4) The predicted rising velocities are also significantly greater than the observed upward velocities.

(5) A complete model of the emerging mechanism has to be able to explain the asymmetry of motion of preceding and following spots.

Acknowledgments

Both of us are grateful to our thesis advisor, Professor H. Zirin, for his suggestions, encouragement, and helpful discussions. We also thank S. Martin, B. Popp, D. Hough, P. Kumar, and K. Akita for reading the manuscript and helpful discussions. This work is supported by NSF under grant ATM-8513577 and NASA under grant NGL 05 002 034.

This work is done in cooperation with Dean-Yi Chou.

APPENDIX

Consider a flux tube with an elevation angle, θ, at the photosphere (Figure 9). Only the component of F_b perpendicular to the tube, which is $F_b\,cos\theta$, can move the tube; the component parallel to the tube moves material along the tube. Since all regions have been transformed to the center of the disk, as the tube moves upward (from $\overline{DE}$ to $\overline{GH}$), the apparent displacement of the tube at the photosphere is AB, which is equal to $CB/sin\theta$. Therefore, for each leg of the tube, the apparent horizontal velocity is different from equations (15) and (17) by a factor $cot\theta$. The apparent separation velocity of two legs is twice the horizontal velocity of each leg, so

$$v = 2\,cot\theta \cdot V_A \cdot (\frac{\pi}{2\,C_d})^{1/2} \cdot (\frac{a}{\Lambda})^{1/2}, \qquad (A1)$$

if $a < \Lambda$; and

$$v = 2\,cot\theta \cdot V_A \cdot (\frac{\pi}{2\,C_d^2})^{1/4} \cdot (\frac{\Lambda}{a})^{1/4}, \qquad (A2)$$

if $a > \Lambda$.

REFERENCES

Akasofu, S.-I.: 1984, *Planet. Space Sci.* **32**, 1257.

Born, R.: 1974, *Solar Phys.* **38**, 127.

Brants, J. J.: 1985, *Solar Phys.* **98**, 197.

Frazier, E. N.: 1972, *Solar Phys.* **26**, 130.

Harvey, K. L. and Martin, S. F.: 1973, *Solar Phys.* **32**, 389.

Kawaguchi, I. and Kitai, R.: 1976, *Solar Phys.* **46**, 125.

Kiepenheuer, K. O: 1953, in G.P. Kuiper(ed.), *The Sun*, The University of Chicago Press, Chicago, p. 322.

Landau, L. D. and Lifshitz, E. M.: 1959, *Fluid Mechanics*, Pergamon, London, Chap. 2.

Livi, S. H. B., Wang, J., and Martin, S. F.: 1985, *Aust. J. Phys.* **38**, 222.

Martin, S. F.: 1983, in S. Keil(ed.), *Sacramento Peak Workshop on Small Scale Dynamical Processes*, Proc. Nat. Solar Obs. Conf., Sunspot, NM, p. 30.

Martin, S. F., Livi, S. H. B., Wang, J., and Shi, Z.: 1985, in M. J. Hagyard(ed.), *Measurements of Solar Vector Magnetic Fields*, NASA Conference Publication 2374, NASA, Washington DC, p. 403.

Moreno-Insertis, F.: 1983,, *Astron. Astrophys.* **122**, 241.

Parker, E. N.: 1955, *Ap. J.* **121**, 491.

Parker, E. N.: 1975, *Ap. J.* **198**, 205.

Parker, E. N.: 1979, *Cosmical Magnetic Fields*, Oxford, New York, Chap. 8 and 10.

Roberts, P. H.: 1970, *'Velocity Fields in Magnetically Disturbed Regions of the Hα Chromosphere'*, Thesis, Calif. Inst. of Technology.

Schmidt, H. U., Simon, G. W. and Weiss, N. O.: 1985, *Astron. Astrophys.* **148**, 191.

Schüssler, M.: 1977, *Astron. Astrophys.* **56**, 439.

Schüssler, M.: 1979, *Astron. Astrophys.* **71**, 79.

Shi, Z., Wang, J. and Patterson, A.: 1979, *'Calibration of Dopplergrams and Magnetograms at BBSO'*, BBSO Preprint, No. 257.

Simon, G. W. and Leighton, R. B.: 1964, *Ap. J.* **140**, 1120.

Simon, G. W. and Wilson, P. R.: 1985, *Ap. J.* **295**, 241.

Spruit, H. C.: 1974, *Solar Phys.* **34**, 277.

Topka, K. and Tarbell, T.: 1983, in S. Keil(ed.), *Small-Scale Dynamical Processes in Quiet Stellar Atmospheres*, Proc. Nat. Solar Obs. Conf., Sunspot, NM, p. 278.

Tritton, D. J.: 1977, *Physical Fluid Dynamics*, Van Nostrand Reinhold, England, Chap. 3.

Tsinganos, K. C.: 1980, *Ap. J.* **239**, 746.

Unno, W. and Ribes, E.: 1976, *Ap. J.* **208**, 222.

van Ballegooijen, A. A.: 1982, *Astron. Astrophys.* **106**, 43.

Wang, H.: 1987, in preparation.

Wilson, P. R. and Simon, G. W.: 1983, *Ap. J.* **273**, 805.

Wilson, P. R.: 1986, *Solar Phys.* **106**, 1.

Zirin, H.: 1972, *Solar Phys.* **22**, 34.

Zirin, H.: 1985, *Aust. J. Phys.* **38**, 961.

Zirin, H.: 1986, private communication.

Zwaan, C.: 1978, *Solar Phys.* **60**, 213.

FIGURE CAPTIONS

Fig. 1a Separation of opposite poles *versus* time for the nineteenth bipole in Table 1. The statistical error is about 1000 km, which is marked by an error bar in the lower-right corner of the figure. The straight line is a least-square linear fit of the steepest portion of the curve, which is chosen by eye.

Fig. 1b Magnetic flux of two poles *versus* time for the nineteenth bipole in Table 1. The statistical error in flux measurements is about 15%.

Fig. 2a Same as Figure 1a, but for the sixth bipole in Table 1. The variation in the beginning is caused by the uncertainty in defining the position of the emerging flux at the very early stage.

Fig. 2b Same as Figure 1b, but for the sixth bipole in Table 1.

Fig. 3 Separation velocity of borders, v_b, *versus* separation velocity of maxima, v_m. The statistical error in v_b and v_m is about 20%.

Fig. 4 Separation velocity of maxima, v_m, *versus* magnetic flux.

Fig. 5 Separation velocity of maxima, v_m, *versus* line-of-sight component of mean magnetic field, $B_{//}^{(mean)}$. The statistical error in $B_{//}^{(mean)}$ is about 15%.

Fig. 6 Temperature difference, ΔT, as a function of depth below the photosphere, calculated from Spruit's convection zone model. The initial position is set at a depth of 5000 km.

Fig. 7 Measured separation velocity, v_m, *versus* v_o, which is $B_{//}^{(mean)}\, a^{-1/4}$.

Fig. 8 Minimum elevation angle, θ_{min}, *versus* mean separation.

Fig. 9 Schematic picture of a flux tube at the photosphere. The lower part is a close view of a segment near the surface. The flux tube moves from (from $\overline{DE}$ to $\overline{GH}$) as it rises. The apparent displacement of the tube at the photosphere is AB, which is equal to $CB/sin\theta$.

TABLE 1

Date	Flux (10^{18}Mx)	V_m (km/s)	V_b (km/s)	V_o (km/s)	Radius (km)	$B_{//}^{mean}$ Gauss	Ini. Sepa. (km)	Mean Sepa. (km)	Arch	Pore	θ_{min} (degree)
04/08/84	694.0	0.28	0.36	5.03	4700	1000	17500	21900	Y	Y	87
06/21/84	198.0	0.75	0.67	3.18	3300	579	17900	22000	Y	Y	77
07/12/83	122.0	0.31	0.57	3.65	2500	621	14200	17200	Y	Y	85
12/17/81	110.0	0.60	0.43	3.30	2500	560	5100	9700	Y	N	80
06/21/84	57.0	0.36	0.33	2.28	2200	375	11400	13600	Y	Y	81
10/14/85	43.0	0.88	0.98	1.72	2200	283	9000	11000	N	N	63
10/14/85	32.0	0.66	0.69	1.28	2200	210	11000	14000	N	N	63
07/12/83	30.0	0.44	0.35	1.88	1800	295	4000	5900	N	N	77
07/21/81	30.0	0.30	0.32	2.45	1600	373	5500	8000	Y	N	83
07/22/85	30.0	0.34	0.51	0.60	3000	106	3700	8500	N	N	60
06/22/85	21.0	0.69	0.64	1.04	2000	167	6500	12000	N	N	56
10/15/85	20.0	0.44	0.49	1.25	1800	196	7500	9700	N	N	71
06/22/85	20.0	0.80	0.85	1.43	1700	220	3500	5400	N	N	61
06/22/85	15.0	0.24	0.38	1.66	1400	244	5500	6400	N	N	82
10/15/85	14.0	0.92	0.74	2.66	1100	368	5000	7000	N	N	71
08/29/84	13.0	0.19	0.17	0.39	2500	66	5000	7500	N	N	64
06/21/84	12.0	0.20	0.46	1.87	1200	265	4800	8100	N	-	84
07/12/83	11.0	1.07	1.18	1.72	1200	243	2200	3400	N	N	58
10/15/85	10.0	0.83	1.05	1.56	1200	221	4000	9200	N	N	62
10/15/85	8.0	0.88	0.52	1.05	1300	151	5000	7800	N	N	50
06/21/84	7.9	0.55	0.39	1.50	1100	208	6000	8300	N	-	70
10/15/85	7.2	0.61	0.59	0.51	1700	79	5500	9200	N	N	40
06/22/85	5.5	0.49	0.64	1.29	1000	175	4000	5300	N	N	69
06/22/85	3.3	0.98	0.81	2.46	600	292	5500	7400	N	N	68

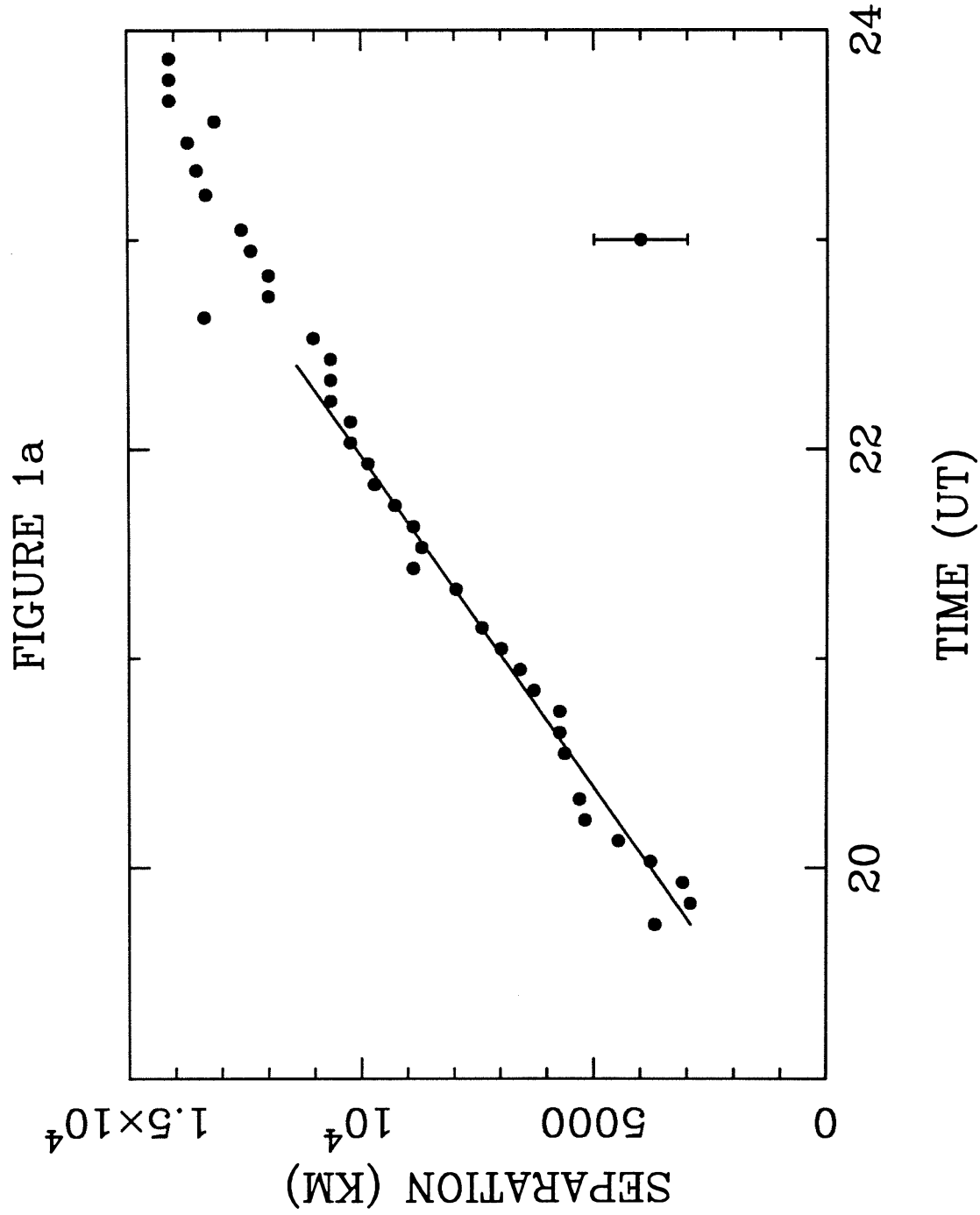

FIGURE 1a

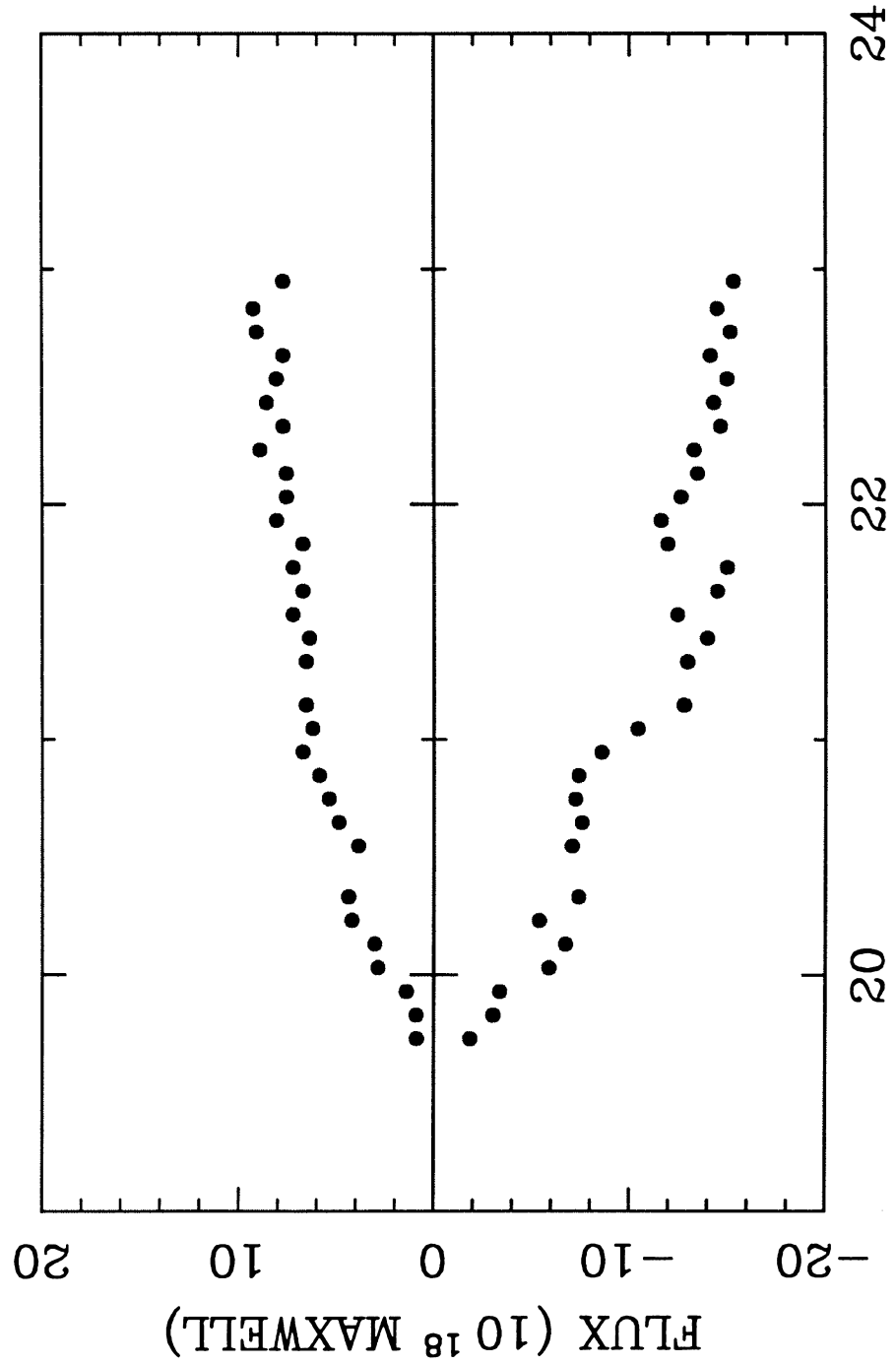

FIGURE 1b

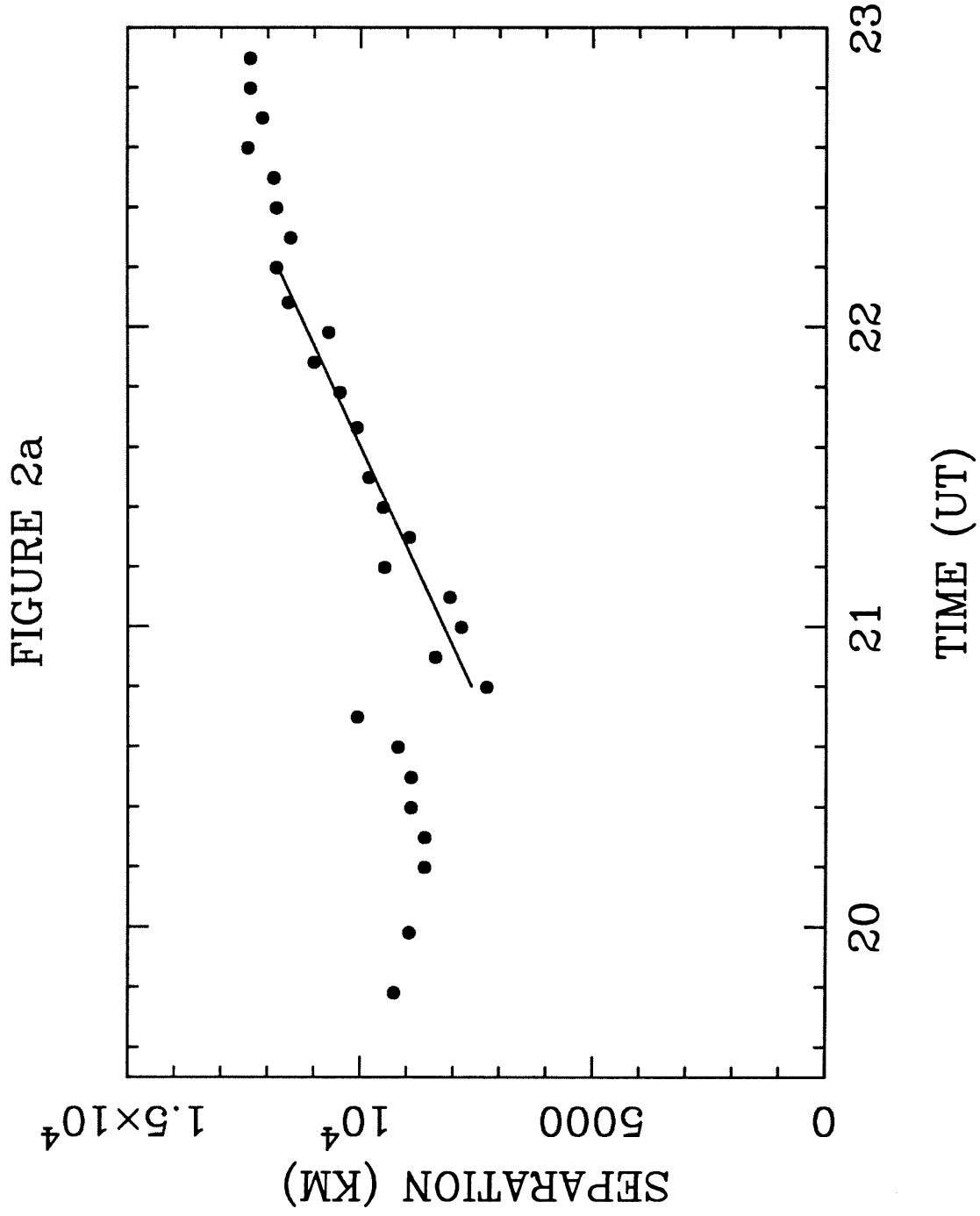

FIGURE 2a

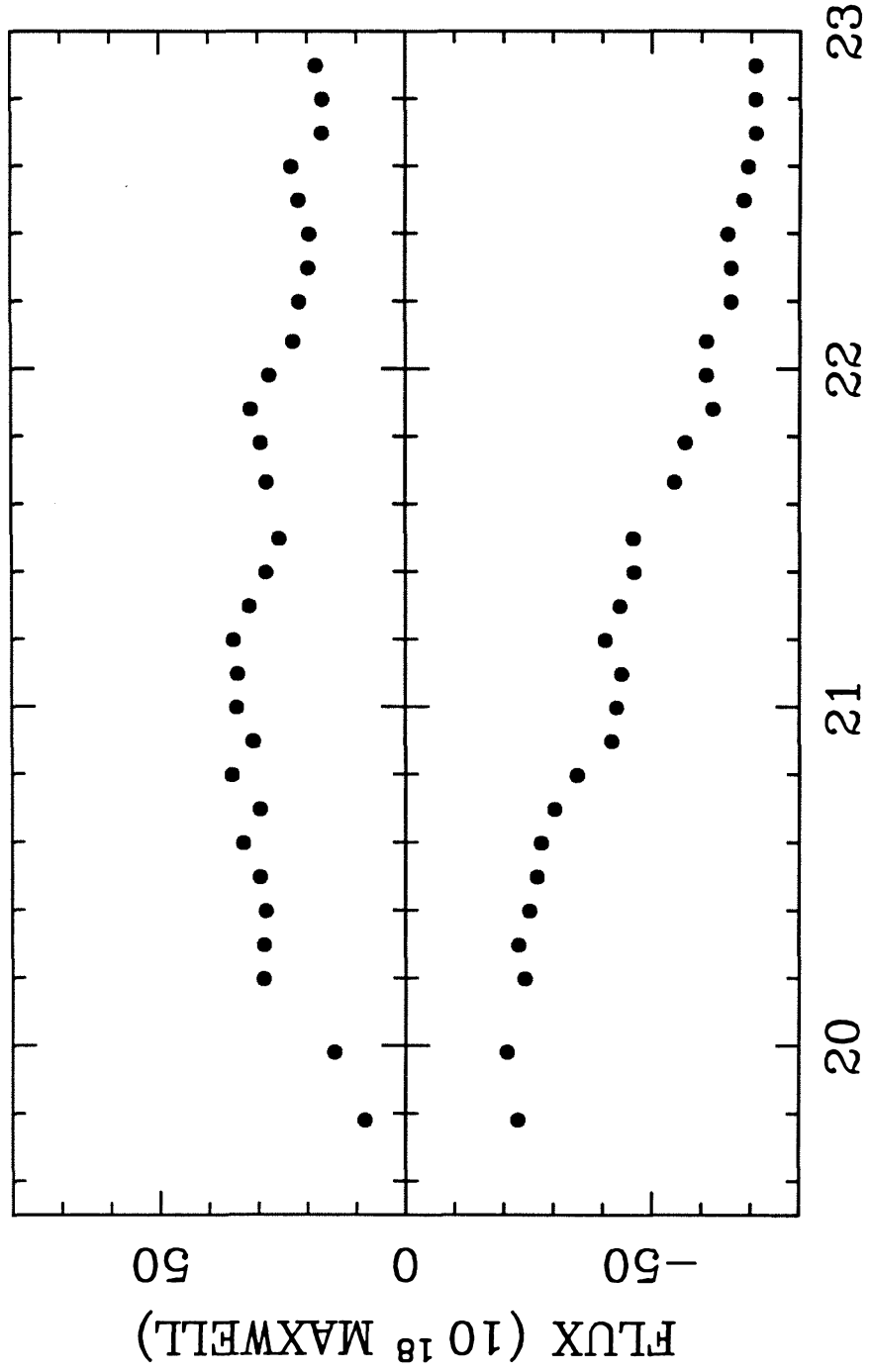

FIGURE 2b

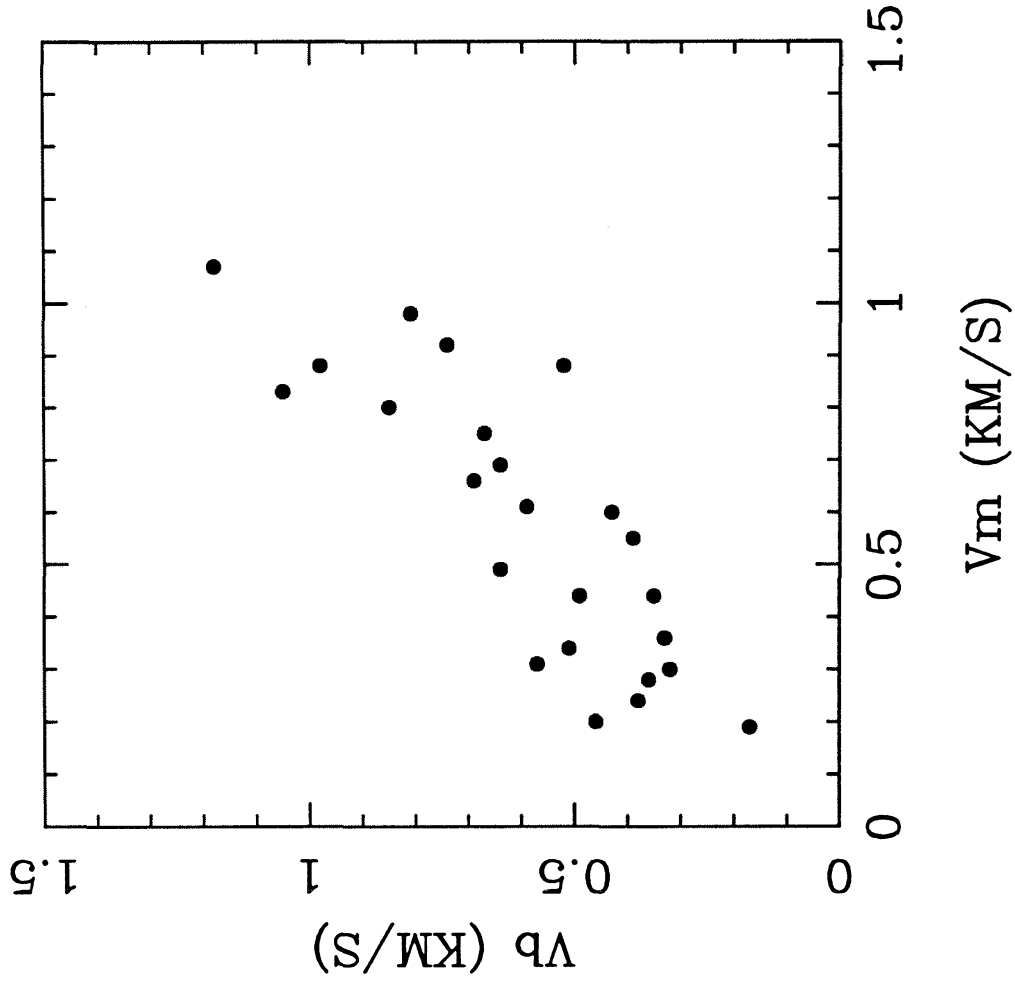

FIGURE 3

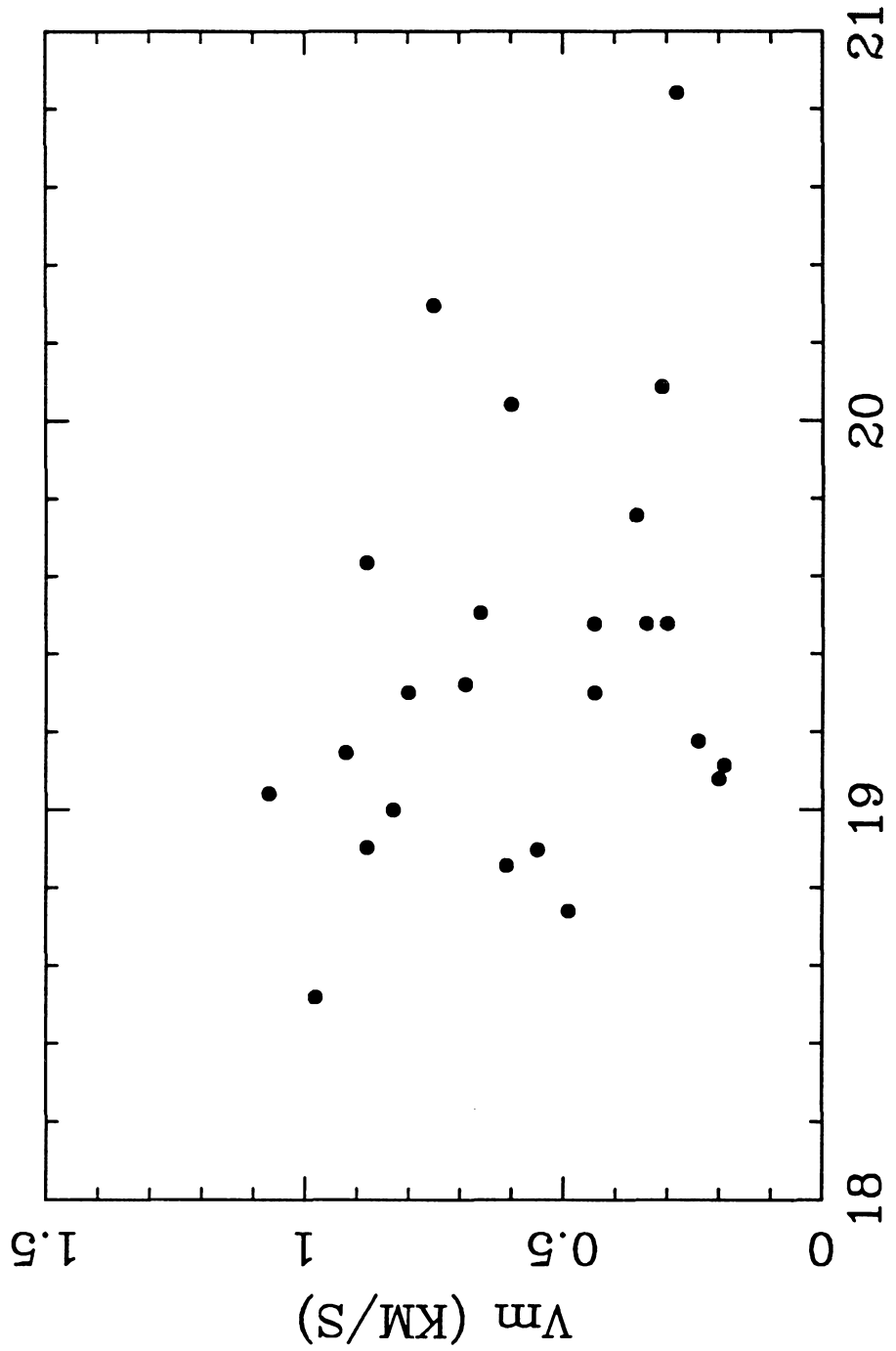

FIGURE 4

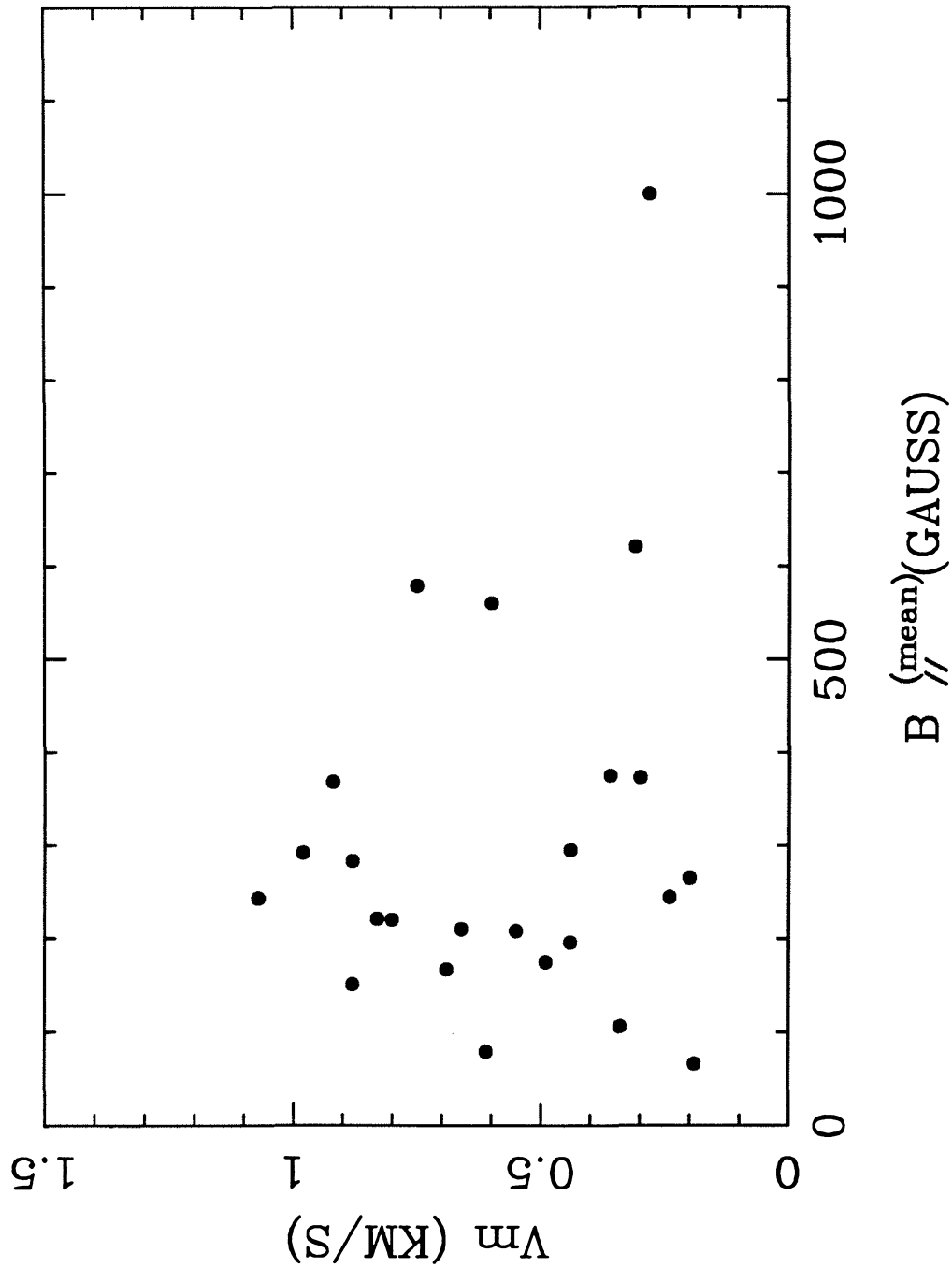

FIGURE 5

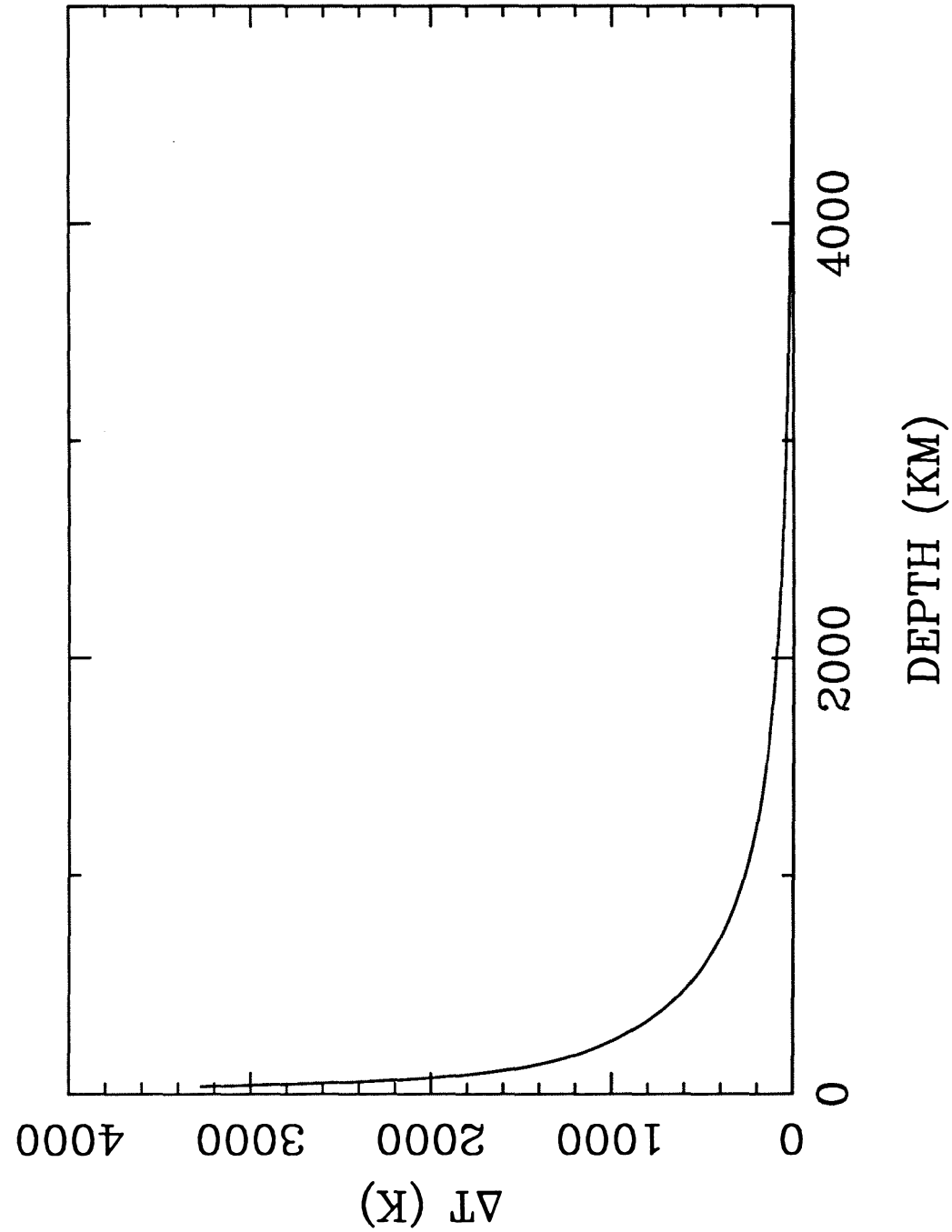

FIGURE 6

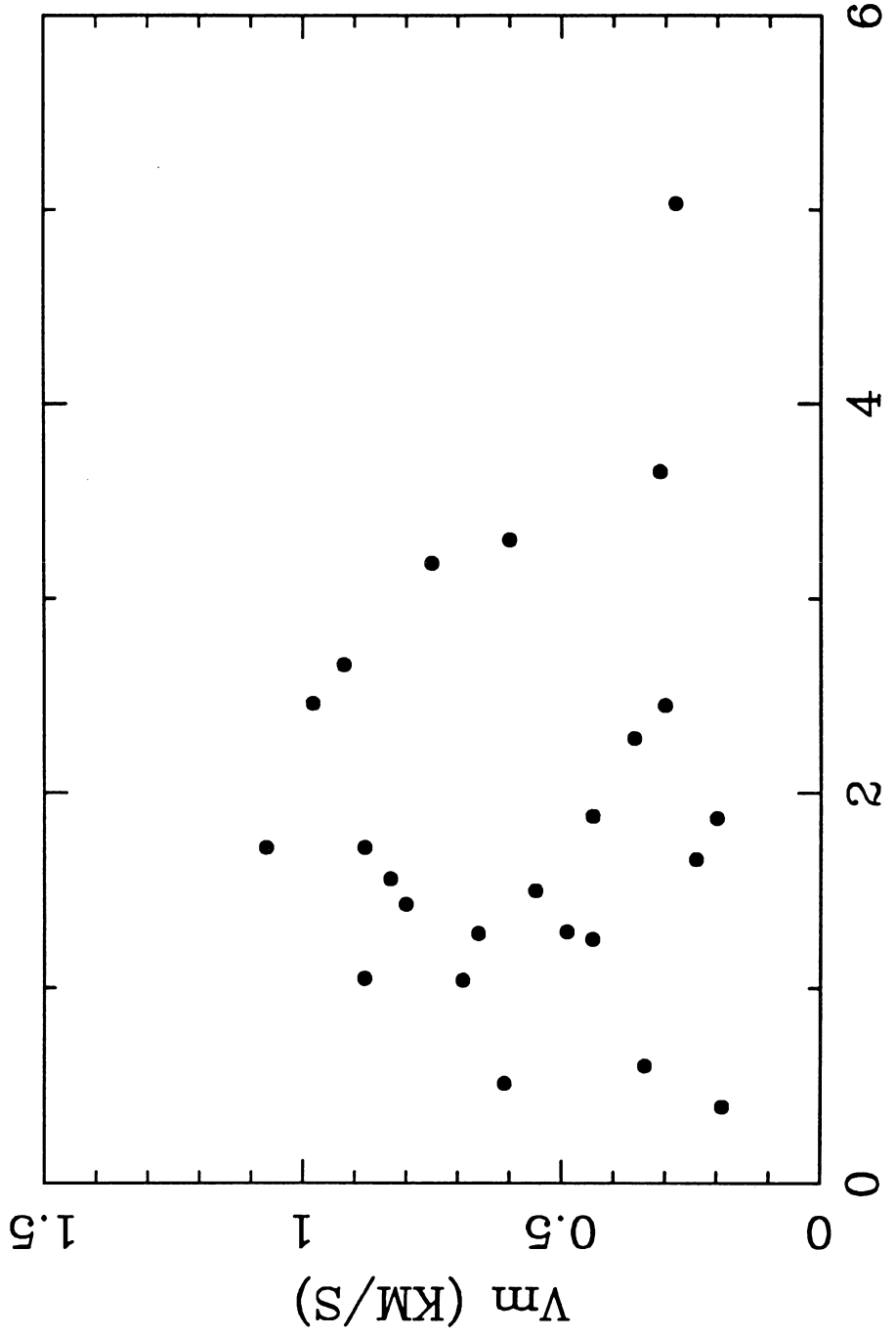

FIGURE 7

FIGURE 8

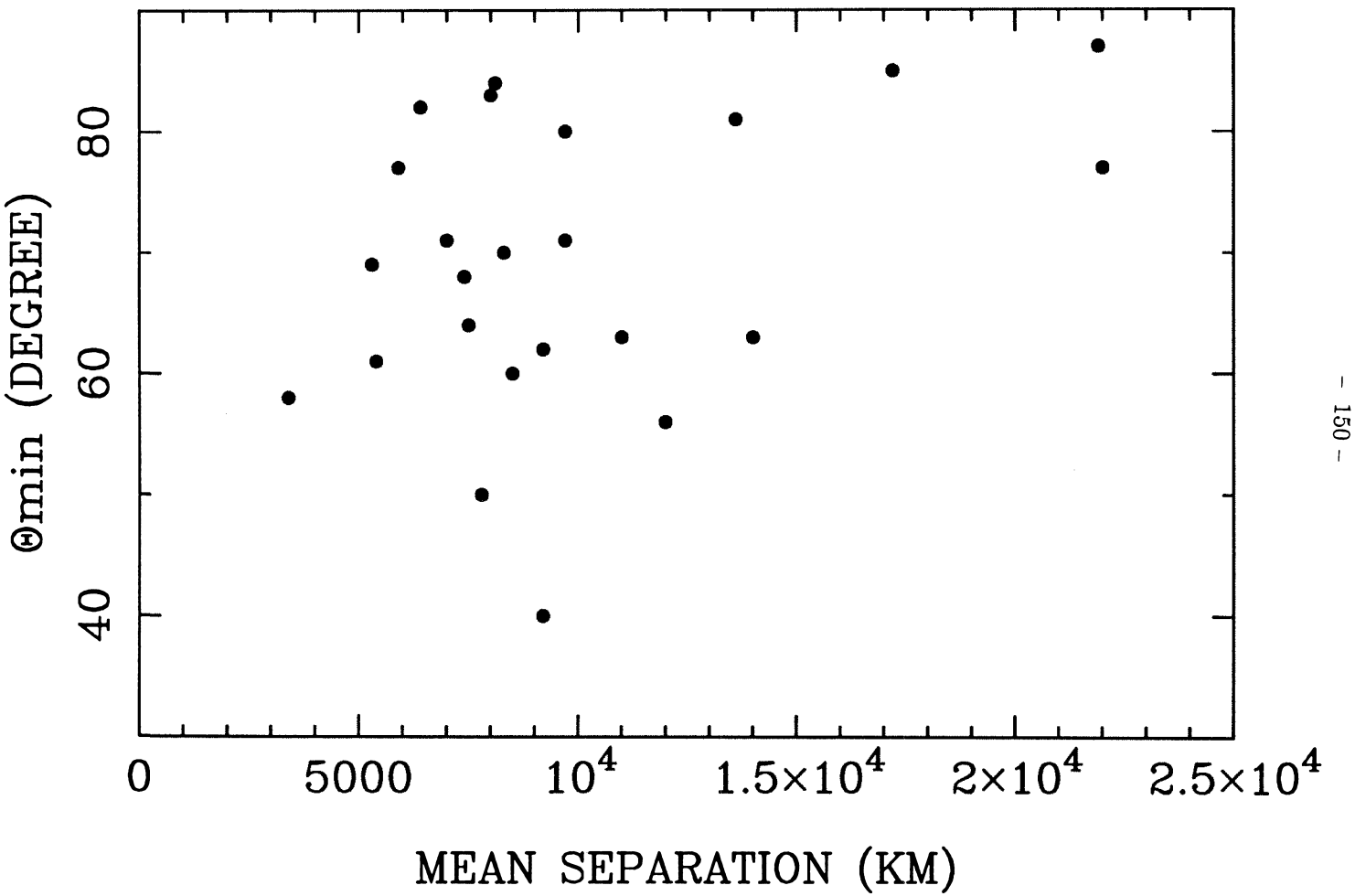
Θmin (DEGREE)
80
60
40
0
5000
10^4
1.5×10^4
2×10^4
2.5×10^4
MEAN SEPARATION (KM)

FIGURE 9

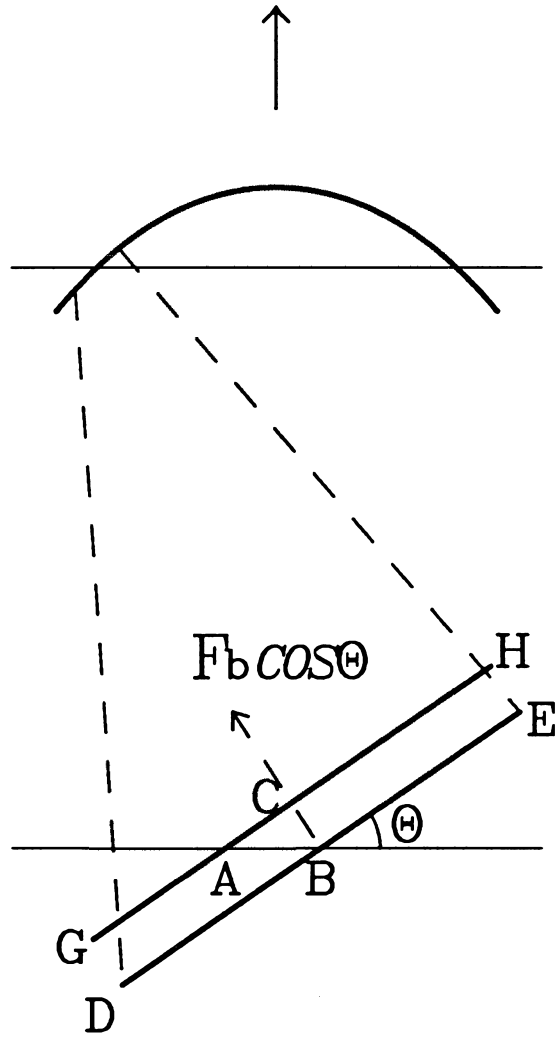

Chapter 6

The Velocity Pattern of Weak Solar Magnetic Fields

Accepted by **Solar Physics**

ABSTRACT

We have measured the proper motion of magnetic elements on the quiet Sun by means of local correlation tracking. The existence of a pattern in the intranetwork (IN) flow is confirmed. This velocity field is roughly consistent with the direct Doppler measurement of the horizontal component of the supergranular velocity field. The IN elements generally move toward the network boundaries. By tracking test points we confirm that the magnetic elements converge in areas corresponding to the magnetic network. But because the IN elements are of random polarity, they cannot contribute to the growth or maintenance of the magnetic network.

By calculating the cross correlation between the magnetogram and Dopplergram, we confirm that the supergranule boundaries and the magnetic network are roughly correlated.

1. Introduction

The supergranule velocity pattern was discovered by Hart (1954, 1956). It was first named and studied extensively by Leighton *et al.* (1962) and Simon and Leighton (1964). They described this phenomenon as the cellular convective motion. They also found a strong spatial correlation between the supergranule boundaries and several other features, e.g. chromospheric CaK, Hα networks and the network magnetic fields. Some theoretical work has been done to study the interaction of isolated magnetic flux tubes or uniformly distributed magnetic fields with convection in the Sun (Clark, 1968; Meyer *et al.* 1979; Galloway and Weiss 1981; Spruit 1981; Parker 1982; Schmidt *et al.* 1985). On theoretical grounds these authors conclude that: Uniformly distributed magnetic fields should be swept to the boundaries of the supergranules; flux tubes of magnitude $\leq 10^{19}$ Mx should follow the motion of convection pattern, while larger flux tubes would respond to the magnetic buoyancy force.

The intranetwork (IN) magnetic fields were first discovered by Livingston and Harvey (1974), who found the following characteristics: mixed polarity; flux elements as small as 5×10^{16} Mx; lifetime 5 to 90 minutes and possible radial proper motion. This paper was only an abstract with limited information.

Following the recent improvements in the videomagnetograph (VMG) system at the Big Bear Solar Observatory, a number of studies of the small-scale quiet Sun magnetic fields have been carried out, including network and IN fields, ephemeral

regions and cancelling features (Martin 1983; Wang *et al.* 1985a; Martin *et al.* 1985, Livi *et al.* 1985; Chou and Wang 1987; Zirin 1985, 1987). Zirin (1985) studied the IN elements and their possible role in replenishing elements of the quiet network. He found a mean velocity of 0.35 km/sec for elements lasting over 90 min. Martin (1987) proposed the term Intranetwork Flow (INF) for the possible systematic motion of IN elements. In general the BBSO data show the IN elements to move rectilinearly and live until they reach the network boundaries.

Title *et al.* (1987) used the SOUP instrument to obtain white light movies of the solar photosphere free of atmospheric seeing and distortion. These data permitted measurement of the supergranular flow by correlation tracking of individual granules.

In the present work we use reregistered and processed versions of Big Bear VMG movies to measure the INF by correlation tracking of magnetic elements. If we assume that the motion of the IN elements is due to local flows, then these relatively long-lived and fast moving features make excellent tracers of the flow. The cross-correlation curve between magnetic and velocity fields shows a rough relationship between the supergranule boundaries and the network magnetic fields. Local correlation tracking of IN elements confirms the cellular INF pattern.

2. Instrument and Observation

Observations were made on June 22, 1985 and October 15, 1985 with the VMG system at BBSO (Mosher 1976 and Zirin 1985). A series of VMG images of October 15, 1985 are shown in Figure 1. The contour-like curves are caused by wrapping the signal around to the opposite sign when the 12-bit memory is filled. Magnetograms were obtained by differencing 4096 pairs of Zeeman frames in the 12-bit memory and outputting the most significant 8 bits. Because of interpolation of Hα frames with the same 25-cm telescope, the interval between frames was 8-10 minutes (presently about 150 sec are required). Observations were carried out for 10 to 12 hours per day and all images were stored to both film and magnetic tape.

During the October 1985 run, simultaneous magnetograms and Dopplergrams were made at the National Solar Observatory at Kitt Peak. Because observations of longitudinal magnetic fields are best made at the disk center while the supergranular horizontal velocity is best observed near the limb, we chose a target region at a heliocentric angle of 30 degrees. The vacuum tower and 512-channel magnetograph system at Kitt Peak have been described by Livingston *et al.* (1976a, b). To correct for the 5-minute oscillation, the Kitt Peak Dopplergrams were taken at a rate of 150 seconds per scan. The scan area is 256″ by 256″, similar to the field of view at Big Bear. With the aid of Kitt Peak magnetograms, we can compare the Big Bear magnetograms and Kitt Peak Dopplergrams without difficulty.

3. Data Reduction

(a) Registration: The Big Bear magnetograms were reregistered with the Mega-vision Image Processor at Caltech. The software uses the maximum correlation principle. A few bad images were removed; solar rotation and guiding fluctuation were removed.

(b) Unwrapping and Calibration: The contour-like wraps used to extend our dynamic range were removed by software, and the magnetograms were calibrated by using measurements of solar rotation (Shi *et al.* 1985).

(c) Running Means: Four consecutive images were averaged, increasing the signal-to-noise ratio by a factor of 1.7. The sensitivity of the magnetic field measurement is increased from 5 gauss to 3 gauss over the 2×2 arc sec resolution element. Each averaged frame is equivalent to a 25-minute, 16000-frame integration magnetogram. We feel that the averaging of 4 images is an upper limit for the 1985 data. If we average more frames, the evolution and the motion of intranetwork magnetic fields would smear the image.

(d) Correction for Dopplergrams: The details of this procedure are described in another paper (Wang and Zirin 1987a). We made 4-image averages and performed spatial Fourier filtering to remove the 5-minute oscillation and other small-scale velocity patterns such as the granulation.

4. Cross-correlation of Magnetic and Velocity Fields

Previous observational and theoretical work suggested that the magnetic fields are swept to the boundaries of supergranules and form the magnetic network. Simon and Leighton (1964) used a simple sinusoidal model for the horizontal component of the supergranule velocity fields:

$$F_h(\rho) = V_h \sin(2\pi\rho/L), \tag{1}$$

where L is the cell diameter, ρ is the radius vector of a plane-polar coordinate system in the solar surface with origin at the center of the cell. Giovanelli (1980) concluded that the vertical velocity of supergranular flow at the photospheric level is ≤ 0.1 km/s. Our observations confirm this conclusion (Wang and Zirin 1987a). Also we confirm Leighton's result for the horizontal component of the supergranule velocity, i.e. the mean speed is 0.3 km/s with a peak velocity of 0.5 km/s (Leighton *et al.* 1962). So the horizontal velocity dominates the supergranular velocity fields. At the supergranule boundary, $\rho = L/2$, *i.e.* $F_h(\rho) = 0$. If the strong magnetic elements are located at the boundary of the supergranular flow pattern, the distribution of magnetic fields would have a peak at $\rho = L/2$, and the cross-correlation of magnetic field and velocity field would have a dip at $\triangle X = 0$, where $\triangle X$ is the relative shift between the two images.

In order quantitatively to describe the correlation between the supergranule boundary and the magnetic network, we calculated the cross-correlation be-

tween the magnetograms and Dopplergrams. Figure 2a shows a Kitt Peak magnetogram:Dopplergram pair made on October 15, 1985. The white and dark contours represent the receding and approaching motion respectively, while the light and dark gray levels represent the magnetic fields with positive and negative polarity. First, we converted the two images to absolute values, then we calculated the B-V cross-correlation for various relative shifts X in the direction (Figure 3), normal to the solar limb. This cross-correlation is plotted in Fig. 2b. A 13% dip in the cross-correlation coefficient appears at $\Delta X=0$, indicating that the magnetic network is roughly related to the supergranular flow. The curve has a periodic property; the distance between two maxima is the average radius of the supergranule cells. The distance is about 17,000 km giving an average cell diameter of 34,000 km, consistent with Leighton's early result (Leighton *et al.* 1962; Simon and Leighton 1964).

5. Correlation Tracking of the Intranetwork Flow

Figure 4 shows the contour map of a Big Bear magnetogram taken at 19:47 on the same day. The lighter contours represent negative polarity, and the darker, positive. Figure 5 is the local correlation tracking map for the same day, where arrows indicate the local motion derived by moving each window until the correlation between frames is maximized. It is the average map for the whole day, but 2- or 3-hour averaging gives quite similar results. Figure 4 covers about $250'' \times 250''$, so there are about 30 supergranule cell inside the field of view. Each image is di-

vided into many small windows; each window represents an indicator of the local proper motion. The size of each window should be bigger than that of individual magnetic elements. A value of about 7 arc seconds was derived from the FWHM of the auto-correlation (Wang and Zirin 1987b). That size only applies to the network elements; the IN elements are 2 arc sec or smaller. Since the flow pattern we are studying is related to the supergranulation, the window size should be substantially smaller than the size of a supergranule, about 45 arc seconds. We chose 10″ as the window size.

Tracking results for two groups of pairs, separated by 30 min and 60 min respectively, were analyzed. The results for the two time intervals were nearly the same. Figure 5 is the average of these two groups.

Figure 5 shows the resulting map of the proper motion of magnetic elements. We see a diverging flow pattern in a number of locations, some of which are marked by $\oplus$. Comparison with the movie shows that the map really presents the true motion. In Figure 6, we plot the magnetogram (Figure 4) and the tracking map (Figure 5) together. The stronger magnetic elements outline the network and almost every diverging point is located at the center of a network cell, a place of low flux. Of course, no matter which direction the IN elements move they will be pointed at the network, but the map shows that almost all arrows point to the nearest network element.

Figure 7 gives the comparison between the direct Doppler measurement of

supergranule velocity and the correlation tracking for October 15, 1985. We use the contours to represent the Doppler measurement. The east limb of the Sun is at the upper-right corner of the map. Darker contours are approaching motion, lighter contours are receding motion. So one pair of contours with a darker contour at the lower-left and lighter one at upper-right represents a single supergranule cell. The line which divides the lighter and darker contours from upper right to lower left passes through the center of a supergranule, and the opposite pair passes through the boundary. In this figure, we can see that most of the diverging points are located at the center of a supergranule cell, the converging points are located at the boundary, and the proper motion of the magnetic elements derived from correlation tracking is roughly consistent with direct Doppler measurement.

The results of another observing run made on June 22, 1985 are shown in Figure 8. This was a quiet region near the center of the solar disk, but there was no corresponding Doppler measurement. This map gives a result similar to that for October 15, 1985.

We also studied the relationship between the amplitude of the proper motion and the mean magnetic flux density. The result is shown in Figure 9. The X-axis is the average magnetic flux density in gauss of the windows defined above, and the Y-axis is the amplitude of the proper motion for that window. The major conclusion is: if the magnetic flux density is high, i.e. the network field, the upper limit of the proper motion speed decreases with the flux density. However, at low flux densities

proper motion ranges from 0 to 0.8 km/sec. This is consistent with the results of Zirin (1985): the IN elements move fast, and network elements move slowly.

The proper motion speed of INF ranges from 0 km/s to 0.8 km/s; the average speed is 0.20 km/s. If the peak of the supergranular horizontal velocity is V_h as shown in the equation 1, the average horizontal speed over the whole cell is:

$$< V >= \frac{\int_0^{2\pi} \int_0^{L/2} V_h \sin(2\pi\rho/L)\rho d\rho d\theta}{\int_0^{2\pi} \int_0^{L/2} \rho d\rho d\theta} = \frac{2}{\pi} V_h \qquad (2)$$

so the peak speed V_h is about 0.31 km/s, slightly smaller than the supergranule speed obtained by previous authors (e.g. Leighton *et al.* 1962).

Finally, we made a numerical simulation to describe the result of the flow derived from correlation tracking. We uniformly distribute one cursor per window over the field of view. We let the cursors run with the observed 2-dimensional velocity fields and made movies based on this simulation. The motion of the cursors has an obvious cellular pattern and they are swept to areas of convergence. After 20 hours, the distribution of the cursors reaches a stable state and a network is formed. But because the IN magnetic elements are of both signs, the unipolar magnetic network cannot form this way, nor can any substantial flux element be produced.

In the steady state, most of the tracers stay in the area corresponding to the stronger magnetic elements with a few exceptions. Figure 10 shows the results of

numerical simulation for October 15, 1985; Figure 10a is superposed on a magnetogram and 10b is superposed on a Dopplergram. Figure 10b gives strong evidence that the cursors (which represent the magnetic elements) are expelled from the strong velocity region and swept to the boundary of the supergranule cells. Figure 11 shows the result for June 22, 1985.

6. Summary and Discussion

By correlation tracking of intranetwork magnetic elements on Big Bear magnetograms, we have confirmed a flow pattern roughly consistent with the supergranule velocity field. We also found a quantitative relation between the supergranule boundaries and the magnetic network using cross-correlation.

By simulation we confirmed that the intranetwork magnetic fields are swept to the boundary of the supergranule by the INF implying the magnetic network elements are confined by the supergranular flow. But this does not mean that the network elements themselves are formed by the concentration of the IN elements. The IN fields are usually of mixed polarity, each element having flux about 5×10^{16} to 10^{17} Mx (Livingston and Harvey 1974; Wang *et al.* 1985b). The network elements have typical flux 5×10^{18} Mx. If the network is formed by the concentration of the intranetwork elements, 10 to 100 elements with the same polarity must be collected. The probability of one element meeting another with the same polarity is 50%, so the probability that an element will meet 50 to 100 other elements with the same

polarity is essentially zero.

We studied the formation and disappearance of the network elements from the VMG movies and found that of the 50 network elements that existed at the beginning of the observation, eight cancelled with other opposite polarity fields, two fragmented to little elements, and the rest of them retained their identity. Also, we found nine new elements formed from ephemeral regions, and two from the concentration of diffuse fields. To avoid bias in selecting the ephemeral regions and cancelling features, we ran the movie forward to study the disappearance of old magnetic flux elements, and backward to study the emergence of the new flux. Thus the network is not formed by the supergranule flow, but the concentration of the network may be maintained. The detail of the magnetic flux budget and the properties of the ER and cancelling features will be discussed in another paper.

Although in general the motion of the magnetic fields follows the supergranule pattern, some flux tubes with larger flux may move under its buoyancy force. The ephemeral regions separate at about 0.6 km/sec (Zirin 1985), regardless of the local flow.

We should point out that the random rectilinear motion of IN elements, which cannot pass through the network, will invariably lead to the result of a simulated accumulation near the network. But the fact that most of the elements we followed did move toward the cell boundaries supports the idea that the IN elements follow the supergranular flow.

The fact that the elements follow the supergranular flow is in itself interesting. If the IN elements were shallow, they would be linked by field lines to other elements of the opposite polarity which should be seen to move with them. Instead we see individual elements of one sign or the other, which suggests that the elements are the intersection of fairly deep lines of force with the surface. It is also of interest that the moving elements show no random perturbations as might be due to exploding granules.

Acknowledgments

We are indebted to Dr. S. F. Martin for many helpful comments, discussion and suggestions. We wish to thank the Big Bear staff for the support in observation, Dr. B. Popp for his computer programs and J. Nenow for processing films. Also we are grateful for the assistance from National Solar Observatory/Kitt Peak, especially Drs. J. Harvey and K. Harvey for their valuable suggestions and F. Recely for his help in observation. This work is supported by NSF under grant ATM-8513577 and NASA under grant NGL 05 002 034.

References

Chou, D. and Wang, H. 1987, *Solar Physics* **110**, 81.

Clark, A. Jr. 1968, *Solar Physics* **4**, 386.

Galloway, D.J. and Weiss, N.O. 1981, *Ap. J.* **243**, 945.

Giovanelli, R.A. 1980, *Solar Physics* **67**, 211.

Hart, A.B. 1954, *Monthly Notice of Roy. Astro. Soc.* **114**, 2.

Hart, A.B. 1956, *Monthly Notice of Roy. Astro. Soc.* **116**, 38.

Leighton, R.B., Noyes, R.W. and Simon, G.W. 1962, *Ap. J.* **135**, 474.

Livi, S.H.B., Wang, J. and Martin, S.F. 1985, *Australian Journal of Physics* **38**, 855.

Livingston, W.C. and Harvey, J. 1975, *AAS Bull.* **7**, 346.

Livingston, W.C., Harvey, J., Pierce, A.K., Schrage, D., Gillespie, B. Simmons, J. and Slaughter, C. 1976a, *Applied Optics.* **15**, 33.

Livingston, W.C., Harvey, J., Slaughter, C. and Trumbo, D. 1976b, *Applied Optics* **15**, 40.

Martin, S.F. 1983. BBSO Preprint No. 228.

Martin, S.F. 1987. *Presentation on Solar Cycle Workshop, Lake Tahoe.*

Martin, S.F., Livi, S.H.B. and Wang, J. 1985, *Australian Journal of Physics* **38**, 929.

Meyer, F., Schmidt, H.U. and Simon, G.W. 1979, *Astro. and Astrophys.* **76**, 35.

Mosher, J.M. 1976. *BBSO Preprint* No. 159.

Parker, E.N. 1982, *Ap. J.* **256**, 746.

Schmidt, H.U., Simon, G.W. and Weiss, N.O. 1985, *Astro. and Astrophys.* **148**, 191.

Simon, G.W. and Leighton, R.B. 1964, *Ap. J.* **140**, 1120.

Shi, Z., Wang, J. and Patterson, A. 1986. *BBSO Preprint* No. 257.

Spruit, H.C. 1981, *Astro. and Astrophys.* **98**, 155.

Title, A.M., Tarbell, T.D. and SOUP Team 1986, *AAS Bull.* **18**, 992.

Wang, H. and Zirin, H. 1987a., in preparation.

Wang, H. and Zirin, H. 1987b, in preparation.

Wang, J., Shi, Z., Martin, S.F. and Livi, S.H.B. 1985a. Submitted to Solar Physics.

Wang, J., Zirin, H. and Shi, Z. 1985b, *Solar Physics* **98**, 241.

Zirin, H. 1985, *Australian Journal of Physics* **38**, 961.

Zirin, H. 1987, *Solar Physics* **110**, 101.

Figure Captions

Fig. 1 The time sequence Big Bear magnetograms made on October 15, 1985.

Fig. 2a A Kitt Peak magnetogram and the simultaneous Dopplergram. The contours represent the velocity fields and the gray scales represent the magnetic fields. They were made at 17:30 UT, October 15, 1985.

Fig. 2b Velocity and magnetic fields correlation curve.

Fig. 3 Schematic map to explain the geometric direction of the Doppler gram.

Fig. 4 Contour map for the magnetogram made on October 15, 1985.

Fig. 5 The local correlation tracking map; the arrows represent the local proper motion velocity, their length proportional to the speed.

Fig. 6 Combination of the Figures 4 and 5, showing a tendency for the IN elements to move to the nearby network elements.

Fig. 7 Comparison of the Doppler measurement and the correlation tracking. The contours are the supergranule velocity fields, arrows represent the correlation tracking map.

Fig. 8 The correlation tracking with the magnetogram contour map for June 22, 1985.

Fig. 9 The proper motion speed of magnetic elements via the average magnitude of magnetic flux density.

Fig. 10 Results of numerical simulation of the correlation tracking velocity fields for October 15, 1987. 10a is superposed on a magnetogram, 10b is superposed on a Dopplergram.

Fig. 11 Results of numerical simulation for June 22, 1985. It is superposed on a magnetogram.

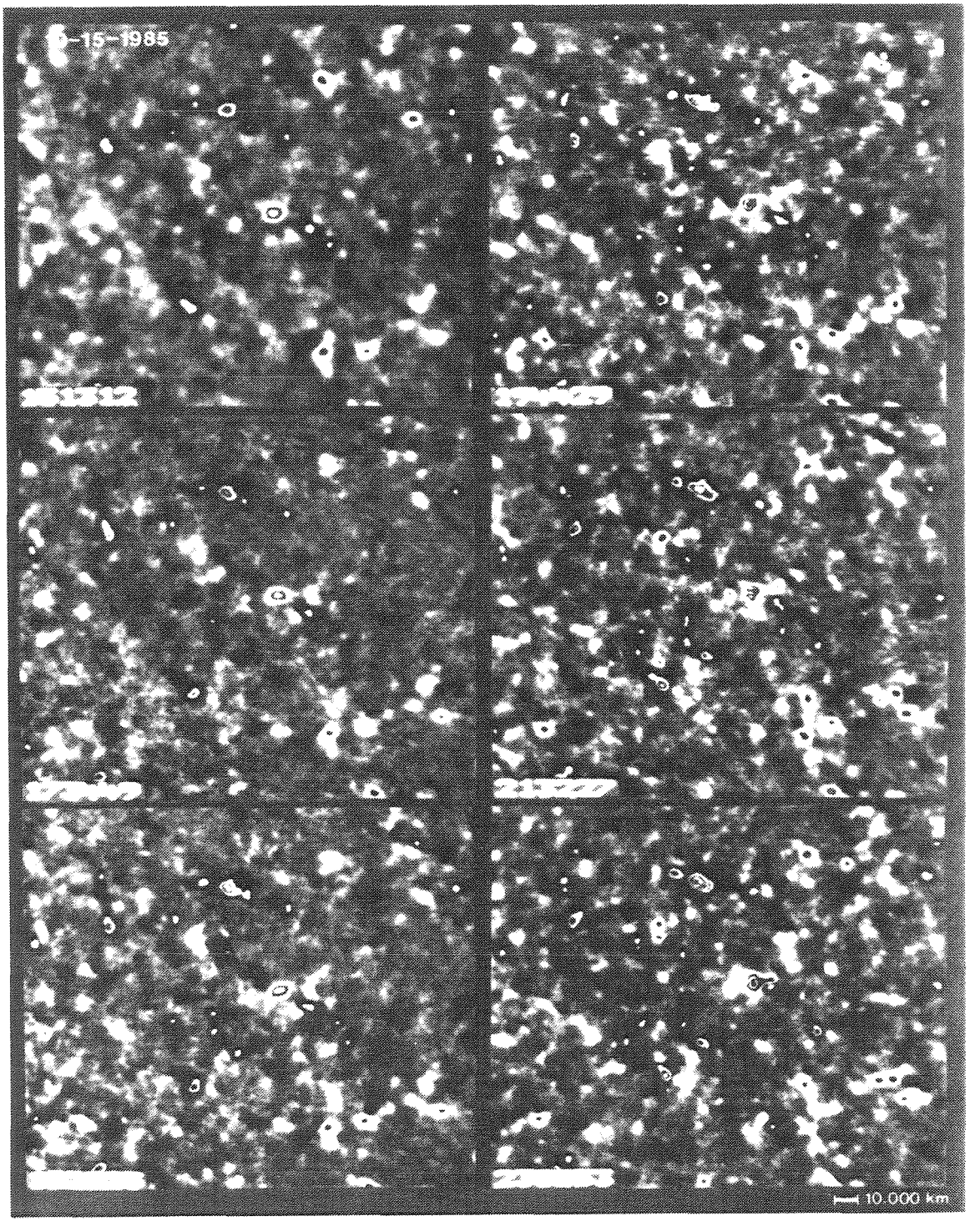

FIGURE 1

FIGURE 2a

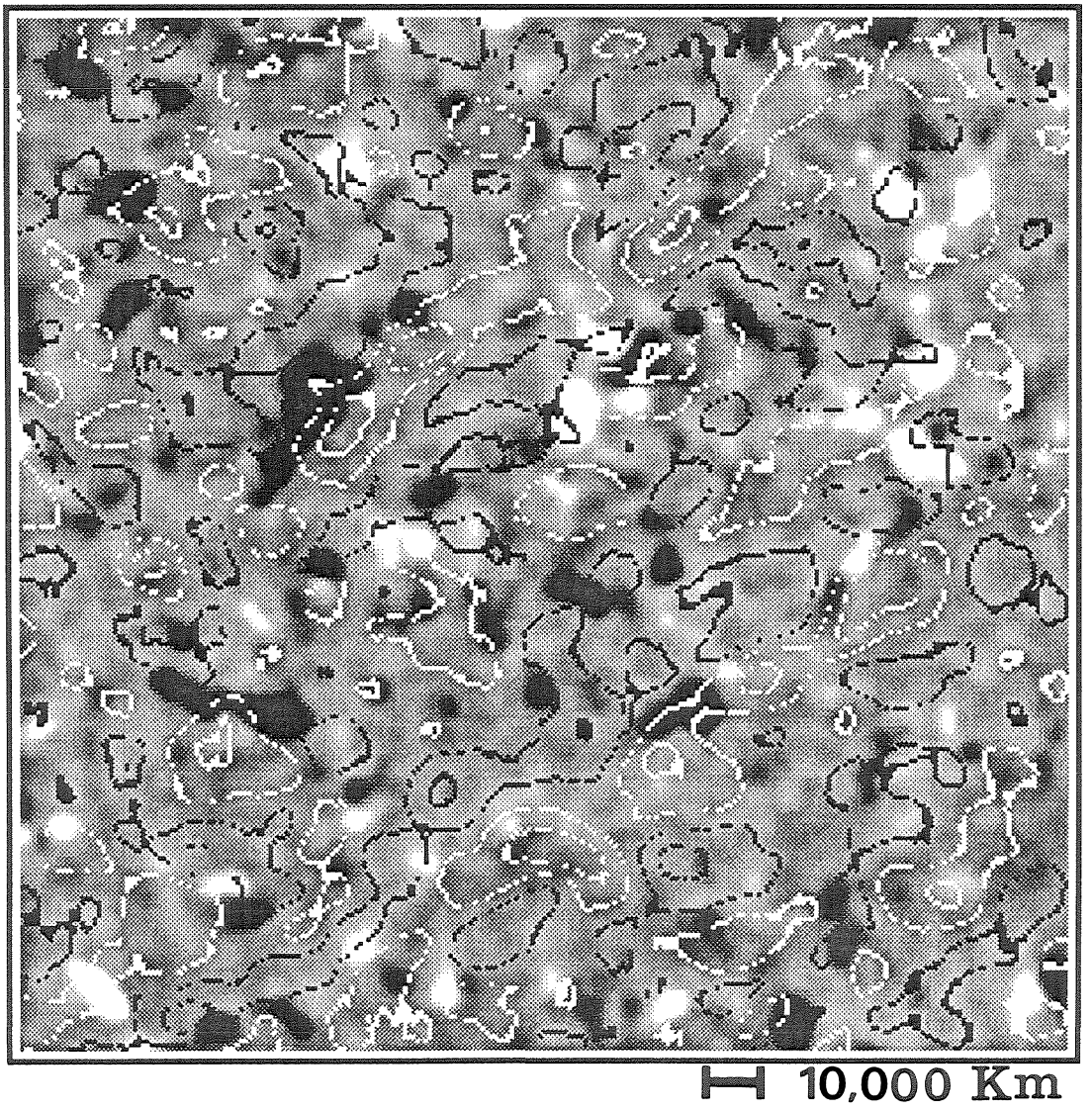

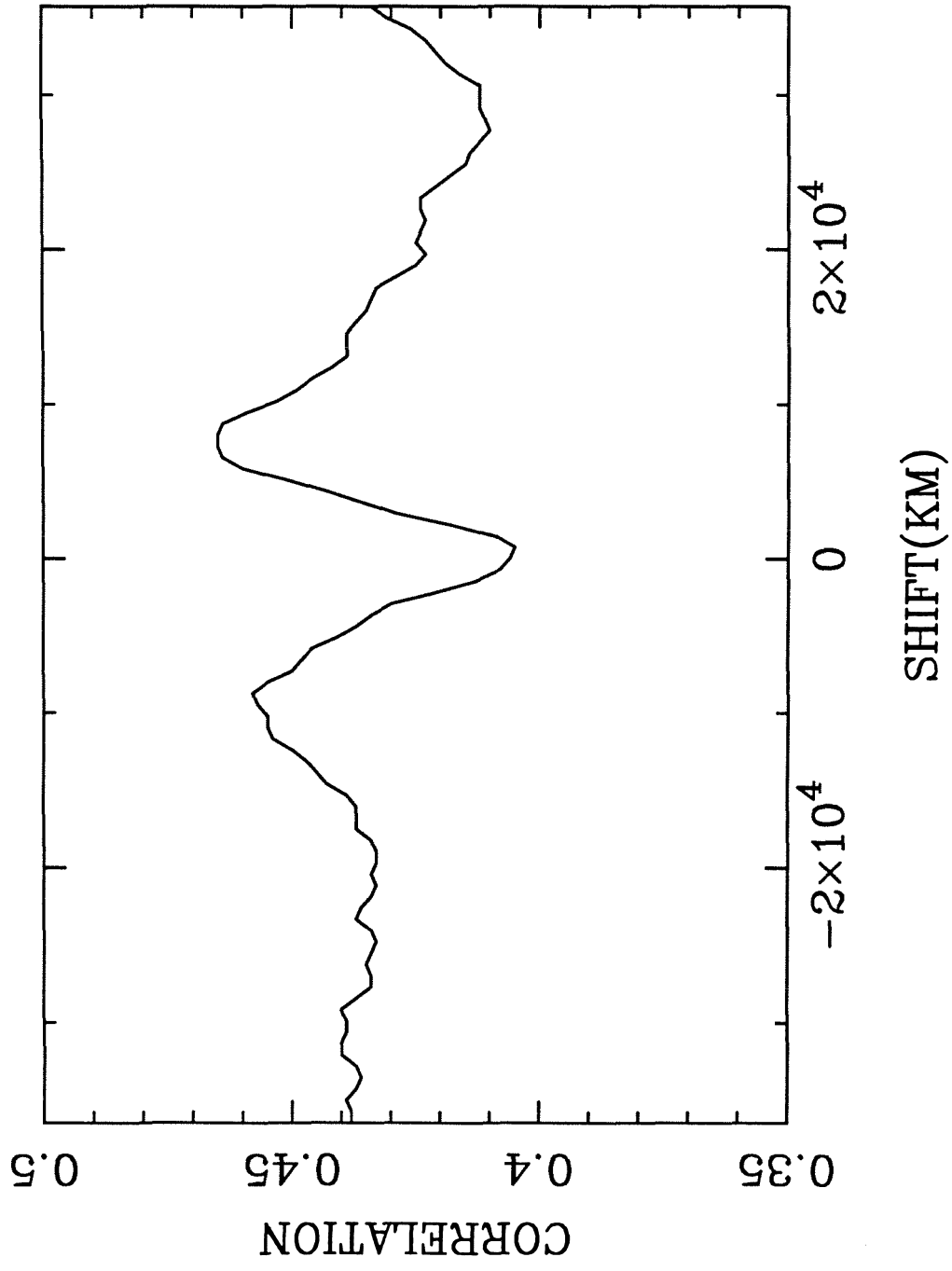

FIGURE 2b

FIGURE 3

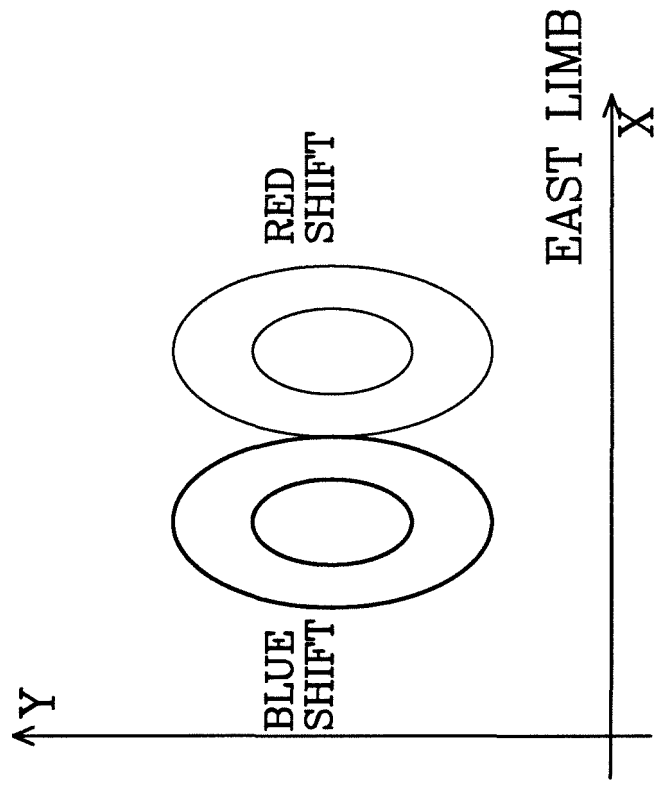

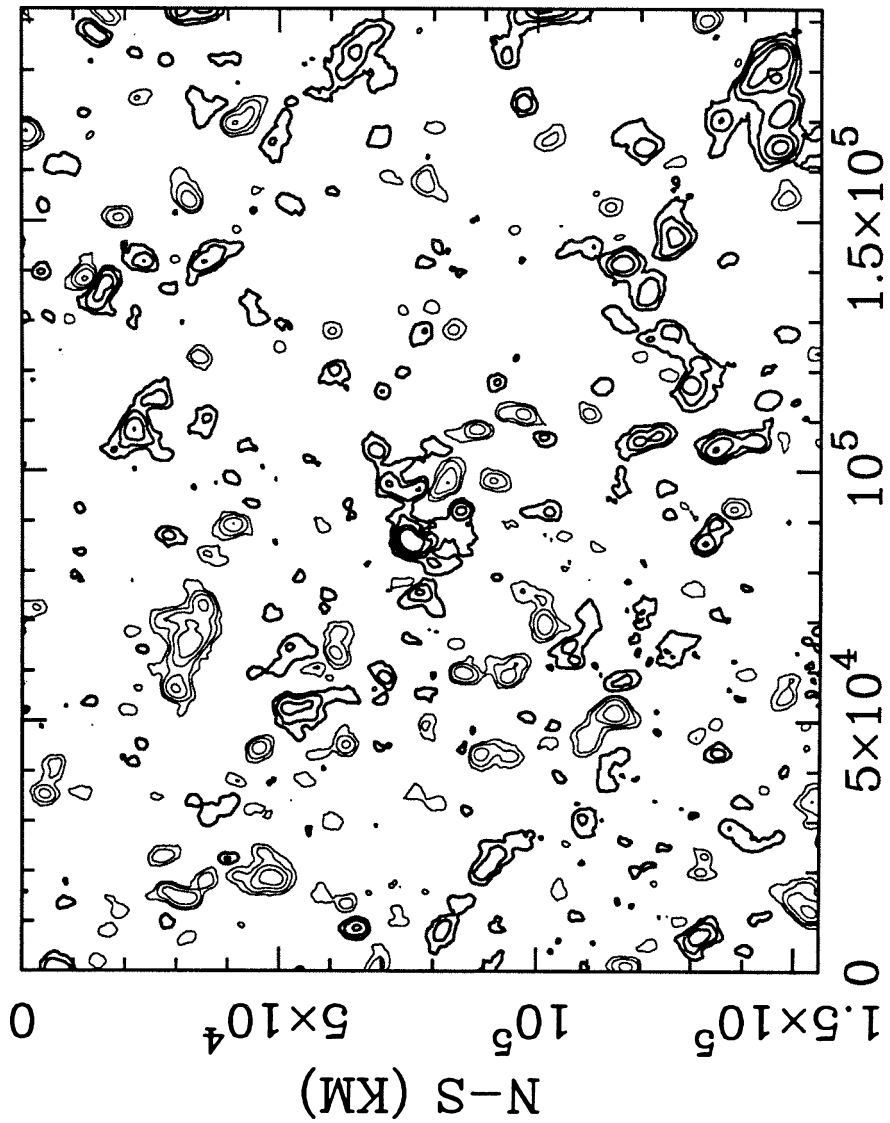

FIGURE 4

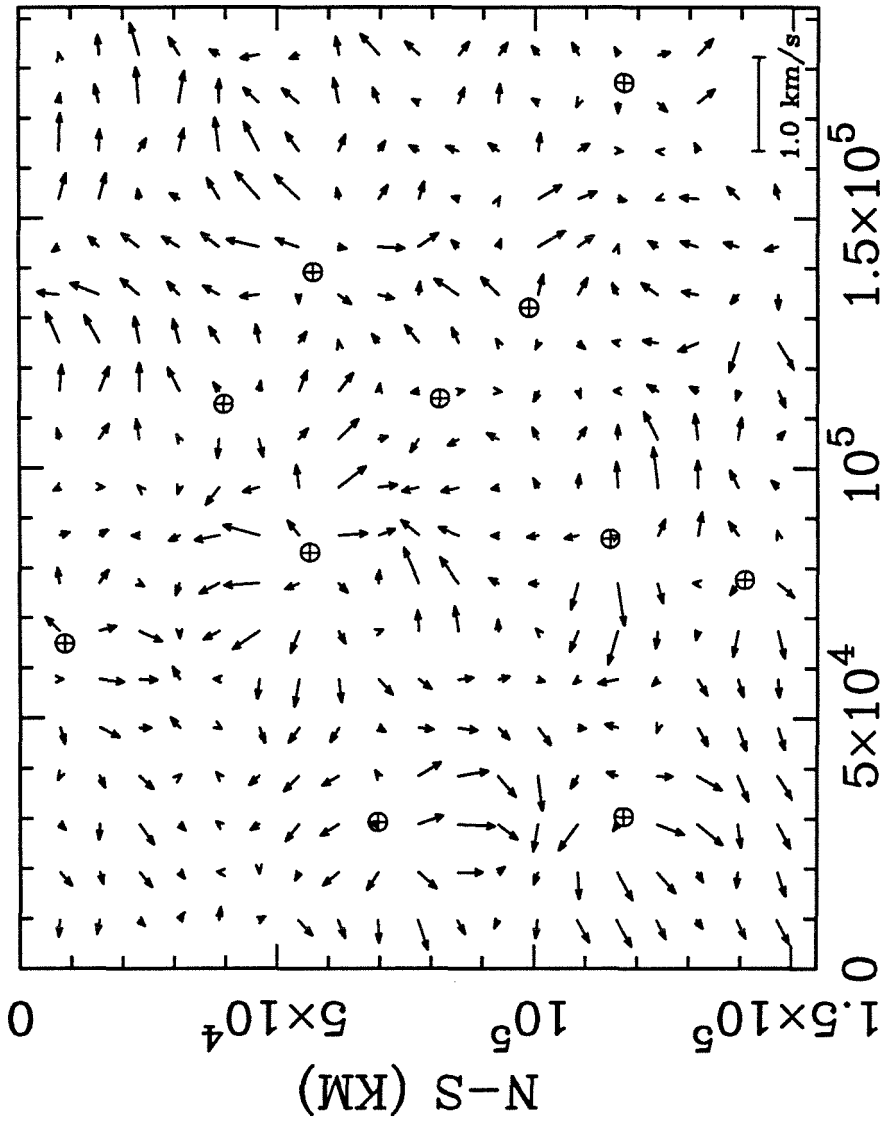

FIGURE 5

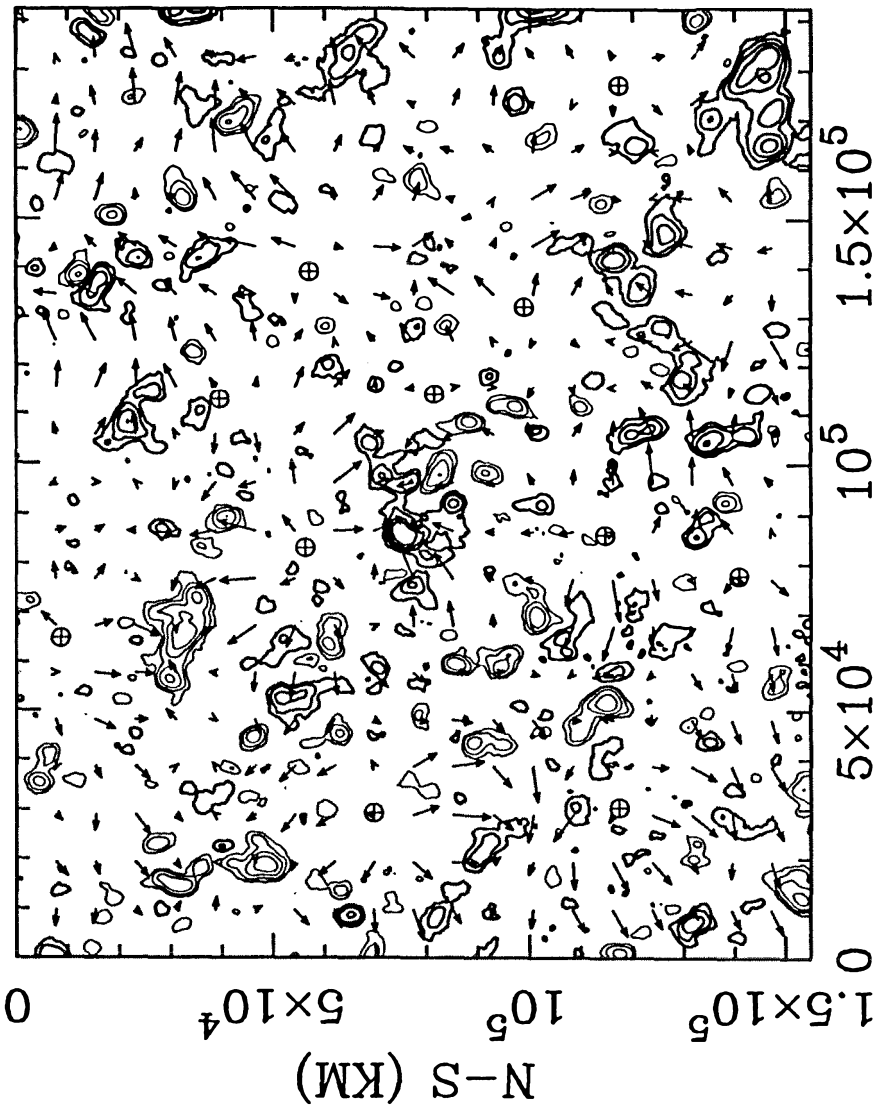

FIGURE 6

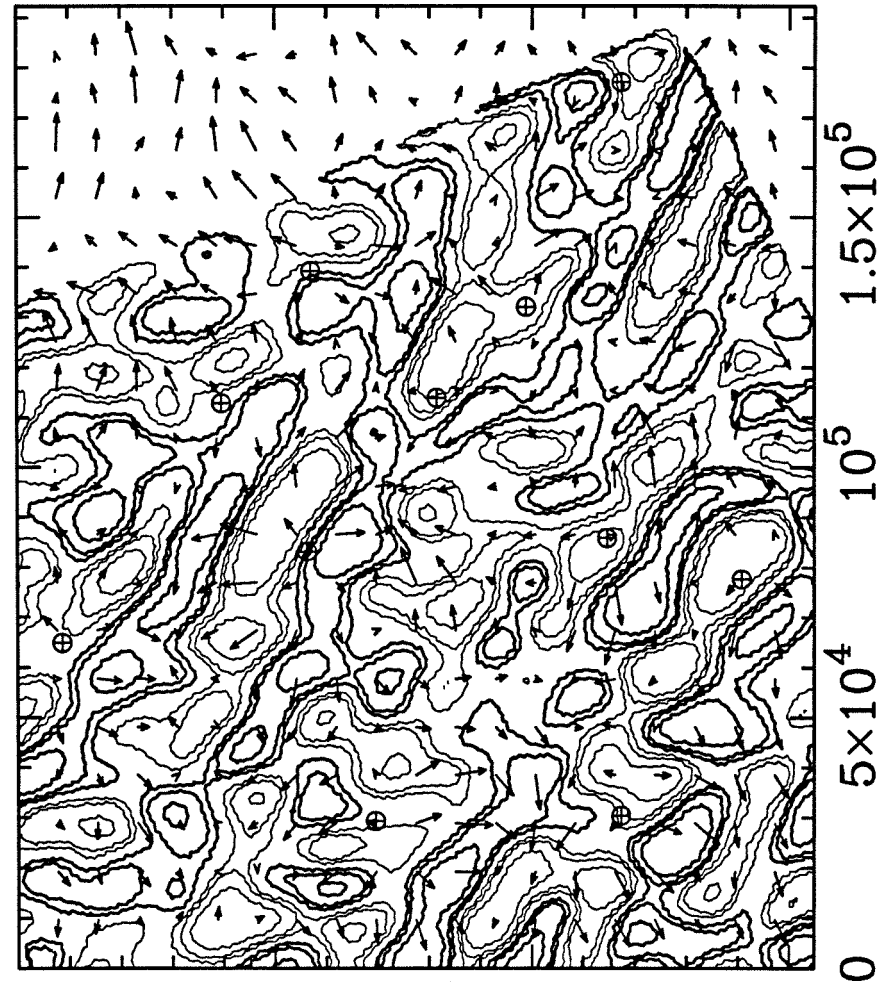

FIGURE 7

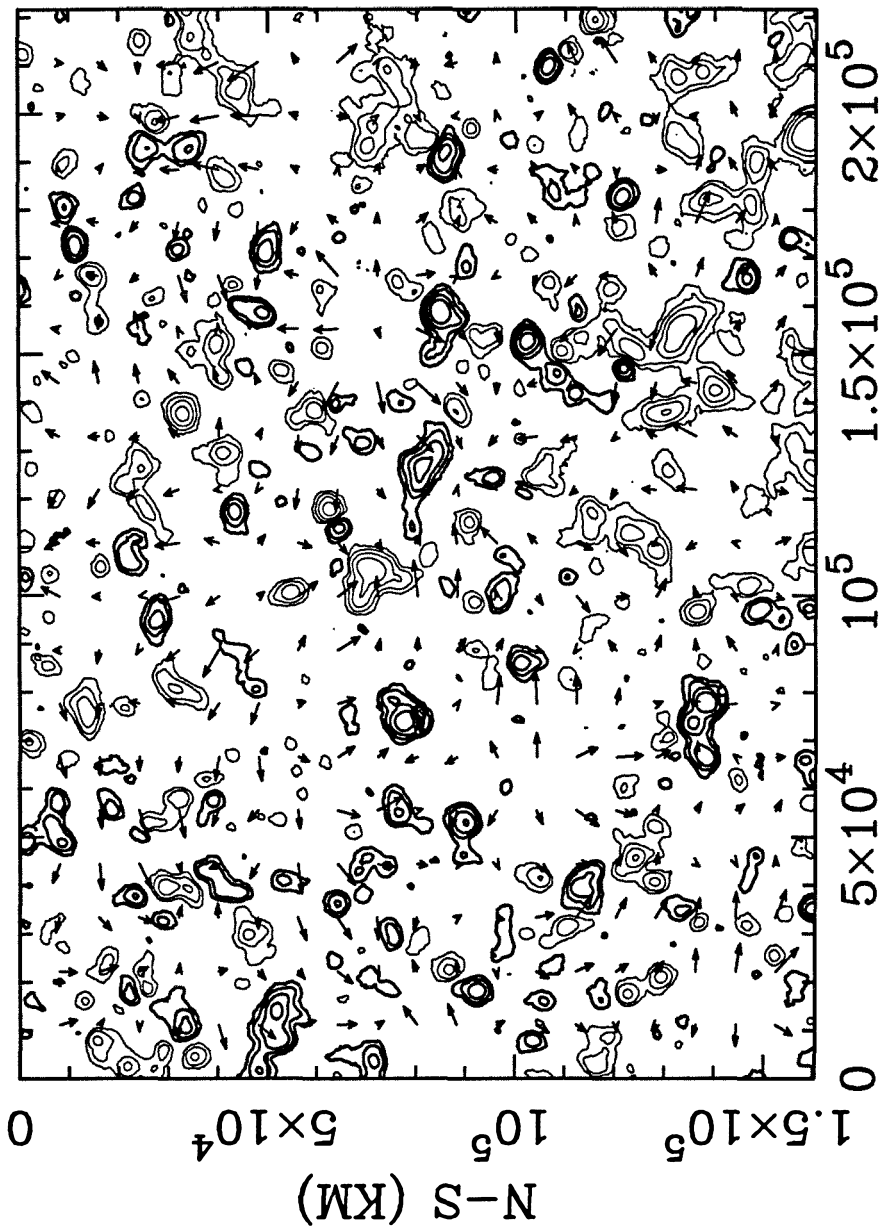

FIGURE 8

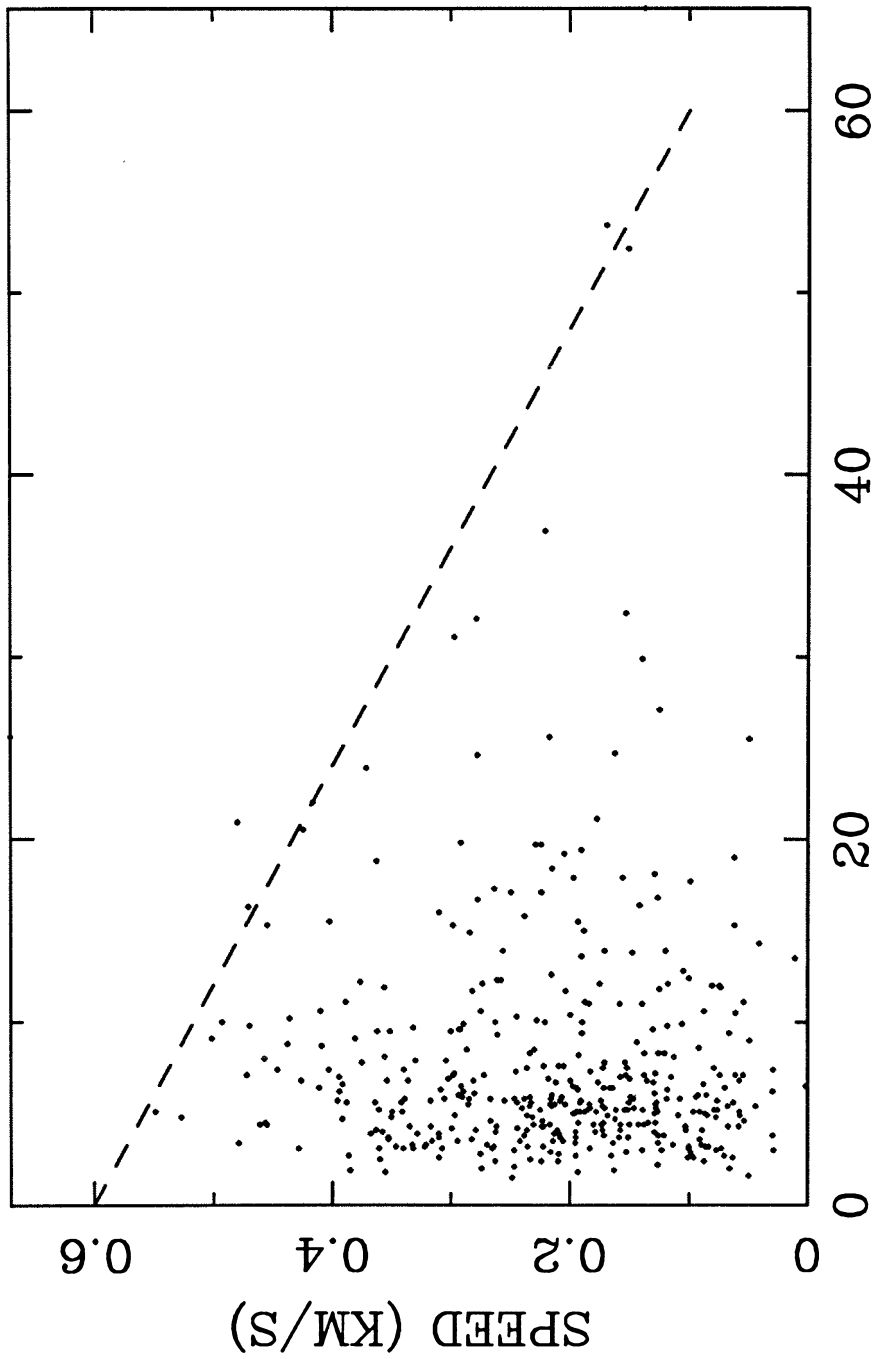

FIGURE 9

FIGURE 10a

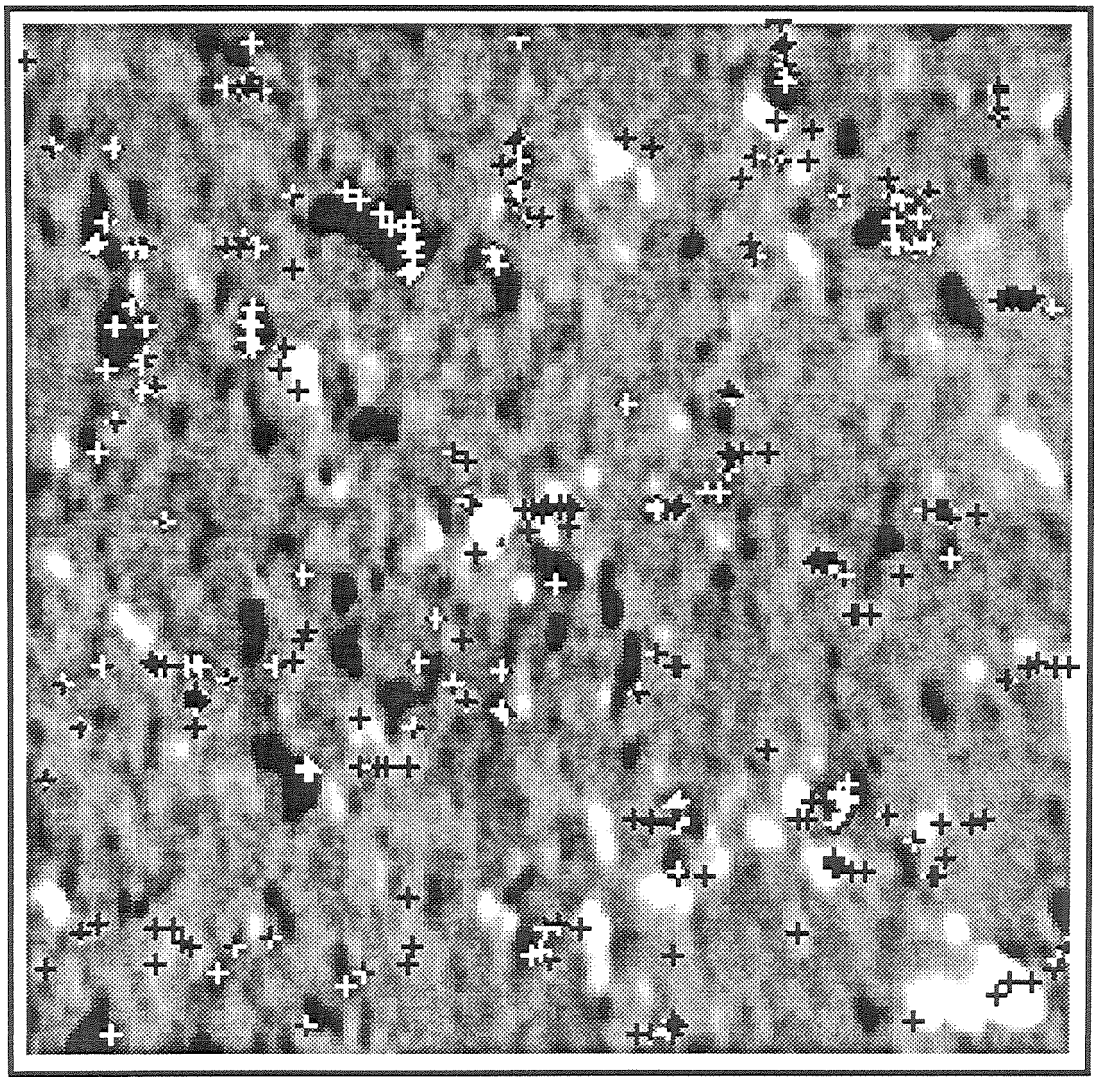

FIGURE 10b

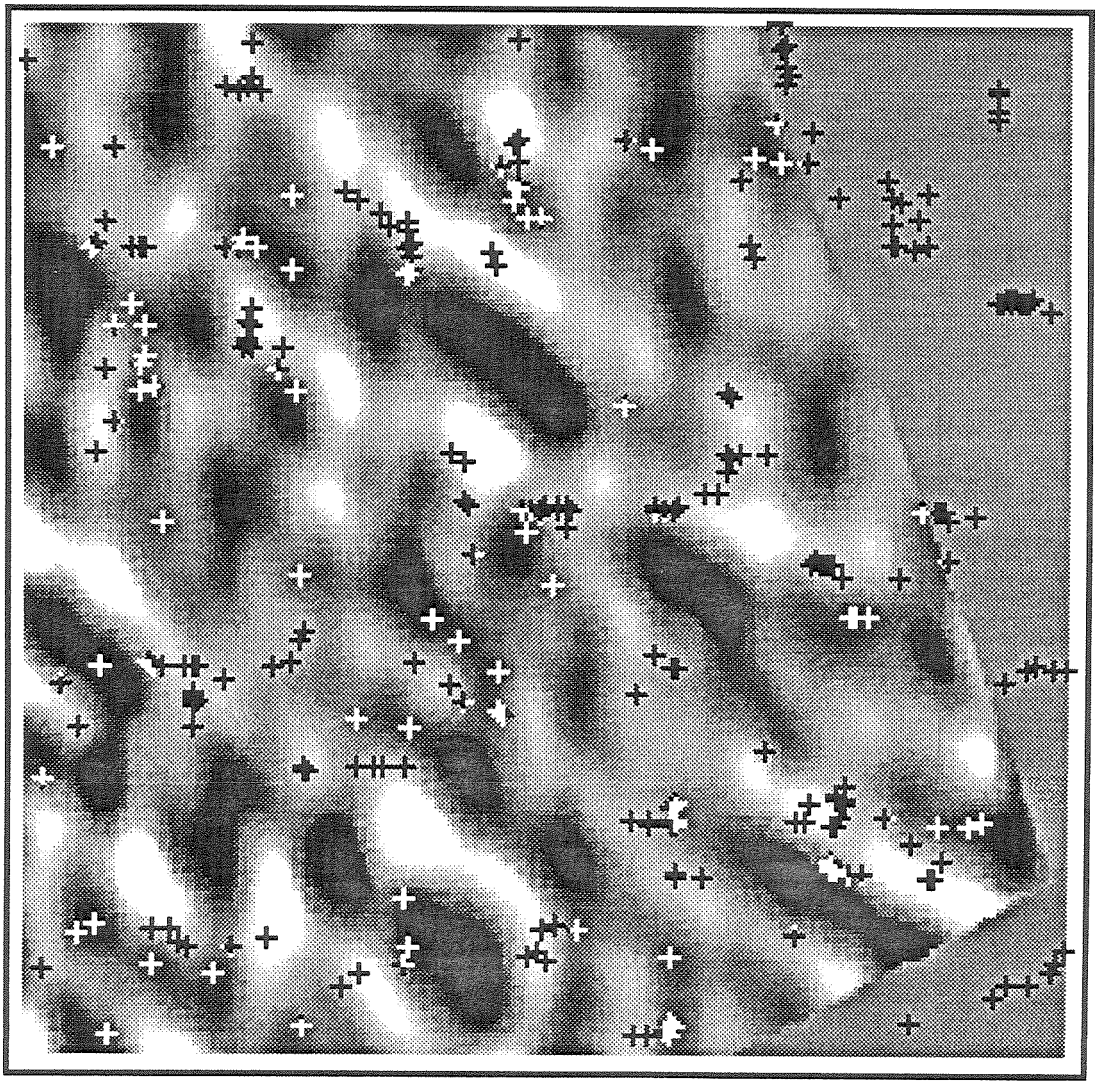

FIGURE 11

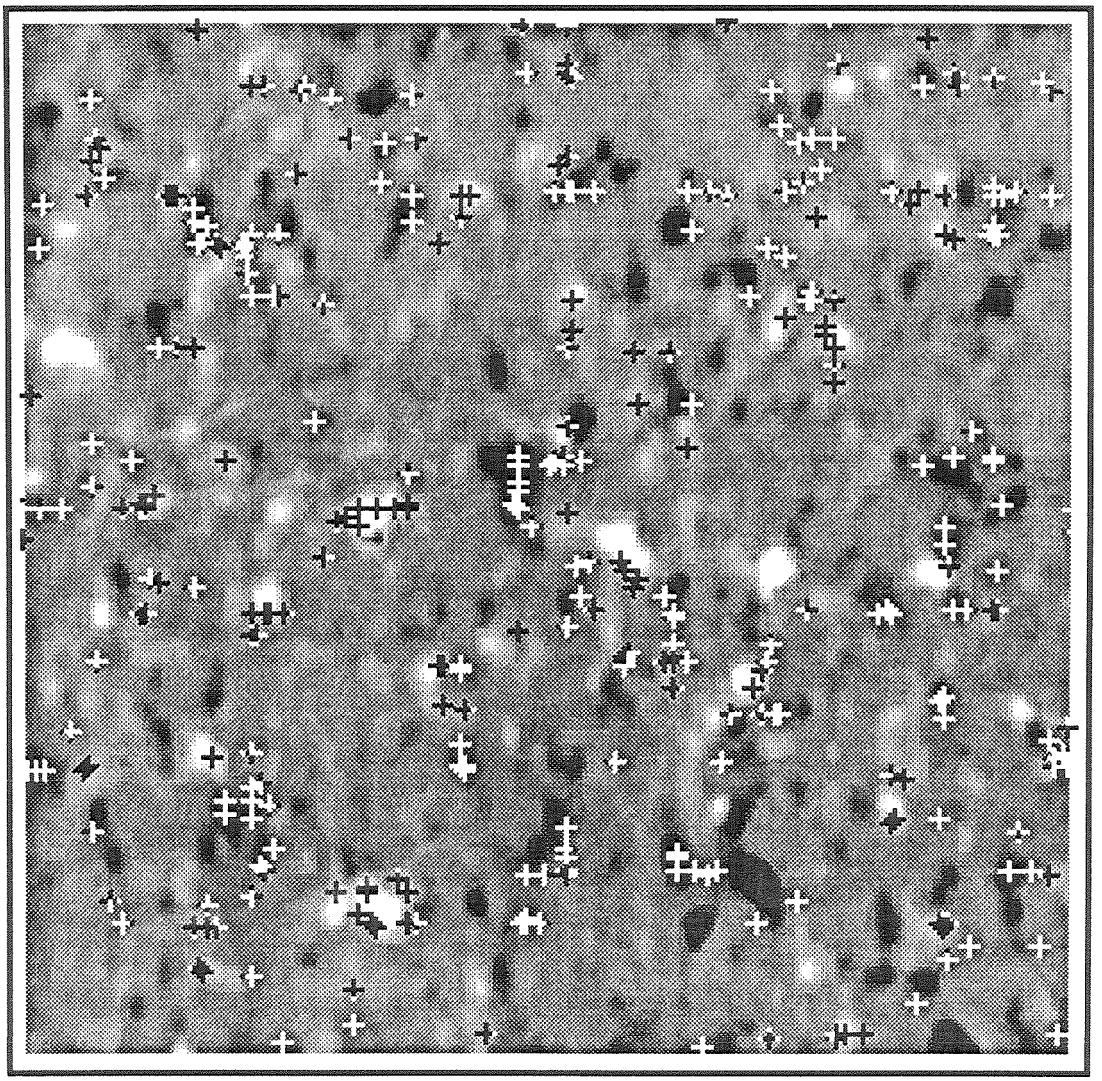

Chapter 7

On the Relationship Between Magnetic Fields and Supergranule Velocity Fields

To be submitted to **Solar Physics**

ABSTRACT

We studied the size, correlation lifetime and horizontal velocity amplitude of supergranules in regions with different magnetic activity. We found that the supergranule velocity cells have similar scale, correlation lifetime and horizontal velocity amplitude in the unipolar enhanced magnetic network regions and in the mixed-polarity quiet sun. However, the correlation lifetime of magnetic structure is much longer in the enhanced network. We investigated the velocity pattern of moving magnetic features(MMF) surrounding a decaying sunspot. The velocity of MMFs is consistent with the outflow surrounding the sunspot as measured by Dopplergrams. The velocity cell surrounding the sunspot has a much larger velocity amplitude and a longer lifetime than regular supergranule cells. We also concluded that ephemeral regions(ER) have a slight tendency to emerge at or near boundaries of supergranules. Almost all the magnetic flux disappears at the supergranule boundaries. In most cases, two poles of cancelling features with opposite magnetic polarities approach along the boundaries of supergranules.

1. Introduction

Supergranulation was first studied extensively by Leighton *et al.* (1962). The general properties of supergranules were reviewed and studied further by us in another paper (Wang and Zirin, 1988). We also studied in detail the structure and velocity pattern of small scale magnetic fields on the quiet sun (Wang and Zirin 1987, Wang 1988). The task of this paper is to provide observational information about the interaction between the magnetic fields and supergranule velocity fields.

The problem of interacting magnetic fields and convective velocity fields has been studied by a number of theorists (Spruit 1984; Clark 1968; Galloway and Weiss 1981; Meyer *et al.* 1979; Schmidt *et al.* 1985). This problem has two aspects: (1) the formation of fluxtubes by the interaction of a weak diffuse field with convection and (2) the interaction of already established fluxtubes with the convective flow. With regard to (1), Clark (1968), for example, calculated the motion of chromospheric fields under the influence of supergranule velocity fields. He concluded that magnetic fields are channeled by supergranule velocity fields. Those channeled fields might correspond to the network magnetic fields. Galloway and Weiss (1981) discussed the concentration of magnetic flux into isolated ropes in the turbulent convective zones of the sun or other late type stars. The diffuse magnetic fields are swept to the boundaries of convection cells after a few turn-over times. Regarding (2), Schmidt *et al.* (1985, Meyer *et al.* 1979) constructed 2-D and 3-D models to study isolated magnetic fluxtubes and convection in the sun. They concluded that small

fluxtubes are swept to the boundaries, while larger, more buoyant tubes are dragged to the axis of a convection cell. New flux emerges at the center of the cell. However, none of these models considered the effect of convective motion on mixed polarity magnetic fields.

Naturally, study of the locations of various magnetic features within a convection cell could provide some observational test of theories of interaction between magnetic fields and convection velocity fields. For example, Leighton *et al.* (1962; Simon and Leighton 1964) found the magnetic network which corresponds to the supergranule boundaries. To understand the physical processes occurring in ERs and cancelling features we need to know the relationship of these features to supergranules. ERs are small bipoles which emerge with a typical flux of 10^{18} Mx to 10^{20} Mx. They were first extensively studied by Harvey and Martin (1973; Martin and Harvey, 1979). Cancelling features are major sources of flux disappearance on quiet sun. They have been studied in detail by members of the Caltech group (Martin, 1984; Livi *et al.* 1985; Martin *et al.* 1985; Zirin 1985, 1987). Howard *et al.* (1979) studied the birthplaces of active regions and of X-ray bright points which were believed to correspond to ephemeral regions. They concluded that the X-ray bright points emerged randomly throughout the CaK network. Active regions emerged at the boundaries of network cells. They also suggested that the magnetic flux of active regions comes from deeper in the convection zone than the flux that gives rise to bright points.

Moving magnetic features (MMF) are also relevant to the interaction of magnetic fields with convection. MMFs are magnetic features which flow radially away from well developed sunspots (Vrabec, 1974; Harvey and Harvey, 1973; Sheeley, 1969). Meyer *et al.* (1974) gave a theoretical explanation of MMFs as follows: because of its strong magnetic fields, the spot inhibits normal convection causing the upflow to be diverted radially outward from the sunspot.

In this paper we will first discuss the locations of ERs and cancelling features relative to the supergranules. Then we will present the results of the study of the MMFs using simultaneous Dopplergrams, magnetograms and CaK filtergrams. We will also discuss the size, correlation lifetime and horizontal velocity amplitude of supergranules in regions with different types of magnetic activity.

2. Observation and Data Reduction

The data we used for this paper were obtained on Oct. 15-16, 1985 (quiet region); May 11-15, 1986 (quiet region); Sept. 18-19, 1987 (enhanced network region) and Oct. 15-16, 1987 (decaying spot). The magnetograms were obtained simultaneously at Big Bear Solar Observatory (BBSO) and at the National Solar Observatory, Kitt Peak (NSO/KP). Dopplergrams were obtained at NSO/KP at a rate of 1 image per 2.5 minutes. A Kitt Peak Type 1 scan was used in an area 256"× 360". Observations for each day lasted 6 to 8 hours at NSO/KP, 10 to 12 hours at BBSO.

The BBSO videomagnetogram(VMG) system, data collection and calibration have been discussed in other papers (Wang and Zirin 1987; Wang 1988 and the references therein). The NSO/KP data collection, calibration, image averaging and filtering were also described in a previous paper (Wang and Zirin 1988). Since the magnetic field observation has the best sensitivity at the center of the disk and the horizontal velocity of supergranules can be seen best near the limb, the targets we selected are within θ=30°to θ=50°, where θ is the heliocentric angle.

During the October 1987 run, broad band CaK data were obtained with the 26" telescope at BBSO. The video images were recorded by a Super-VHS video recorder. The best images were selected and digitized by a Megavision Image Processor System at a rate of roughly 1 image per 5 minutes. This technique was also used for the white light granulation movie study (Zirin and Wang, 1987).

3. ERs, Cancelling Features and Supergranule Velocity Fields

It is generally believed that quiet sun magnetic fields are closely related to solar convection. ERs and cancelling features are two important magnetic phenomena on the sun (Harvey and Martin 1973; Martin and Harvey 1979; Martin 1984; Livi *et al.* 1985). The study of the positions of these features relative to the supergranule velocity fields may shed light on the physical processes behind those features. Frazier (1972) proposed that the magnetic flux is carried to the solar surface by supergranule motion. If Frazier's theory is true, ERs should emerge near the centers

of supergranules.

On the quiet sun, the network usually is not well defined, due to the scarcity of flux elements. Therefore, VMG or CaK data alone are not sufficient to determine the locations of ERs and cancelling features with respect to supergranule boundaries. Simultaneous Dopplergrams are also needed. We found that an effective way to study ER locations is to make magnetogram movies with Dopplergrams superposed on them (Wang and Zirin 1988). Dopplergrams were plotted as contour maps, magnetograms as gray scale maps. From the movies, we have the impression that most ERs emerged at the boundaries of supergranules. Figure 1 shows an ER emerging at the boundary of a supergranules.

In Figure 2, we plot the distribution of ERs as a function of R, the distance between the location of ER emergence and the nearest supergranule cell center in units of the radius of the cell. Thirty-one ERs, selected from six days of observation, whose location can be identified clearly were included in the histograms If we count ERs within the bin between R=0.9 and R=1.0 as ERs emerged at the supergranule boundaries, then twenty six, i.e. 84%, of ERs emerged at or near the supergranule boundaries.

One question needs to be answered before we can draw any conclusion from Figure 2: i.e., how many ERs would be in the bin between R=0.9 and R=1.0 if ERs emerge randomly relative to supergranules? When Howard *et al.* (1979) compared the X-ray photographs and CaK spectroheliograms, they found that 76% of

X-ray bright points, which were believed to represent emergence of ERs (Golub *et al.*, 1974), are located on or adjacent to Cak network cell boundaries. However, when Howard *et al.* did a random distribution test by misaligning X-ray and CaK images, 69% bright points remained on or adjacent to cell boundaries after misaligning. They therefore concluded that the X-ray bright points tend to emerge randomly throughout the CaK network. We did a similar randomness test by rotating Dopplergrams 180° relative to magnetograms. 60% of ERs were found at boundaries of supergranule cells after misaligning. This number is indicated in Figure 2 by a dashed line. Since the observed number in the first bin is 40% larger than the random number, we suggest that the ERs have a slight tendency to emerge at supergranule boundaries.

It is not surprising that almost all the major magnetic cancellation happens at supergranule boundaries. The three most common modes of cancellation are (Livi *et al.* 1985): (1) Two network elements with opposite magnetic polarities meet and disappear mutually. This is the principal way in which the quiet sun magnetic fields disappear. (2) A network element is cancelled by one pole of an ER. (3) Intranetwork (IN) fields move to the supergranule boundary and are cancelled by the network elements. Cancellation among the IN fields is very rare. We note that in almost every case of category (1) cancellation, two poles of cancelling features approach along the boundary of supergranules. Figure 3 shows an example. Cancellation has not been explained adequately by theory.

4. Moving Magnetic Features

Observations of decaying sunspots show small magnetic features moving outwards from the penumbra towards the surrounding moat with a velocity of about 1.0 km/s (Vrabec, 1974; Harvey and Harvey, 1973; Sheeley, 1969). Doppler measurements in the vicinity of sunspots (Sheeley and Bhatnagar, 1971; Sheeley, 1972) provide evidence for a horizontal outflow extending roughly 10,000 to 20,000 km into the extrapenumbral photosphere. The average outflow velocity from Doppler measurements is between 0.5 and 1.0 km/s. It is important to test whether both MMFs and Doppler velocity fields of a given spot are consistent. This is difficult to accomplish because MMFs are very difficult to observe toward the limb, where the observations have to be made in order to detect the Doppler signals produced by the horizontal outflow. We provide the results of our first attempt to measure the velocity of MMFs and the Doppler velocity fields simultaneously.

Both magnetograms and CaK filtergrams may be used to study MMFs. Under the best seeing at BBSO, CaK images have better spatial resolution than magnetograms. Only two hours of CaK data, under ideal seeing, were obtained each day, whereas typically 10-12 hours of magnetogram data were obtained per day. It has been well established that the chromospheric plage or bright network as shown on CaK spectroheliograms is cospatial with photospheric magnetic fields (e.g. Frazier 1970). Figure 4a is a magnetogram and 4b is the corresponding CaK image of BBSO region No. 1006, a decaying sunspot region observed on Oct. 15, 1987. Figure 5

shows the relationship between the magnetic flux density and the CaK contrast. We divided data points into bins by magnetic flux density with a bin width of 5 Gauss. The CaK contrast is the averaged value for each bin. This plot is consistent with studies by other authors (e.g. Frazier 1970).

Figure 6 is a Dopplergram made at NSO/KP corresponding to the magnetogram and CaK image shown in Figures 4a and 4b. The five-minute oscillation was removed by averaging two hours of Dopplergrams. A smooth component, corresponding to solar rotation, was fitted to and subtracted from the original Dopplergrams. The coordinates of the image center are 4°W, 40°S. The image is oriented with west at the right, south at the bottom. Because only the line-of-sight velocity component is observed in Dopplergrams, a radial outflow cell should appear as a white area beneath a black area. Many supergranule cells are apparent in this map.

The BBSO magnetograms, CaK images and NSO/KP Dopplergrams were carefully registered. Figure 7 shows a BBSO CaK image superposed on a NSO/KP Dopplergram after registration. The velocity fields are represented by contours, white contours receding, black approaching. There are two contour levels shown in the map, 0.15 km/s and 0.5 km/s. Obviously the outer edge of the moat, toward which the moving magnetic features move, is the boundary of the velocity cell associated with the sunspot in the figure. Sheeley (1972) has previously shown that the velocity cell is not symmetric relative to the spot. Note that, in Figure 7, the side towards the limb extended further from the spot and has stronger flow.

Figures 8a and 8b compare the structure of Doppler outflow surrounding a sunspot and a regular supergranule. Figure 8a is a velocity profile through the sunspot, 8b is a profile of a typical supergranule cell. Both velocity profiles were corrected for geometric foreshortening. The peak of the outflow surrounding the spot can reach 1.3 km/s; however for a regular supergranule, it is only about 0.5 km/s. Further comparisons will be shown in the next section.

In addition to the direct Doppler measurement, we measured the velocities of 42 moving magnetic features by tracking their positions in the magnetograms. The data which we used were obtained on October 15 and 16, 1987. The average radial velocity of MMFs, obtained by tracking individual features, is 0.65 ± 0.25 km/s, consistent with the average velocity of 0.67 ± 0.19 km/s obtained from Doppler measurement.

Meyer *et al.* (1974) pointed out that moving magnetic features generally occur in pairs with opposite polarities. To explain MMFs theoretically, Spruit *et al.* (1987) proposed that MMFs presumably correspond to the kinks travelling along an underlying flux tube, the average velocity of MMFs would be greater than the velocity obtained from Dopplergrams, since the kinks move outwards with the Alfvén velocity relative to the streaming gas. We estimated the Alfvén speed for the observed magnetic flux density of MMFs as about 1.0 km/s. Therefore, our results did not confirm Spruit *et al.*'s theory.

Finally, we would like to point out that MMFs are not uniformly distributed

throughout the region of Doppler outflow.

5. Influence of Magnetic Activity on Supergranulation

Having discussed the influence of convection on magnetic fields, we now consider the effect of magnetic fields on convection. An obvious example is that a sunspot, having strong magnetic fields and large flux, inhibits convection motion (Biermann, 1941). As a second example, it is believed that the lifetime of supergranule cells in enhanced network is much longer than that of normal supergranules on the quiet sun because of magnetic confinement (Zwaan 1978). Livingston and Orrall (1974) demonstrated the existence of some long lived cells near active regions, which they called "Magnetic Pukas". Pukas may live for 4 to 7 days. As a third example, Sýkora(1970) showed that the sizes of supergranules increase with the level of magnetic activity. Observational study of properties of supergranule cells in regions with different magnetic activity levels may increase our understanding of the effect of magnetic fields on convection motion.

5.1 Scale

The size of supergranules can be studied by the means of auto-correlation curves of Dopplergrams (Leighton *et al.*, 1962; Simon and Leighton, 1964; Wang, 1988). The average size of features of an image is defined as the distance between two minima in the auto-correlation curve. All the authors find a supergranule scale

around 32,000 km.

Our observations were made in the regions described in section 3. The results listed in the Table 1 are averages over all the regions in each category. The average size of supergranules in the quiet sun and enhanced network region is derived from the auto-correlation curve of Dopplergram as described above. The size of the radial outflow region surrounding the spot is estimated visually from the Dopplergrams. Supergranules in the enhanced network are slightly larger than in the quiet sun. However, this difference is smaller than the measurement errors, so it not significant. The radial outflow cell surrounding sunspots is 37,000 km, larger than the supergranule cells in general.

5.2 Horizontal Speed

As we showed in section 4, the outflow velocity in the cell surrounding a sunspot is larger in size and velocity amplitude than that of regular supergranule cells. We measured the average horizontal velocity in different regions discussed in section 3. However, the velocity obtained from Dopplergrams is the line-of-sight component of supergranule velocity. We convert it to a more meaningful parameter, i.e. the average horizontal velocity of supergranules, as follows. The observed line-of-sight velocity, V_L, is related to the supergranule velocities by Simon and Leighton (1964) as:

$$V_L = \frac{y \sin\theta}{\rho \cos\theta} F_h(\rho) + \cos\theta F_v(\rho) \qquad (2)$$

where θ is the heliocentric angle of the cell center, x and y are rectangular coordinates on the Doppler image originating at the cell center such that the y axis passes through disk center. $F_v(\rho)$ and $F_h(\rho)$ are the vertical and horizontal components of supergranule velocity, and $\rho^2 = x^2 + y^2/\cos^2(\theta)$.

The line-of-sight projection of the vertical component of supergranule velocity is significantly smaller than that of the horizontal component, especially when the observation is made far from disk center (Giovanelli, 1980; Wang and Zirin, 1988). So the second term in the right side of equation (2) can be neglected.

Simon and Leighton (1964) used:

$$F_h = V_h \sin(\pi\rho/R) \tag{3}$$

where R is the radius of the supergranule cell.

The average absolute value of V_L over the entire cell $|\overline{V_L}|$, is $\int |V_L| dS/\pi R^2$. We derived:

$$|\overline{V_L}| = \frac{4}{\pi^2} V_h \frac{\sin\theta}{\cos\theta} \tag{4}$$

Since there are gaps between the cells, we should make an area correction. We estimate the ratio of the area occupied by cells to the whole image area as $\pi R^2/4R^2 = \pi/4$, the ratio of the area of a a circle with a radius of R to that of a square with a side-length of 2R. Finally, we derived:

$$V_h = \pi |\overline{V_L}| \frac{\cos\theta}{\sin\theta} \tag{5}$$

where $|\overline{V_L}|$ is observed average velocity over the whole Dopplergram, V_h is the average peak horizontal velocity of supergranule. Our observed $|\overline{V_L}|$ is consistent with the result by Chou *et al.* (1988).

The results are included in the Table 1. The observations show that the horizontal velocities of supergranules are similar in the quiet sun and in the enhanced network region. i.e. V_h=0.45 to 0.47 km/s. However, the outflow cell surrounding the sunspot has V_h = 1.02 km/s, which is more than twice as strong as the average regular supergranule cell.

5.3 Correlation Lifetime

Correlation lifetime is defined as the time lag required for the temporal cross-correlation coefficient to drop to 1/e (Simon and Leighton 1964). As we stated in another paper (Wang and Zirin 1988), due to the shape change of supergranules, the correlation lifetime of supergranules is much shorter than their actual average lifetime. By observing the evolution of individual supergranules, we found the average lifetime of supergranules to be longer than 50 hours. However correlation analysis is more objective than inspecting images visually. Cross-correlation coefficients of magnetogram and Dopplergrams are calculated for all those regions mentioned in section 3. Figure 9 plots the cross-correlation coefficients and least square fits for a quiet region and an enhanced network region. Both magnetograms and Dopplergrams were analyzed. Figure 10 shows cross-correlation coefficients for a sunspot.

The results are summarized in Table 1. The standard deviations for all the fits are between 0.5 to 2.0 hours.

It was expected that the supergranule lifetime in the enhanced network region would be longer than in the regular quiet sun (Livingston and Orrall, 1974, Zwaan, 1978). From our observations, correlation time of magnetograms in the enhanced region is 7 times as long as in the quiet sun. However, the velocity correlation times are almost the same for the two regions. Finally, we notice that the radial outflow pattern surrounding the spot is 7.5 times as stable as the regular supergranule cells.

6. Summary and Discussion

Our observations confirmed the outflow velocity cells surrounding decaying sunspots. This paper provides the first comparison between the speed of MMFs and the Doppler measurements of the outflow. The average speed of MMFs is approximately the same as the average speed of the outflow. However, the outflow is not symmetric relative to the spot. In some places, no MMFs were found although there exists a clear outflow.

Neither the scales nor the horizontal velocity amplitudes of supergranules depend on the average magnetic flux density of the regions in which the supergranules are found. It is hard to understand why the velocity structure of supergranule cells has the same correlation lifetime in the enhanced network region and in the mixed polarity quiet region even though the magnetic structure is much more stable in

the enhance network region than in the mixed polarity quiet sun. We suggest that the magnetic fields do not affect the evolution of supergranule velocity fields in the enhanced network regions and the mixed polarity quiet sun. One fact which might be worth noting is that the relationship between the network magnetic fields and the supergranule boundaries in enhanced network regions is not as close as in the quiet region.

The convective velocity fields can be controlled and rearranged by magnetic fields at or nearby the sunspots, where a radial outflow pattern is formed with the spot at its center. The outflow pattern has larger scale, stronger radial velocity and much longer lifetime than the regular supergranules.

We found, unlike Howard *et al.* (1979), that ERs have a tendency to form near the boundaries of supergranules. Since we have demonstrated that supergranule cells exhibit upflow near the cell center and downflow at boundaries, we conclude that ERs are not brought to the surface by convection motion. In this sense, ERs are similar to new active regions, they also tend to emerge at the boundaries of supergranules (Born 1974, Howard *et al.*, 1979).

References

Biermann, L. 1941, *Vierteljahrsschr Astr. Gesellsch* **76**, 194.

Born, R. 1974, *Solar Physics* **38**, 127.

Chou, D., LaBonte, B.J., Braun, D.C. and Duvall, T.L. 1988, in preparation.

Clark, A. 1968, *Solar Physics* **4**, 386.

Frazier, E.N. 1970, *Solar Physics* **14**, 89.

Frazier, E.N. 1972, *Solar Physics* **26**, 130.

Galloway, D.J. and Weiss, N.O. 1981, *Ap. J.* **243**, 945.

Giovanelli, G.R. 1980, *Solar Physics* **67**, 211.

Golub, L., Krieger, A.S., Silk, J.K., Timothy, A.F. and Vaiana, G.S. 1974, *Ap. J.* **189**, L93.

Harvey, K. and Harvey, J. 1973, *Solar Physics* **28**, 61.

Harvey, K. and Martin, S.F. 1973, *Solar Physics* **32**, 389.

Howard, R., Fritzova-Svestkova, L. and Svestka, Z., *Solar Physics* **63**, 105.

Leighton, R.B., Noyes, R.W. and Simon, G.W. 1962, *Ap. J.* **135**, 474.

Livi, S.H.B., Wang, J. and Martin, S.F. 1985, *Australian Journal of Physics* **38**[6], 855.

Livingston, W.C. and Orrall, F.Q. 1974, *Solar Physics* **39**, 301.

Martin, S.F. 1984, *BBSO 228.*

Martin, S.F., Livi, S.H.B. and Wang, J. 1985, *Australian Journal of Physics* **38**[6], 929.

Martin, S.F. and Harvey, K. 1979, *Solar Physics* **64**, 93.

Marsh, K. A. 1978, *Solar Physics* **59**, 105.

Meyer, F., Schmidt, H.U., Weiss, N.O. and Wilson, P.R. 1974, *Mon. Not. R. Astro. Soc.* **169**, 35.

Meyer, F., Schmidt, H.U., Simon, G.W. and Weiss, N.O. 1979, *Astro. and Astrophys.* **76**, 35.

Schmidt, H.U., Simon, G.W. and Weiss, N.O. 1985, *Astro. and Astrophys.* **148**, 191.

Sheeley, N.R. 1969, *Solar Physics* **9**, 347.

Sheeley, N.R. 1972, *Solar Physics* **25**, 98.

Sheeley, N.R. and Bhatnagar, A. 1971, *Solar Physics* **19**, 338.

Simon, G.W. and Leighton, R.B. 1964, *Ap. J.* **140**, 1120.

Spruit, H.C. 1984, in S.L. Keil (ed.) *Proceeding of the Symp. on Small Scale Dynamical Processes in Quiet Stellar Atmosphere*, NSO/SP, p249.

Spruit, H.C., Title, A.M. and Van Ballegooijen, A.A. 1987, *Solar Physics* **110**, 115.

Sýkora, J. 1970, *Solar Physics* **13**, 292.

Vrabec, D. 1974, in Athay, R.G. (ed.) *Chromospheric Fine Structure*, p201.

Wang, H. and Zirin, H. 1987, submitted to Solar Physics.

Wang, H. and Zirin, H. 1988, to be submitted to Solar Physics.

Wang, H. 1988, submitted to Solar Physics.

Zirin, H. 1985, *Australian Journal of Physics* **38**, 961.

Zirin, H. 1987, *Solar Physics* **110**, 101.

Zirin, H. and Wang, H. 1987, Presentation in AAS Solar Physics Division Meeting, May 13-15, 1987, Honolulu.

Zwaan C. 1978, *Solar Physics* **60**, 213.

Figure Captions

Fig. 1 An ER emerging at the boundary of a supergranule. The ER is marked 'E1' and was first seen at 20:33 UT. Contours give the supergranule velocity fields. The first contour level is 0.1 km/s and the second level is 0.3 km/s. Pairs of adjacent white and black contours, with white above and to the right of black, represent supergranules.

Fig. 2 The histogram of the ER distribution. R is the distance between the ER location and the cell center in units of the radius of supergranule cell where the ER resides. The dashed line is a fictitious distribution if ERs emerge randomly relative to supergranules.

Fig. 3 A cancelling feature and its relationship to the supergranule velocity fields. The cancelling feature is marked by 'C1'.

Fig. 4a A magnetogram observed at 18:20 UT, Oct-15, 1987, The region is BBSO No. 1006, a decaying active region.

Fig. 4b A CaK image corresponding to magnetogram of Figure 4a.

Fig. 5 Relationship between the magnetic flux density B and the average contrast of CaK emission.

Fig. 6 A Dopplergram after two hour averaging, 2-D smoothing and filtering, showing the same region and shown to same scale as Figure 4a.

Fig. 7 The Dopplergram superposed on the CaK image. White contours are receding motion, black ones approaching. This Dopplergram is the same one shown in Figure 6.

Fig. 8a A profile of velocity through the sunspot. The line of the cut is shown in Figure 7. The geometric foreshortening is taken into account. Two solid vertical lines show the position of the penumbra, and two dash lines show that of the umbra.

Fig. 8b Horizontal velocity profile of a typical supergranule cell.

Fig. 9 Cross-Correlation curves and their least square fits to a decaying exponential for a quiet region and an enhanced magnetic region. (1) Plus signs and dashed line: magnetograms, enhance network; (2) Stars and light solid line: Dopplergrams, enhanced network; (3) Circles and dash-dot line: Dopplergrams, Q.S.; (4) Triangles and dark solid line: magnetograms, Q.S..

Fig. 10 Cross-Correlation curves for a decaying sunspot. (1) Plus signs and light solid line: magnetograms; (2) Triangles and dark solid line: Dopplergrams.

Table 1. Properties of Supergranule Velocity Cells

Region	Mean B(G)	Size(km)	V_L(km/s)	Correlation Time(h)	
				Magnetic	Velocity
Q.S.	5.9±0.9	30500±2500	0.47±0.05	7.9	14.5
Enhanced Network	18.8±2.0	31900±2100	0.45±0.05	58.3	13.3
Decaying Sunspot	170±12	37000±1800	1.02±0.02	411	104

FIGURE 1

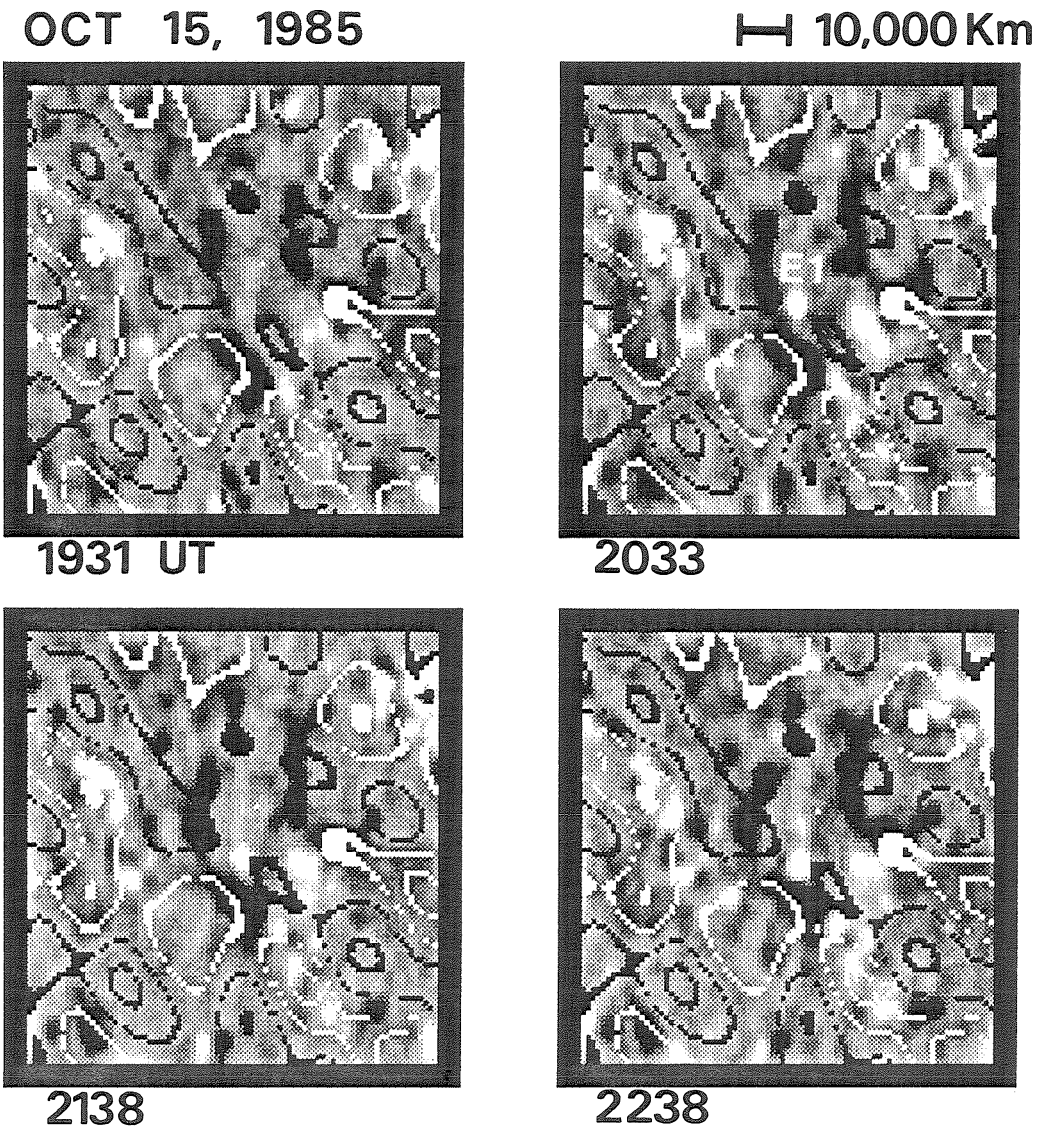

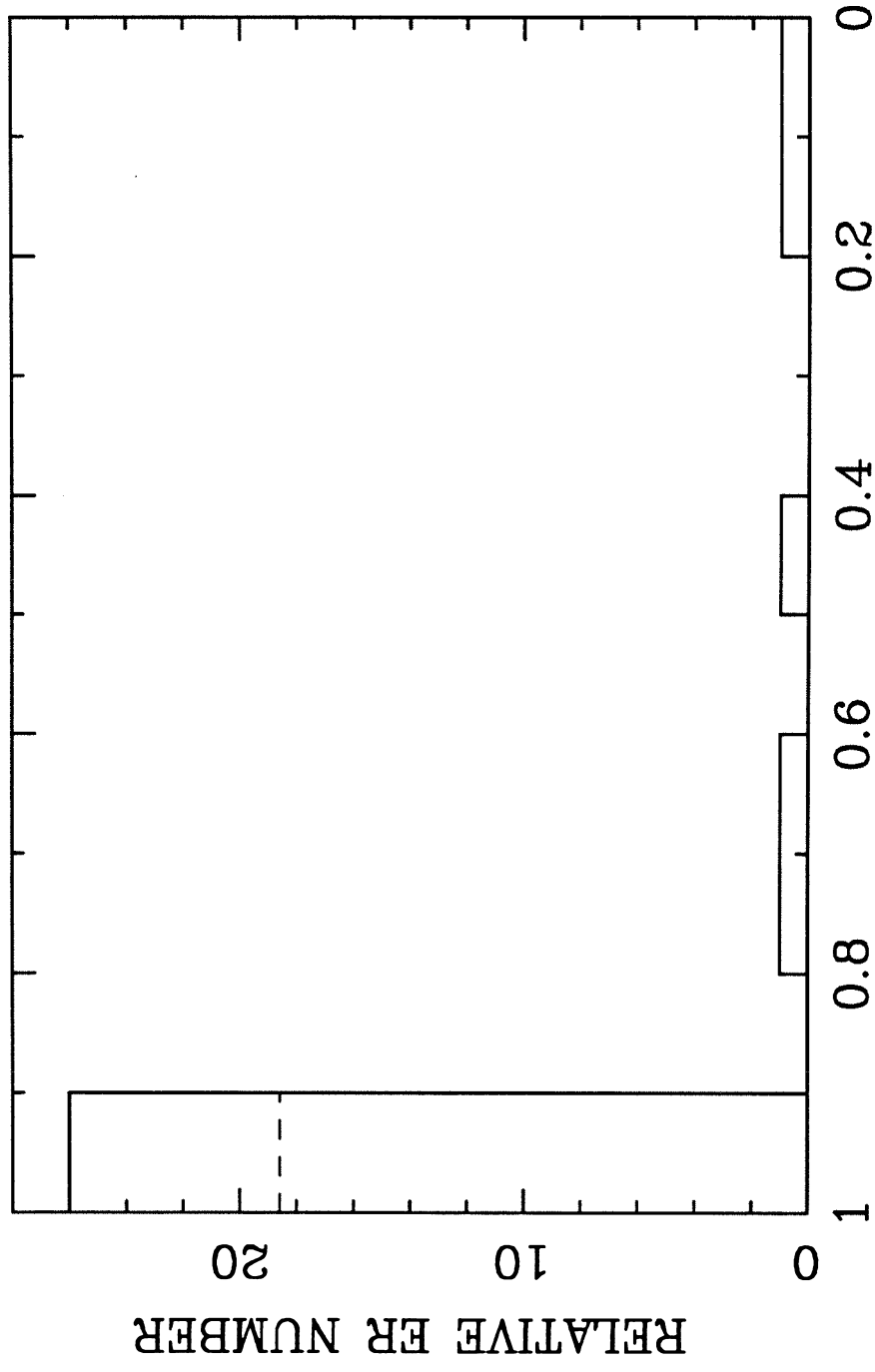

FIGURE 2

FIGURE 3

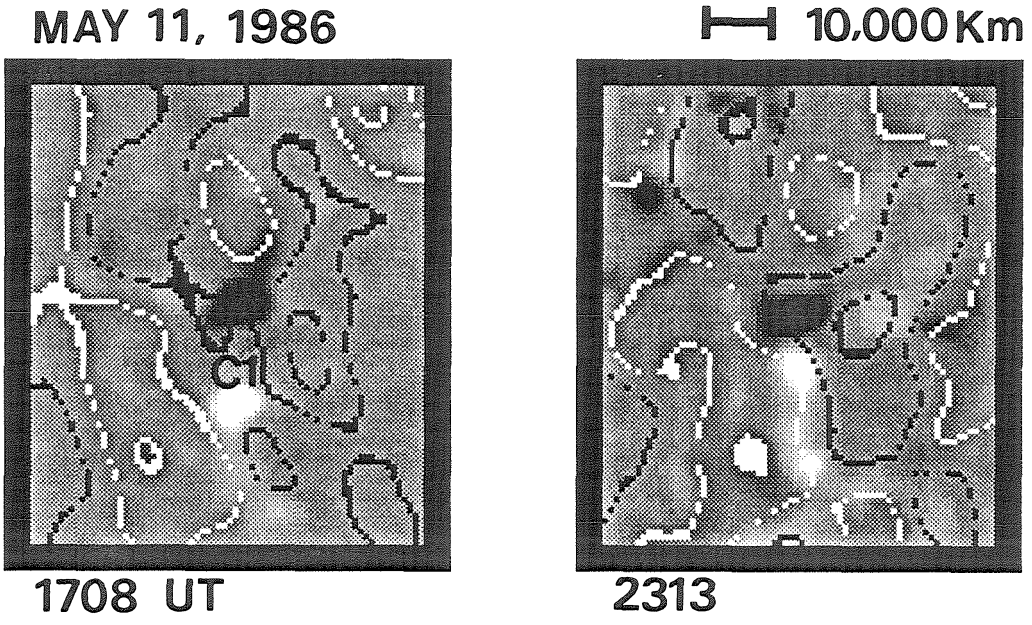

FIGURE 4a

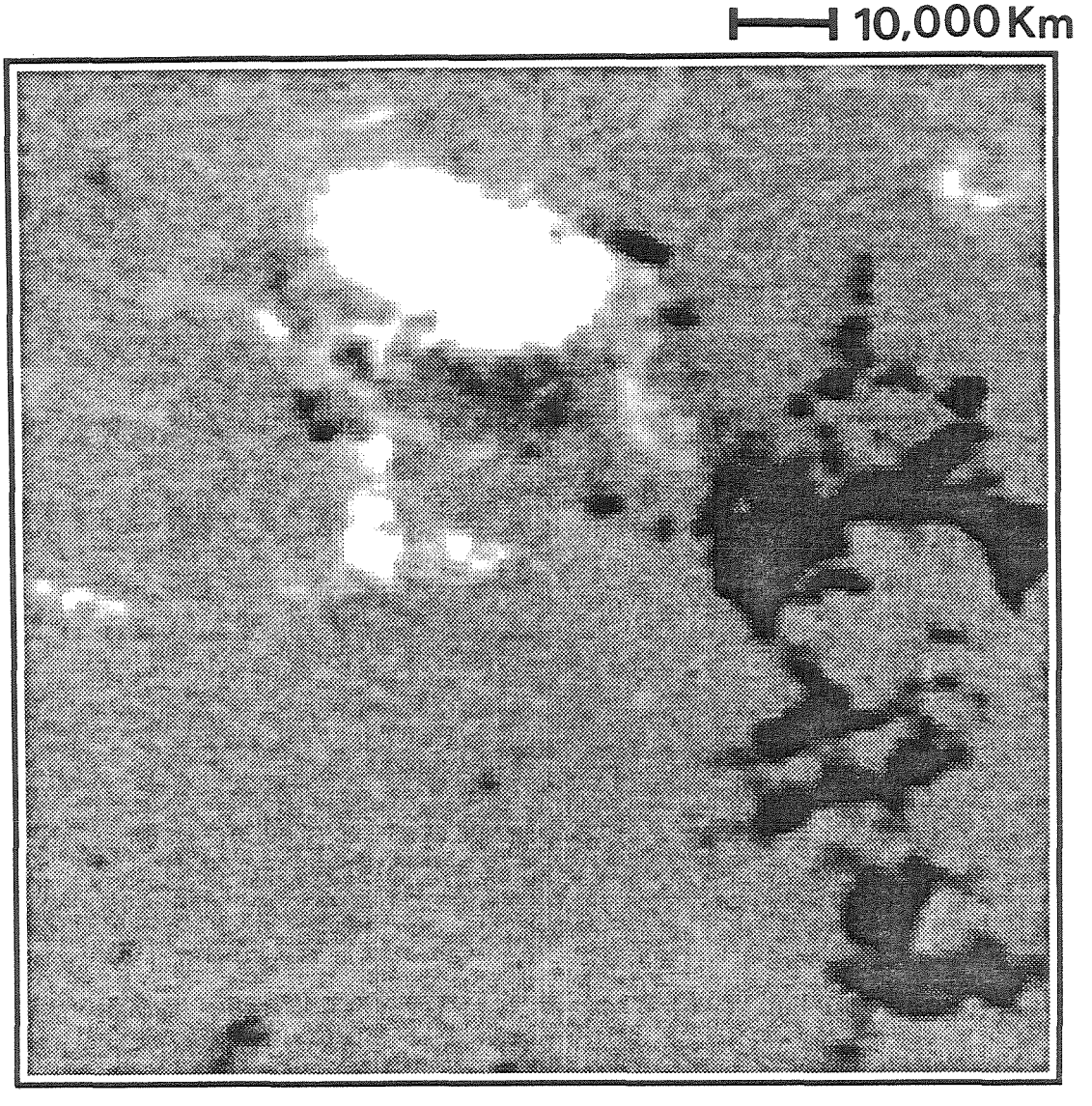

FIGURE 4b

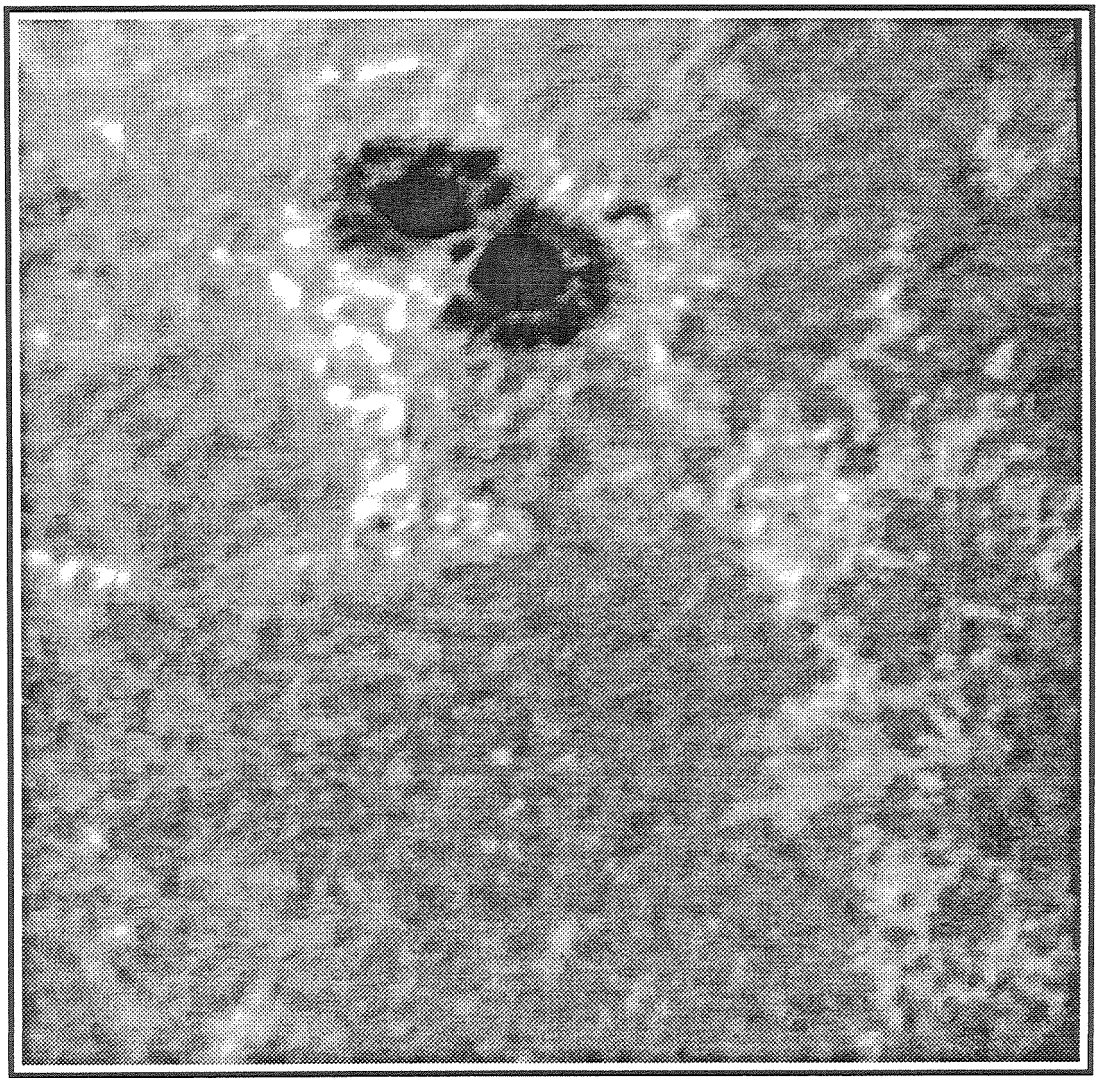

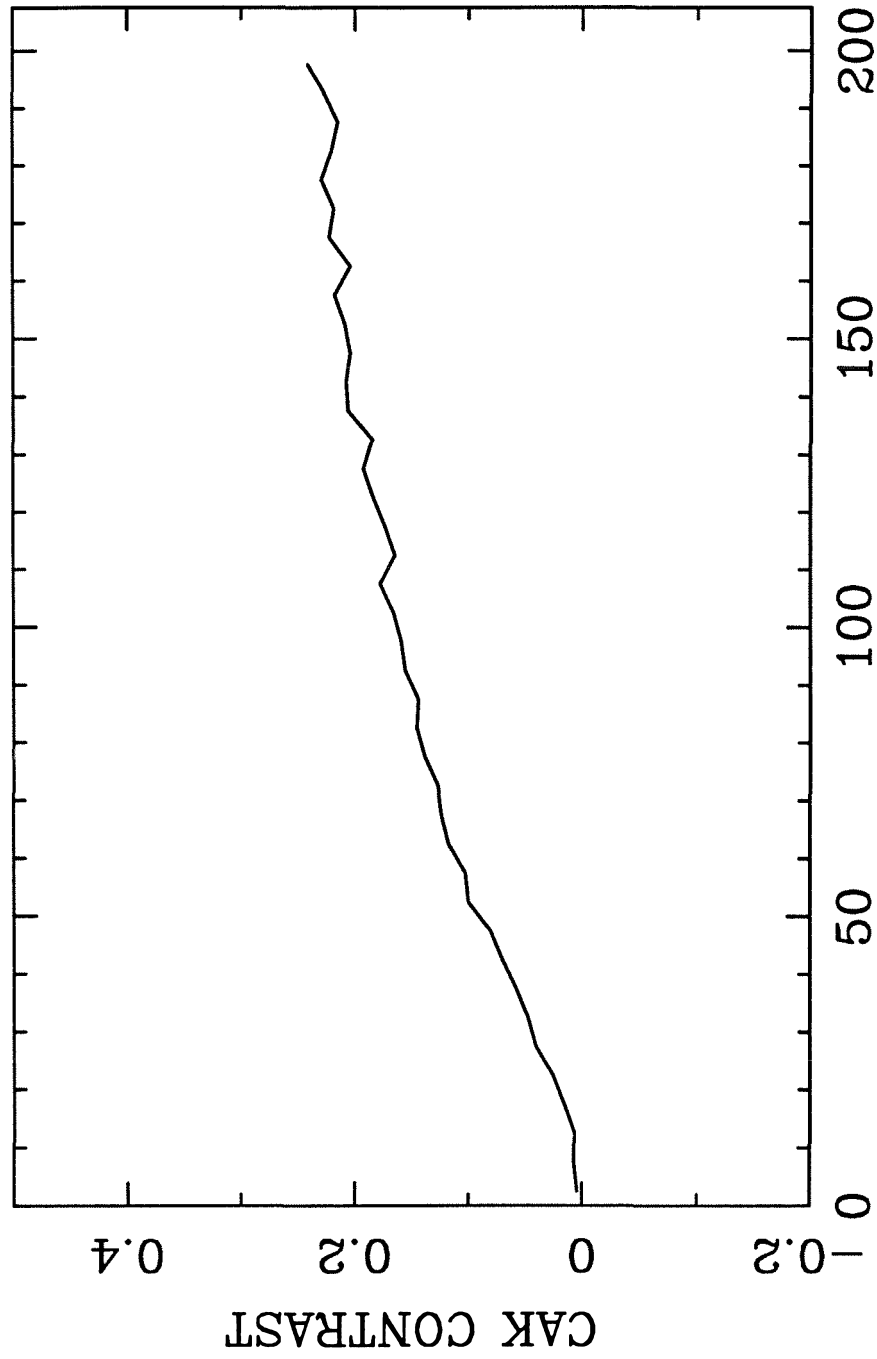

FIGURE 5

FIGURE 6

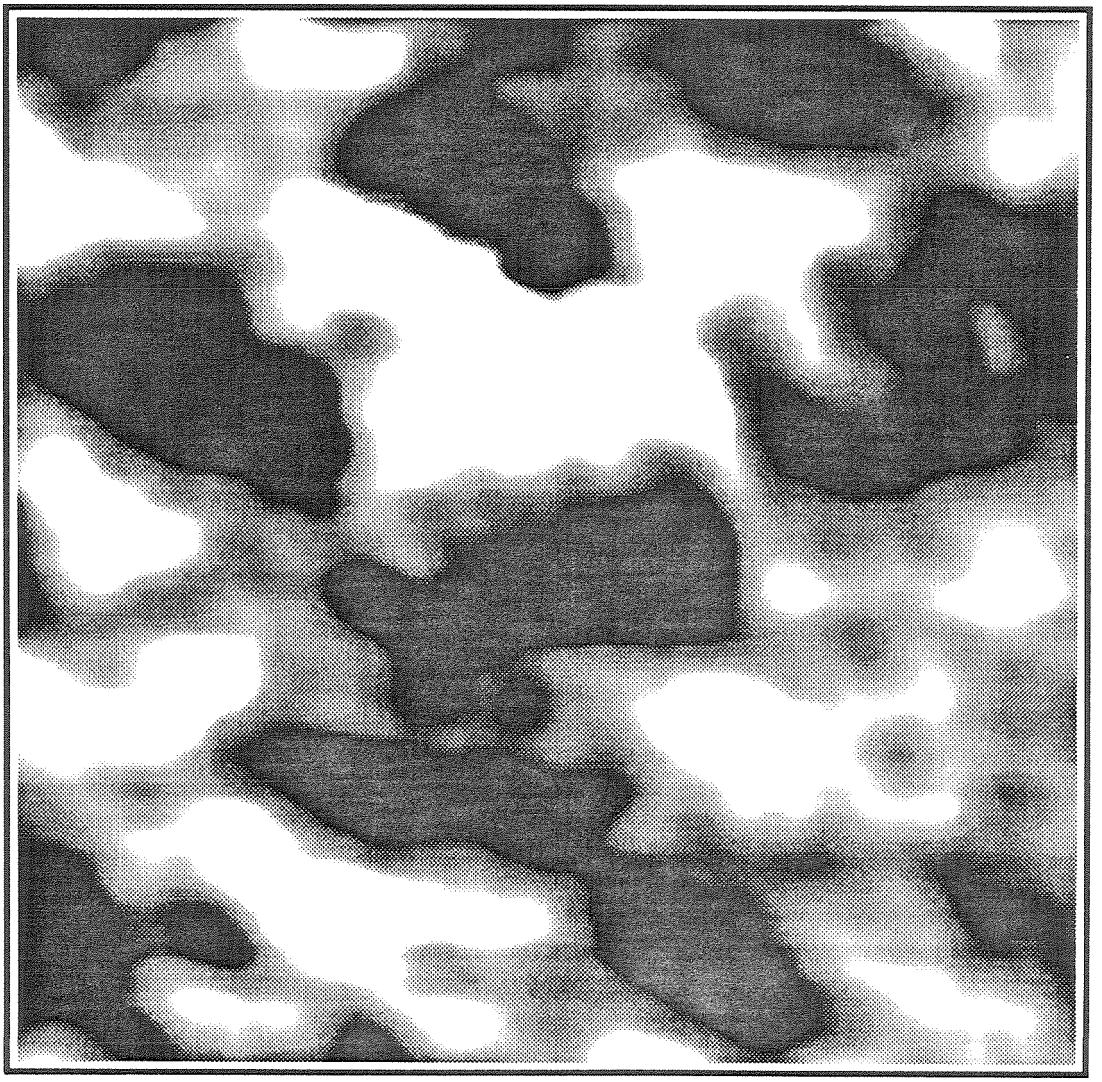

FIGURE 7

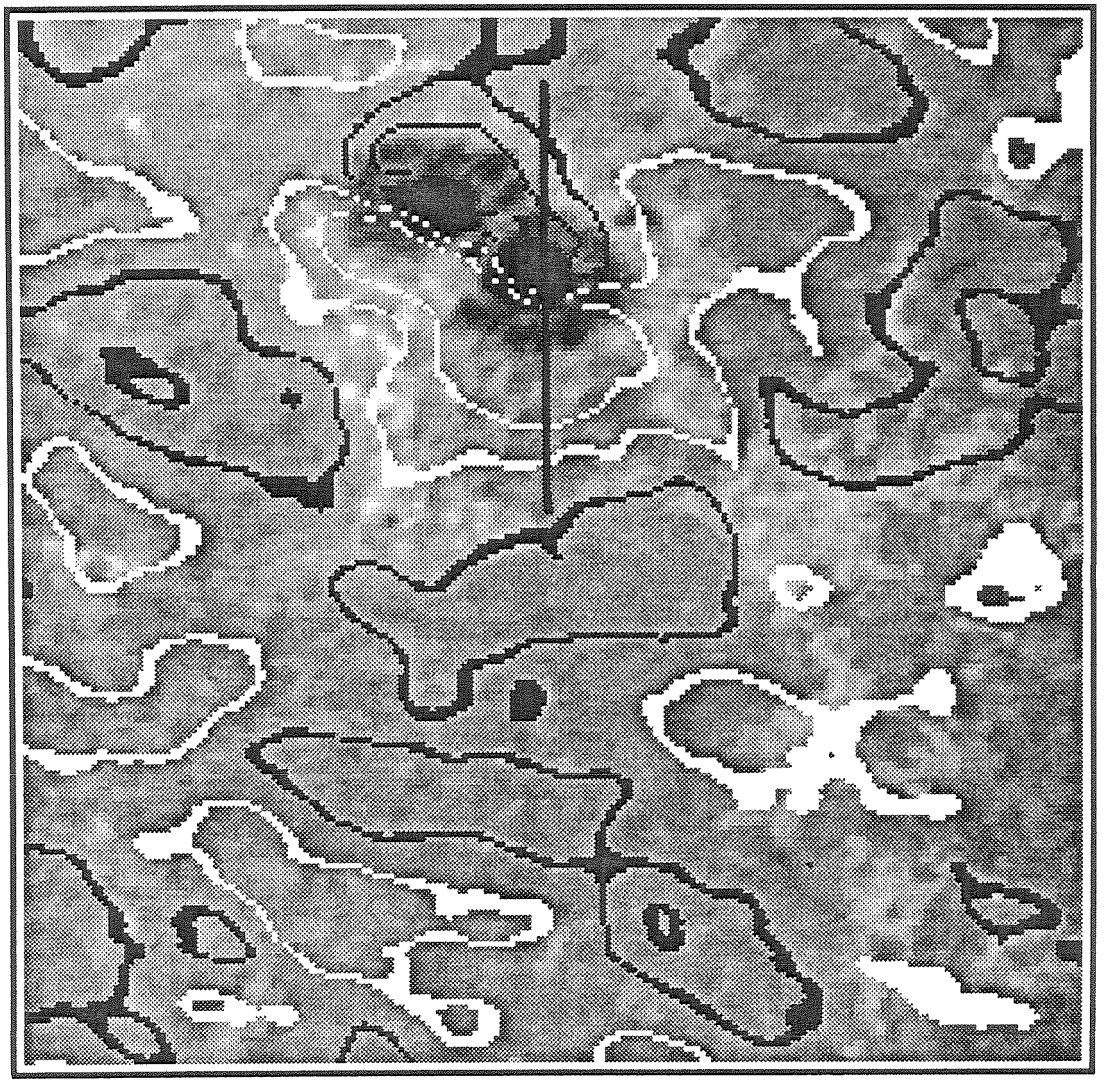

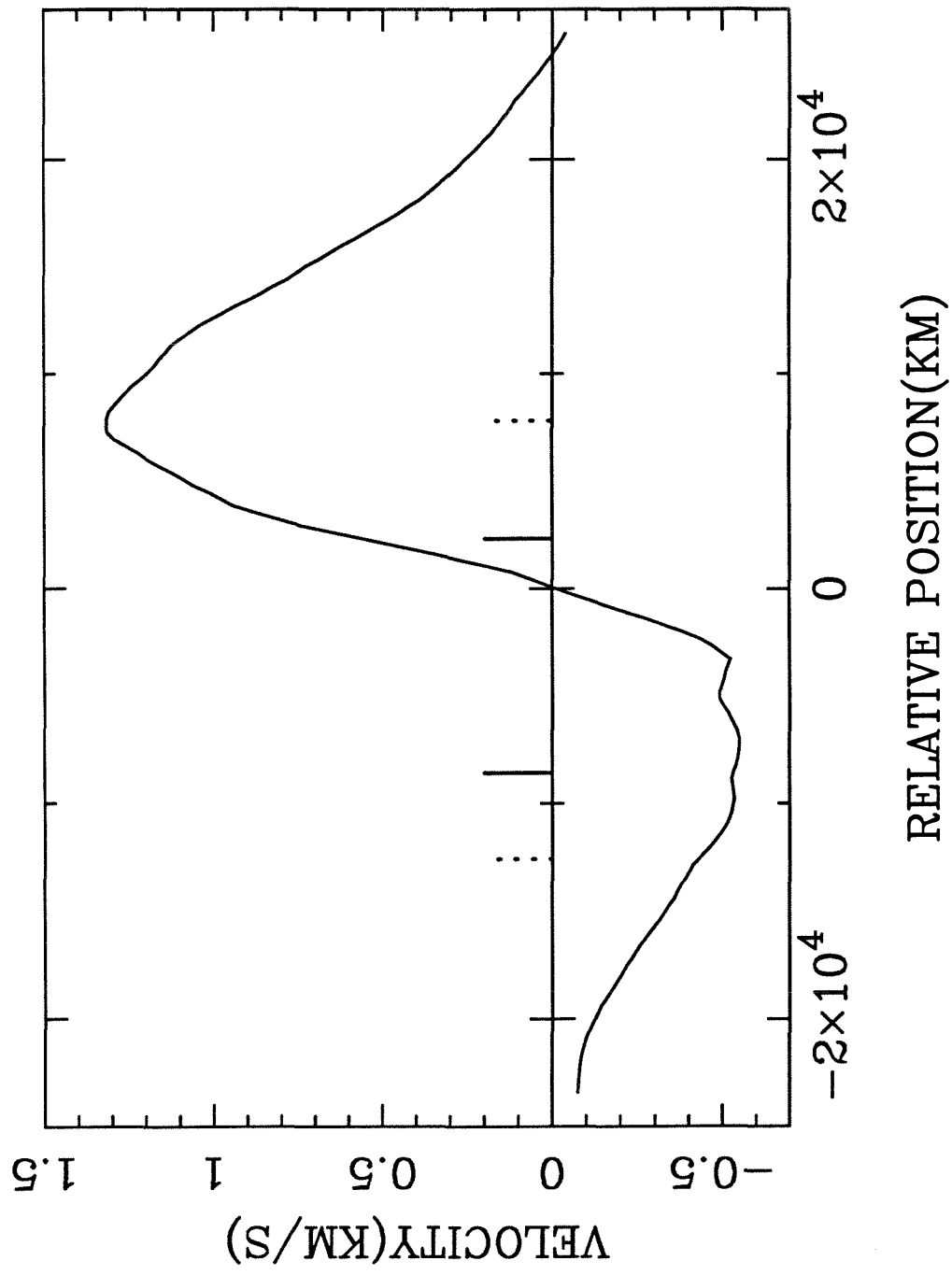

FIGURE 8a

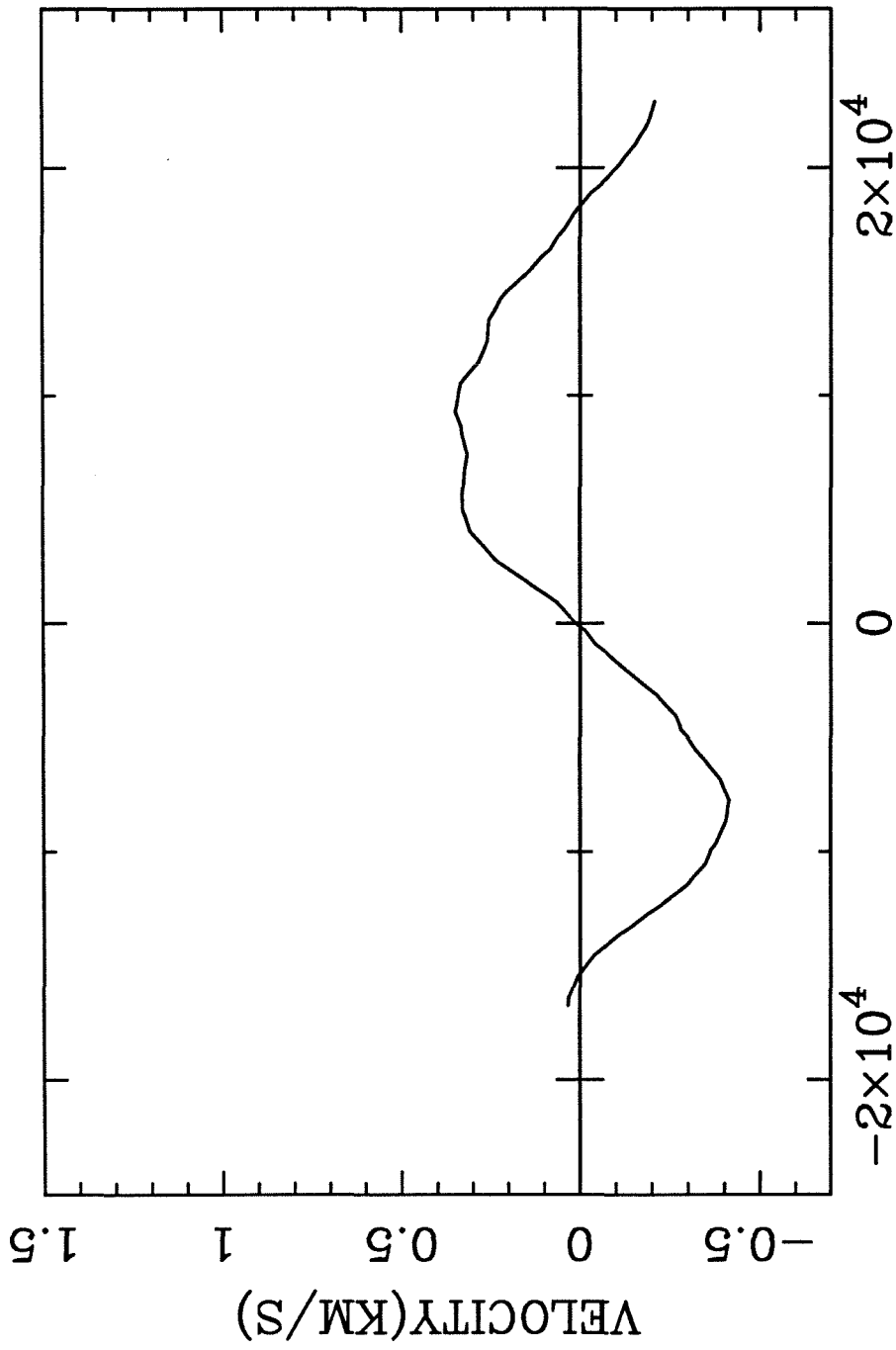

FIGURE 8b

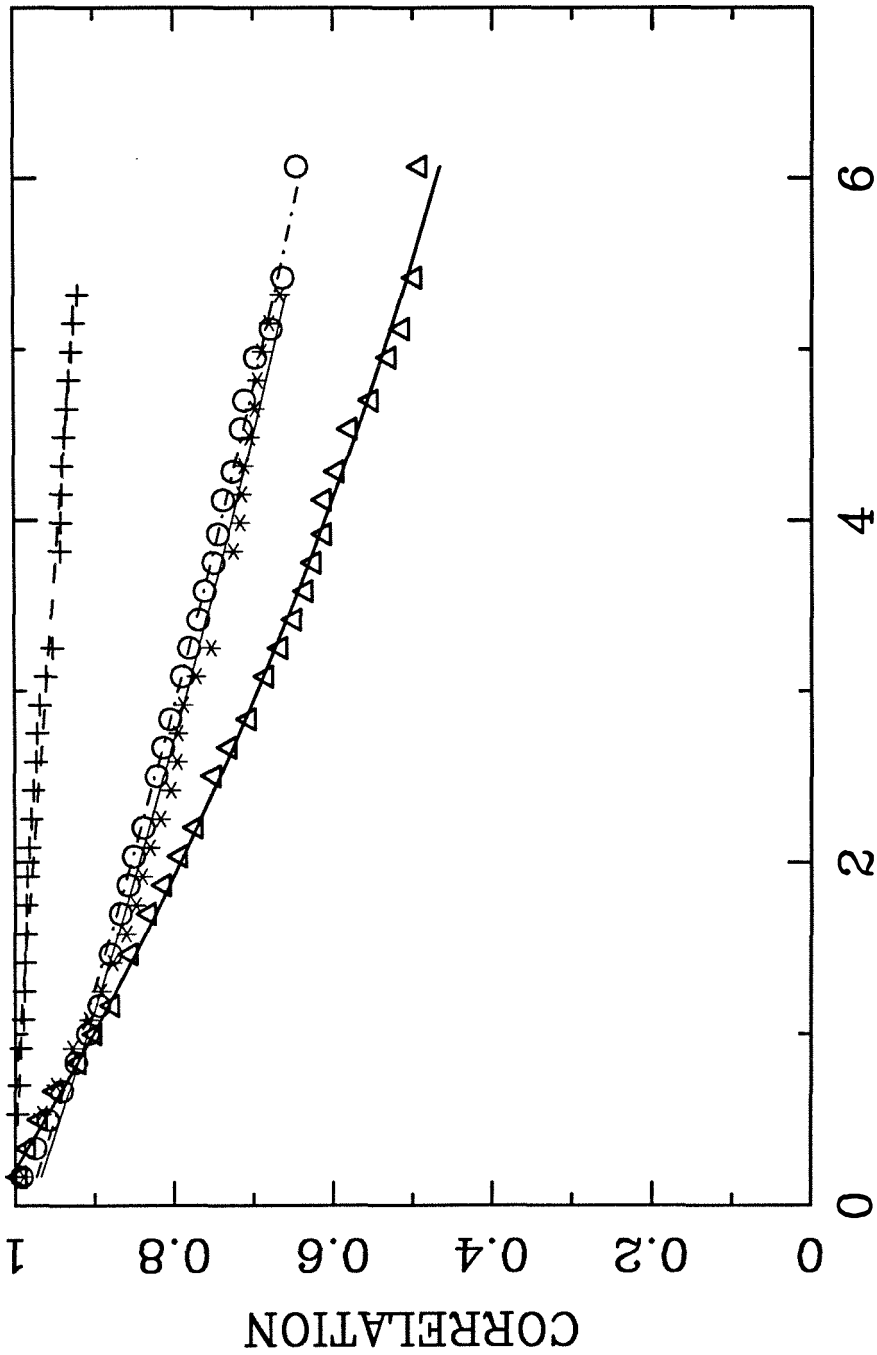

FIGURE 9

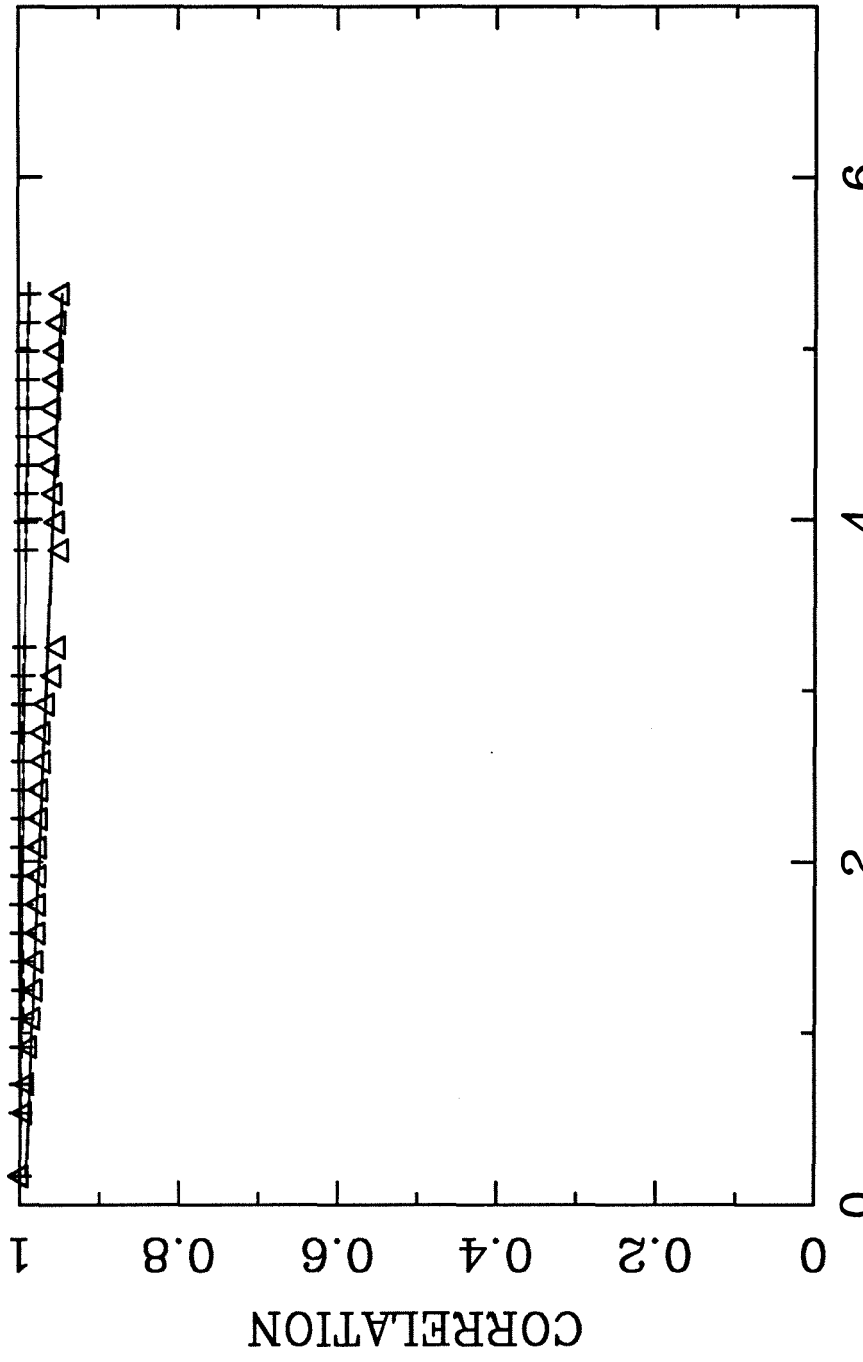

FIGURE 10